*Final Progress Report*

# SCALE-DEPENDENT PHOSPHORUS LEACHING IN ALLUVIAL FLOODPLAINS

## USGS Award No. G10AP00137

*Garey Fox, Todd Halihan, Chad Penn, and Daniel Storm*
*Oklahoma State University*

*Derek Heeren, Ryan Freiberger*
*University of Nebraska-Lincoln*

*Brian Haggard, Andrew Sharpley, and Phil Hayes*
*University of Arkansas and USGS*

*This report is the final progress report for this project.*

# EXECUTIVE SUMMARY

Increased nutrient loads have resulted in several adverse impacts on surface water quality, including excessive algal growth, fish kills, and drinking water taste and odor issues across the United States and especially in the Ozark ecoregion of northeastern Oklahoma and northwestern Arkansas. Nitrogen is a concern, but phosphorus (P) is generally considered the limiting nutrient in most surface water systems. The significance of this problem has been highlighted by litigation, with one case even reaching the U.S. Supreme Court (Arkansas et al. v. Oklahoma et al., 503 U.S. 91) which required the upstream state to meet downstream water quality standards. Scientists and engineers need to identify critical nutrient source areas and transport mechanisms within a catchment in order to cost effectively protect and enhance drinking water systems, recreation activities, and aquatic ecosystems. While surface runoff is considered to be the primary transport mechanism for P, leaching through the vadose zone and subsurface transport through coarse gravel subsoils to gravel bed streams may be significant and represents a source of P not alleviated by current conservation practices (e.g., riparian buffers). It was hypothesized that hydrologic heterogeneities (e.g., macropores and gravel outcrops) in the subsurface of floodplains play an integral role in impacting flow and contaminant transport between the soil surface and shallow alluvial aquifers which are intricately connected to streams. Infiltration is often assumed to be uniform at the field scale, but this neglects the high spatial variability common in anisotropic, heterogeneous alluvial floodplain soils. Therefore, the overarching objective of this line of research was to characterize phosphorus leaching to alluvial aquifers in the coarse gravel floodplains of the Ozark ecoregion across a range of scales (point to 100 $m^2$) in order to evaluate the effect of the scale of measurement.

Electrical resistivity imaging was used to characterize the alluvial deposits at selected floodplain sites. Laboratory flow through P sorption experiments were conducted in order to examine the effect of retention time (RT) and inflow P concentration on P sorption; this was compared to results of isothermal titration calorimetry (ITC) experiments where the heat of reaction was measured with the addition of P to soils. Based on thermograms, the dominant P sorption reaction was ligand exchange onto Al/Fe oxides/hydroxides, with a lesser degree of precipitation. Phosphorus removal for both soils was limited by physical nonequilibrium instead of chemical nonequilibrium (sorption kinetics).

Innovative field studies, including plot scale (1 by 1 m, 3 by 3 m, and 10 by 10 m) solute injection experiments along with geophysical imaging, were performed on both gravel outcrops and non-gravel outcrops. A berm method, using a temporary berm constructed of a water-filled 15 cm diameter vinyl hose with the edges sealed to the soil using bentonite, was developed and utilized for plot-scale infiltration experiments. Guidelines are provided for tank size and refilling frequency for conducting field experiments. Plots maintained a constant head of 2 to 9 cm for up to 52 hours. Infiltration rates ranged from 0.6 to 70 cm/h, and varied considerably even within a single floodplain. Effective saturated hydraulic conductivity ($K_{eff}$) data, based on plot scale infiltration rates, ranged from 0.6 to 68 cm $hr^{-1}$. Plot scale infiltration tests are recommended over double ring infiltrometer tests or point scale estimates, although only small plots (1 m by 1 m) are necessary. Tension infiltrometers showed that macropore flow accounted for approximately 85% to 99% of the total infiltration.

Solutes in the injection water included P (highly sorptive), Rhodamine WT (slightly sorptive), and chloride (conservative). Observation wells were installed outside the plots to monitor for water table rise and tracers that leached into the groundwater. Electrical resistivity imaging was used to identify zones of preferential flow as well as characterize subsurface soil layering. Fluid samples from observation wells outside the plot (0.5 m from the boundary) indicated nonuniform subsurface flow and transport. Phosphorus was detected in the groundwater for 6 of the 12 plots and was positively correlated to the presence of gravel outcrops. Results indicated that flow paths are sub-meter scale for detecting infiltrating solutions. The surface soil type (ranging from silt loam to clean gravel) and macroporosity were found to have a significant impact on P leaching capacity. This research highlighted the difference between the conceptual infiltration model of a diffuse wetting front characterized by Richards Equation and actual infiltration in field conditions. Results were modeled with HYDRUS-2D/3D, a two/three-dimensional, finite-element model for flow and contaminant transport (both equilibrium and physical/chemical nonequilibrium transport) through soils. A gravel outcrop trial found significant P transport to the water table boundary after 15 years. HYDRUS was unable to simulate observed P detections in silt loam plots, indicating that better modeling techniques or programs need to be developed to better simulate highly complex soil profiles dominated by macropore flow.

Since floodplains are well-connected to alluvial aquifers and streams in gravelly watersheds, a higher level of agricultural stewardship may be required for floodplains than upland areas. This has implications for the development of best management practices specifically for floodplains in the Ozark ecoregion due to their close proximately and connectedness to streams.

# TABLE OF CONTENTS

# LIST OF FIGURES

# LIST OF TABLES

# SCALE-DEPENDENT PHOSPHORUS LEACHING IN ALLUVIAL FLOODPLAINS

# USGS AWARD NO. G10AP00137

**Principal Investigators:**

Garey Fox, Todd Halihan, Chad Penn, and Daniel Storm
Oklahoma State University

Derek Heeren
University of Nebraska

Brian Haggard and Andrew Sharpley
University of Arkansas

Phil Hayes
University of Arkansas and Arkansas USGS

**Start Date:** 9/1/2010

**End Date:** 8/31/2013

**Congressional District:** 2nd and 3rd in Oklahoma; 3rd in Arkansas

**Focus Category:** AG, GEOMOR, GW, HYDROL, NPP, NU, ST, SW, WQL

## (1) PROBLEM AND RESEARCH OBJECTIVES

This research hypothesizes that macropores and gravel outcrops in alluvial floodplains have a significant, scale-dependent impact on contaminant leaching through soils; therefore, both soil matrix and macropore infiltration must be accounted for in an analysis of nutrient transport. However, quantifying the impact and spatial variability of macropores and gravel outcrops in the subsurface is difficult, if not impossible, without innovative field studies. This research proposes an innovative plot design that combines these and other methods in order to characterize water and phosphorus movement through alluvial soils.

The specific objectives of this research are twofold. The first objective is to quantify the phosphorus (P) transport capacity of heterogeneous, gravel soils common in the Ozark ecoregion. Two characteristics of the soil are expected to promote greater infiltration and contaminant transport than initially expected: (1) macropores or large openings (greater than 1-mm) in the soil (Thomas and Phillips, 1979; Akay et al., 2008; Najm et al., 2010) and (2) gravel outcrops at the soil surface (Heeren et al., 2010). This research will estimate P concentration and P load of water entering the gravelly subsoil from the soil surface in several alluvial floodplains with varying topsoil thicknesses. Second, the impact of experimental scale on results from P leaching studies will be evaluated. If a material property is measured for identical samples except at various sample sizes, a representative element volume (REV) curve can be generated showing

large variability below the REV. This provides a helpful framework for evaluating scales in P leaching. What minimum land area is necessary to adequately measure P leaching? It is hypothesized that measured P leaching (kg/m-s) will generally increase as the scale increases from point ($10^{-3}$ $m^2$) to plot ($10^2$ $m^2$) scales. This will be evaluated by measuring P leaching at the point scale in the laboratory and at plot scales with bermed infiltration experiments for three plot sizes (approximately $10^0$, $10^1$, and $10^2$ $m^2$).

If subsurface transport of P to alluvial groundwater is significant, these data will be critical for identifying appropriate conservation practices based on topsoil thickness. Riparian buffers are primarily aimed at reducing surface runoff contributions of P; however, their effectiveness within floodplains may be significantly reduced when considering heterogeneous subsurface pathways.

# (2) METHODOLOGY AND PRINCIPAL FINDINGS/SIGNIFICANCE

## (A) Site Descriptions

The three selected riparian floodplain sites are located in the Ozark region of northeastern Oklahoma and western Arkansas. The Ozark ecoregion of Missouri, Arkansas, and Oklahoma is characterized by karst topography, including caves, springs, sink holes, and losing streams. The erosion of carbonate bedrock (primarily limestone) by slightly acidic water has left a large residuum of chert gravel in Ozark soils, with floodplains generally consisting of coarse chert gravel overlain by a mantle of gravelly loam or silt loam (Figure 1). The three floodplain sites are located adjacent to the Barren Fork Creek, Pumpkin Hollow and Clear Creek (Figure 2).

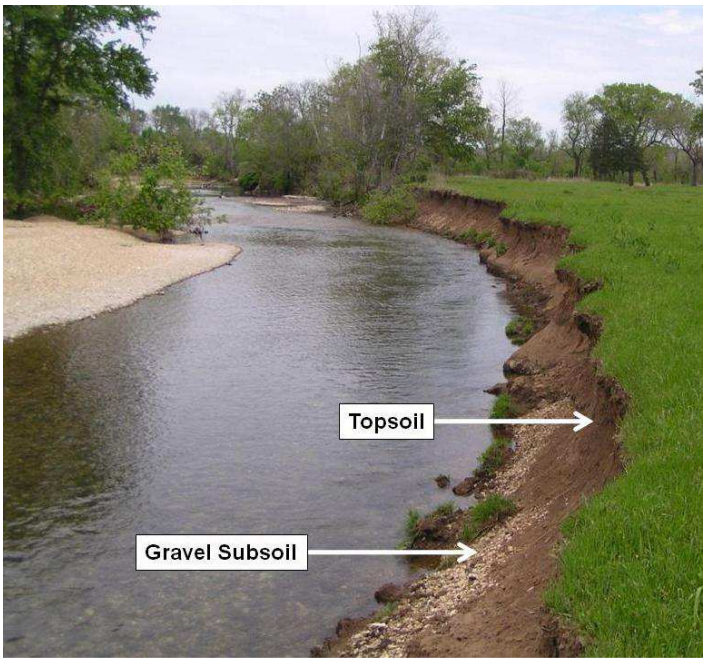


**Figure 1. Floodplains in the Ozark ecoregion generally consist of coarse chert gravel overlain by a mantle (1-300 cm) of topsoil.**


**Figure 2. Location of riparian floodplain sites in the Ozark ecoregion of Oklahoma and Arkansas.**

## Barren Fork Creek Site (Oklahoma)

The Barren Fork Creek site, five miles east of Tahlequah, Oklahoma, in Cherokee county (latitude: 35.90°, longitude: -94.85°), is located just downstream of the Eldon U.S. Geological Survey (USGS) gage station (07197000). A tributary of the Illinois River, the Barren Fork Creek has a median daily flow of 3.6 $m^3/s$ and an estimated watershed size of 845 $km^2$ at the study site. Historical aerial photographs of the site demonstrate the recent geomorphic activity (Midgley et al., 2012) including an abandoned stream channel that historically flowed in a more westerly direction than its current southwestern flow path (Figure 3).

Fuchs et al. (2009) described some of the soil and hydraulic characteristics of the Barren Fork Creek floodplain site. The floodplain consists of alluvial gravel deposits underlying 0.5 to 1.0 m of topsoil (Razort gravelly loam). Topsoil infiltration rates are reported to range between 1 and 4 m/d based on USDA soil surveys. The gravel subsoil, classified as coarse gravel, consists of approximately 80% (by mass) of particle diameters greater than 2.0 mm, with an average particle size ($d_{50}$) of 13 mm. Estimates of hydraulic conductivity for the gravel subsoil range between 140 and 230 m/d based on falling-head trench tests (Fuchs et al., 2009). Soil particles less than 2.0 mm in the gravelly subsoil consist of secondary minerals, such as kaolinte and noncrystalline Al and Fe oxyhydroxides. Ammonium oxalate extractions on this finer material estimated initial phosphorus saturation levels of 4.2% to 8.4% (Fuchs et al., 2009).


**Figure 3. Aerial photos for 2003 (left) and 2008 (right) show the southward migration of the stream toward the bluff and the large deposits of gravel in the current and abandoned stream channels. The study site is the hay field in the south-central portion of each photo (red arrow).**

The floodplain site is a hay field with occasional trees (Figure 4). The field has a Soil Test Phosphorus (STP) of 33 mg/kg (59 lb/ac) and has not received fertilizer for several years. The southern border of the floodplain is a bedrock bluff that rises approximately 5 to 10 m above the floodplain elevation and limits channel migration to the south. The floodplain width at the study site is 20 to 100 m from the streambank (based on the 100 year floodplain); however, water was observed 200 m from the streambank (to the bluff) during a 6 year recurrence interval flow event (Figure 4).

**Figure 4. The Barren Fork site is a hay field (left). The site becomes completely inundated during large flow events (right).**

## Pumpkin Hollow Site (Oklahoma)

The Pumpkin Hollow site, 12 miles northeast of Tahlequah, Oklahoma, in Cherokee County (Figure 5, latitude: 36.02°, longitude: -94.81°) has an estimated watershed area of 15 $km^2$. A small tributary of the Illinois River, Pumpkin Hollow is an ephemeral stream in its upper

reaches. The Pumpkin Hollow site is pasture for cattle (Figure 6). The entire floodplain is 120 to 130 m across. Soils in the study area include Razort gravelly loam and Elsah very gravelly loam.

**Figure 5. Pumpkin Hollow is a narrow valley ascending from the Illinois River to the plateau.**

**Figure 6. The Pumpkin Hollow site in spring (left) and winter (right). The site includes soils with shallow layers of topsoil and gravel.**

## Clear Creek Site (Arkansas)

The Clear Creek site is 5 miles northwest of Fayetteville, Arkansas, in Washington County (Figure 7, latitude: 36.125°, longitude: -94.235°). Clear Creek is a fourth order stream, and is a tributary to the Illinois River. Streamflow during baseflow conditions is estimated to be around 0.5 cms. The Clear Creek site is also pasture for cattle (Figure 8). The floodplain is approximately 300 to 400 m across. The soils included intermixed layers of gravel and silt loam (Figure 8).


**Figure 7. Clear Creek and an overflow channel at the Clear Creek floodplain site.**

**Figure 8. The Clear Creek site is pasture (left). Soils are composed of gravel and silt loam alluvial deposits (right).**

## (B) Electrical Resistivity Imaging

Electrical Resistivity Imaging (ERI) is a geophysical method commonly used for near-surface investigations which measures the resistance of earth materials to the flow of DC current between two source electrodes. The method is popular because it is efficient and relatively unaffected by many environmental factors that confound other geophysical methods. According to Archie's Law (Archie, 1942), earth materials offer differing resistance to current depending on grain size, surface electrical properties, pore saturation, and the ionic content of pore fluids. Normalizing the measured resistance by the area of the subsurface through which the current passes and the distance between the source electrodes produces resistivity, reported in ohm-meters (Ω-m), a property of the subsurface material (McNeill, 1980). Mathematical inversion of the measured voltages produces a two-dimensional profile of the subsurface showing areas of differing resistivity (Loke and Dahlin, 2002, Halihan et al., 2005).

ERI data were collected using a SuperSting R8/IP Earth Resistivity Meter (Advanced GeoSciences Inc., Austin, TX) with a 56-electrode array. Fourteen lines were collected at the Barren Fork Creek site, three at the Pumpkin Hollow site, and eight lines at the Clear Creek site. One line at the Barren Fork Creek site and all of the lines at Pumpkin Hollow were "roll-along"

lines that consisted of sequential ERI images with one-quarter overlap of electrodes. The profiles at the Barren Fork Creek site employed electrode spacing of 0.5, 1.0, 1.5, 2.0 and 2.5 m with associated depths of investigation of approximately 7.5, 15.0, 17.0, 22.5 and 25.0 m, respectively. All other sites utilized a 1.0-m spacing. The area of interest in each study site was less than 3 m below the ground surface and thus well within the ERI window. The resistivity sampling and subsequent inversion utilized a proprietary routine devised by Halihan et al. (2005), which produced higher resolution images than conventional techniques.

The OhmMapper (Geometrics, San Jose, CA), a capacitively-coupled dipole-dipole array, was effectively deployed at the relatively open Barren Fork Creek site for large scale mapping. The system used a 40 m array (five 5 m transmitter dipoles and one 5 m receiver dipole with a 10 m separation) that was pulled behind an ATV. Two data readings per second were collected to create long and data-dense vertical profiles. The depth of investigation was limited to 3 to 5 m. Positioning data for the ERI and OhmMapper were collected with a TopCon HyperLite Plus GPS with base station. Points were accurate to within 1 cm.

## Barren Fork Creek

Resistivity at the Barren Fork Creek site appeared to conform generally to surface topography with higher elevations having higher resistivity, although the net relief was minor (~1 m). This was most evident in the OhmMapper resistivity profiles which covered most of the floodplain and which revealed a pattern of high and low resistivity that trended SW to NE (Figure 9). More precise imaging with reduced spatial coverage was obtained with the ERI. A composite ERI line collected from the site is shown in Figure 10. The line, which is approximately parallel to the stream, begins only 5 m from the stream. Gravel outcrops are indicated by gray colors reaching closer to the surface and will be the location for induced leaching experiments at different spatial scales at this site.

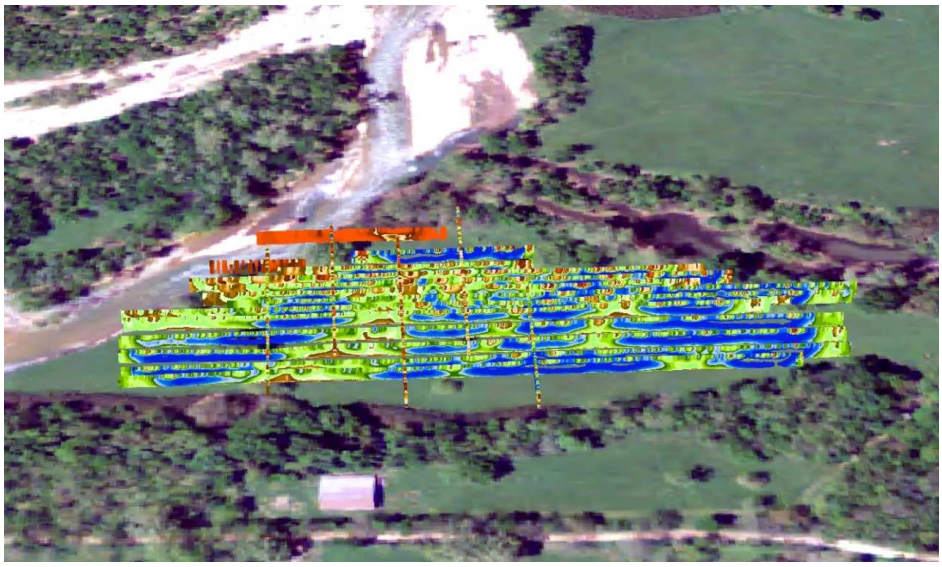

**Figure 9. OhmMapper coverage of the Barren Fork Creek alluvial floodplain showing SW to NE trends of low (blue) and high (orange) resistivity. View is to the North and subsurface resistivity profiles are displayed above the aerial image for visualization purposes. Modified from Heeren et al. (2010).**

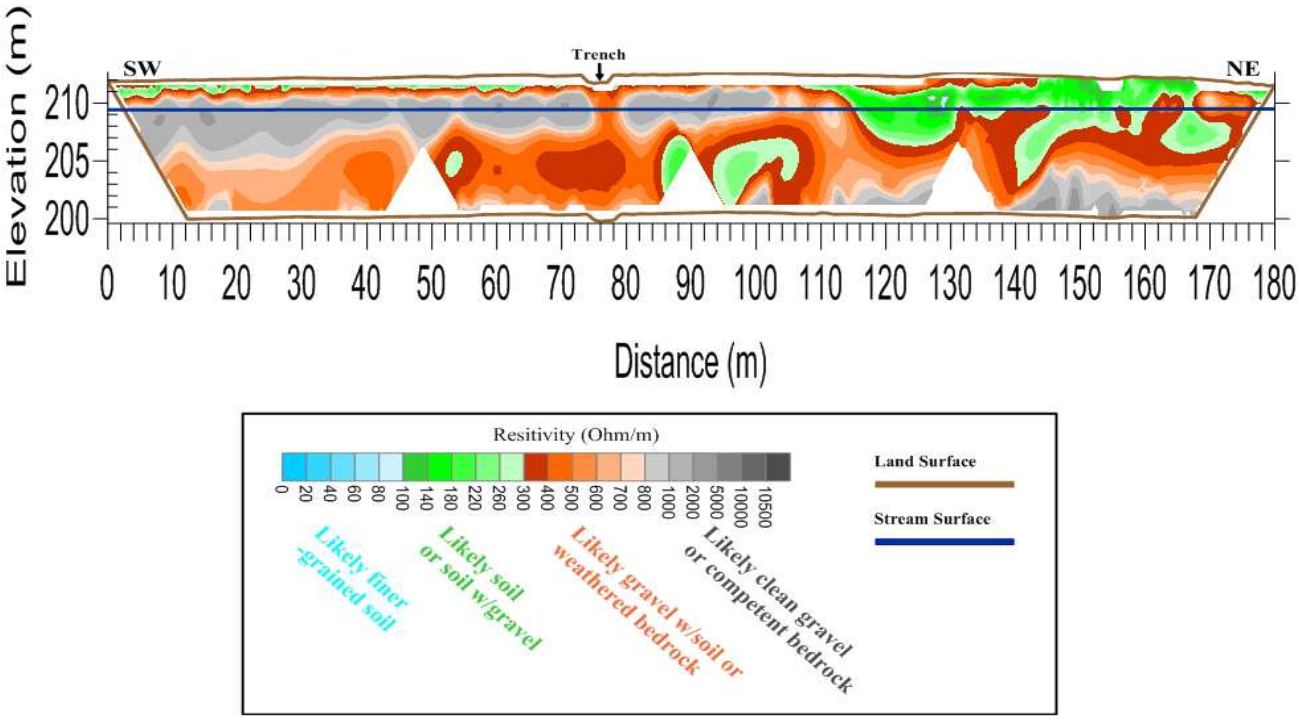


**Figure 10. Composite SuperSting image, showing mapped electrical resistance (Ω-m), running southwest to northeast along a trench installed for studying subsurface phosphorus transport in the gravel subsoils by Fuchs et al. (2009). The x-axis represents the horizontal distance along the ground; the *y*-axis is elevation above mean sea level. Source: Heeren et al. (2010).**

## Pumpkin Hollow

Pumpkin Hollow differed from the other streams because it was a headwater stream with a smaller watershed area. The valley at the study site was approximately 200 m wide and the roll-along lines spanned nearly the entire valley width, crossing Pumpkin Hollow Creek at about the midpoint of the line. The ERI survey at Pumpkin Hollow consisted of three lines oriented W-E with 1 m electrode spacing, 12.5 m depth, and 97 m (lines 1-2 and 3-4) or 139 m (line 5-6-7) length (Figure 11).

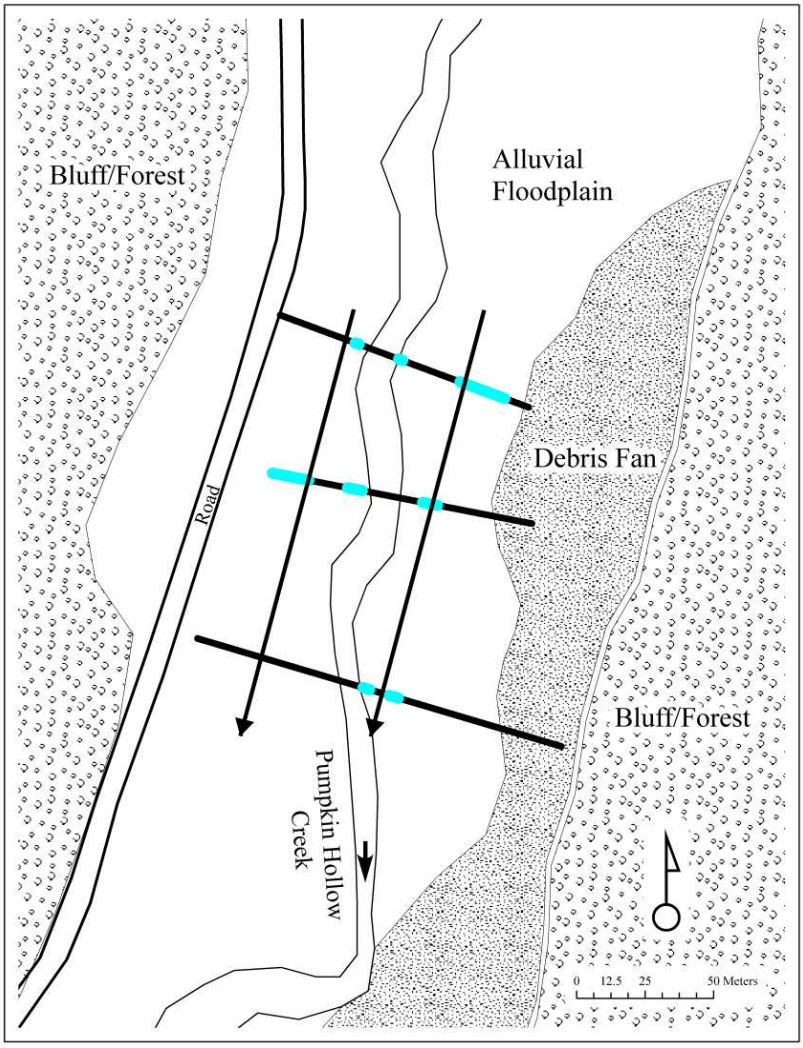


**Figure 11. High resistivity feature locations on ERI lines at the Pumpkin Hollow site are shown in blue. Arrows represent potential connections between them and the direction of flow.**

The Pumpkin Hollow ERI profiles also had a unique configuration consisting of a low resistivity layer between a high resistivity surface layer and high resistivity at depth (Figure 12). Observations at the site included the close proximity of large gravel debris fans originating from nearby upland areas. Jacobson and Gran (1999) noted similar pulses of gravel in Ozark streams in Missouri and Arkansas originating from 19$^{th}$ and early 20$^{th}$ century deforestation of plateau surfaces, implying that a possible interpretation of the low resistivity layer in the ERI profiles was a soil layer buried by gravel from the nearby plateau surfaces. The streambed elevation was approximately 262 m with the general floodplain surface being about 1 m above that elevation. The area of interest included the elevations above 262 m (note that the mean elevation was 262.9 m and that the maximum elevation 265 m occurred at the valley edge) and was therefore thin compared to the other study sites. The resistivity at Pumpkin Hollow ranged from 58 to 3110 Ω-m with a mean of 387 Ω-m. Like the other sites, the Pumpkin Hollow resistivity suggested a pattern of discrete areas of high resistance that indicated gravel outcrops (Figure 12). These were

generally associated with topographic high areas and appeared to have the potential to direct flow down-valley parallel to the stream.

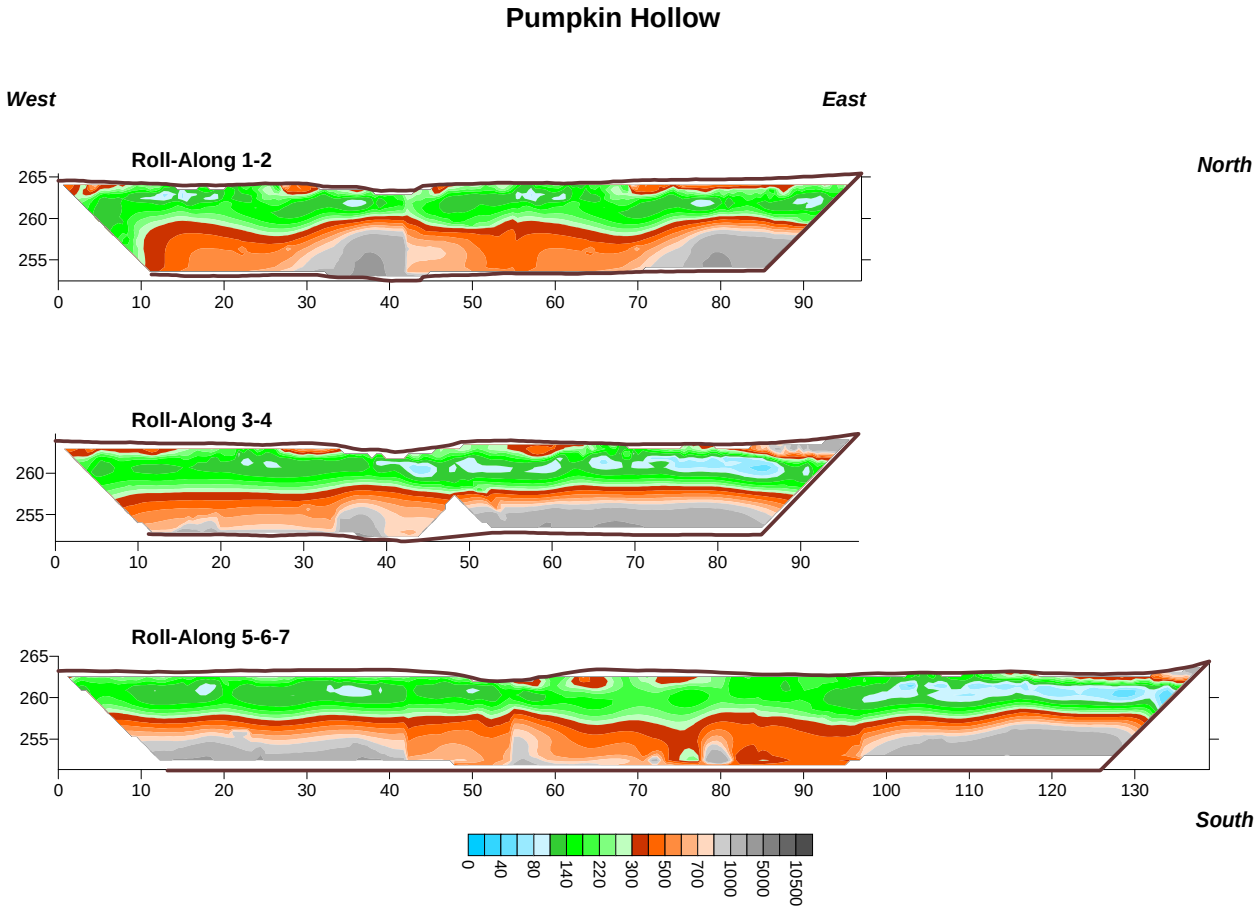


**Figure 12. ERI images of three "roll-along" lines for the Pumpkin Hollow site. The x-axis represents the horizontal distance along the ground; the y-axis is elevation above mean sea level. The color bar is the electrical resistivity in Ohm-meters.**

## Clear Creek

Geophysical mapping was first performed between the overflow channel and Clear Creek shown in Figure 7; however, limited gravel outcrops were observed in this area and therefore the control (non-gravel outcrop) leaching experiments will be performed at this location (Figure 13a). Most of the shallow profile possessed electrical resistivities less than 450 Ω-m. On the east side of Clear Creek, layered profiles demonstrated the potential for lateral flow and transport to the stream, and this feature was clearly visible based on exposed streambanks and supported by the ERI data. Electrical resistivities at the surface were on the order of 600 to 1000 Ω-m with lower resistivity soils below this surface feature (Figure 13b).

**(a)**

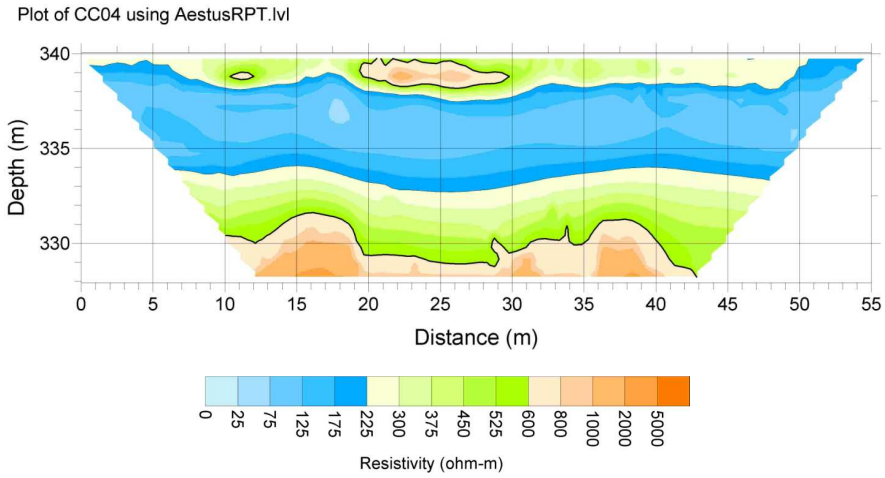


**(b)**

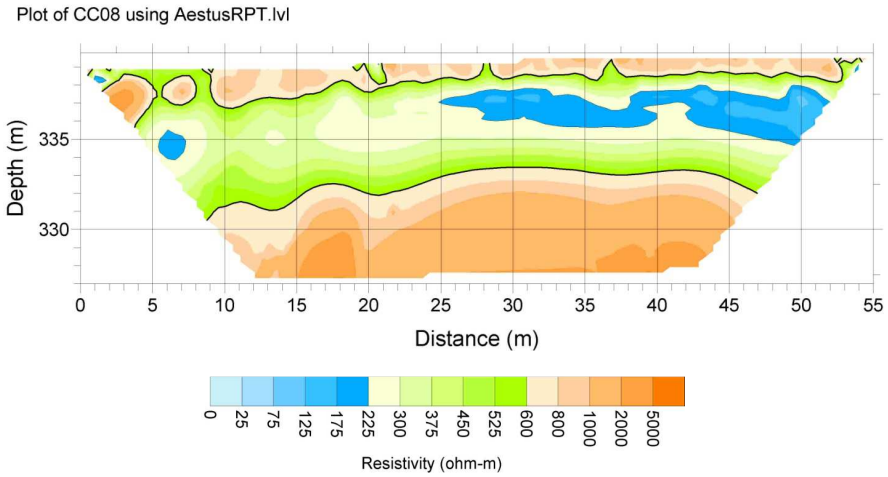


**Figure 13. ERI images of two lines at the Clear Creek site where (a) is a line between the overflow channel and the creek with limited gravel outcrop area and (b) is a line on the east side of Clear Creek with gravel outcrops at the surface. The x-axis represents the horizontal distance along the ground; the *y*-axis is elevation above mean sea level.**

## (C) Point-Scale Studies - Phosphorus Sorption onto Soils in a Flow-Through System (Penn, Heeren, and Fox, 2013, Application of isothermal calorimetry to the study of phosphorus sorption onto soils in a flow-through system, *Soil Science Society of America Journal*, In press)

Phosphorus (P) transport from soils to surface waters is an important contributor to eutrophication (Ryther and Dunstan, 1971). Phosphorus losses from soils occur in both the particulate and dissolved forms. Particulate P consists of sediment that has P sorbed on it, and is typically transported in runoff. Dissolved P is simply P that is already in solution, free from the solid phase. Most best management practices (BMPs) focus on reducing particulate P that is

transported in runoff through erosion control and capturing sediment prior to runoff exiting a field or entering a water body (Fox and Penn, 2013; Rao et al., 2009). Such practices include no-till management, grassed waterways, vegetated buffer strips (VBS), and contour farming. Among floodplains, use of VBS along the riparian areas of the surface water is common (Osborne and Kovacic, 2006; Sabbagh et al., 2009; Muñoz-Carpena et al., 2010; Fox et al., 2010; Fox and Penn, 2013). However, while effective at reducing particulate P, VBS and other traditional BMPs are less effective at reducing dissolved P transport among soils recently amended with P and soils that have become excessive with regard to soil P concentrations (Owens and Shipitalo, 2006; Fox and Penn, 2013). In addition, most BMPs have little impact on reducing P leaching under such scenarios.

In general, P will leach mostly in the dissolved form, except in cases of excessive preferential flow (Simard, et al., 2000; Djodjic et al, 2004). As dissolved P leaches downward from the high P topsoil or applied P amendment, the lower soil horizons can sorb P through several reactions depending on soil properties. Factors that control the quantity of P leaching are mostly related to soil chemical properties which dictate the capacity and kinetics of the soil to sorb P (Maguire and Sims, 2002), and physical properties that impact the rate of water movement through the soil profile (Fuchs et al., 2009) which can also impact the rate of P sorption. The kinetics of P sorption is critical to the P leaching process since the soil will have limited contact time (i.e. retention time) with the moving P-rich solution. Simply put, if the contact time required for adequate P sorption is greater than the contact time of the moving P solution, then limited P sorption will occur resulting in greater transport of P to the subsurface.

Movement of P downward is especially important in the riparian floodplains of northeastern Oklahoma and northwestern Arkansas since these alluvial soils possess a relatively shallow topsoil with underlying gravelly silt loam to gravelly loam. Not only do these gravelly subsoils have an extremely high hydraulic conductivity (Sauer and Logsdon, 2002; Sauer et al., 2005) that range from 0.2 to 844 m/d (Fuchs et al., 2009), but they have also been shown to be directly hydrologically connected to adjacent streams via the gravel subsurface behaving as a stage-dependent storage zone (Fuchs et al., 2009; Hereen et al., 2010; Hereen et al., 2011). Therefore, sorption of a leaching P solution by the thin topsoil is especially critical to preventing transport of dissolved P to surface waters.

Phosphorus transport requires both a P source and physical connectivity (Nelson and Shober, 2012). It is clear that as soils increase in P concentration, particularly as they become more saturated with P, the risk for P leaching increases if the hydraulic conditions are appropriate. Such information is easily obtained through soil testing. However, there are factors that influence the "gap" between P source and the physical transport of P, including P sorption mechanisms and kinetics of sorption. In regard to mechanisms, not only is the degree of P sorption important to potential P leaching, but the mechanism in which P is sorbed will dictate how strongly the P is held and under what conditions. For example, P bound with Ca typically becomes more soluble as the pH decreases. Kinetics can also influence P transport in the context of a moving solution (i.e., leaching) because of the time required for a sorption reaction to occur. Fuchs et al. (2009) found that a decreased contact time (increased flow rate) of a P solution through the fine fraction of a riparian subsoil resulted in a decrease in P sorption and therefore increase in P leaching.

This study proposes a new and simple tool to aid in studying P leaching; isothermal titration calorimetry (ITC) measures the heat of reaction while solutions or soil suspensions are titrated with chemicals (such as P). The quantity and patterns of heat measured can provide information on the degree of reaction, type of reaction, and kinetics (Rhue et al., 2002; Kabengi et al., 2006a; Harvey and Rhue, 2008). For example, Penn and Warren (2009) were able to distinguish between P sorbed by ligand exchange vs. surface precipitation in titration of kaolinite with a P solution. Calorimetry also provided useful information on kinetics in regard to ammonium exchange with potassium in zeolite materials (Penn et al., 2010). The objectives of this study were to measure the impact of contact (retention) time on P sorption in a flow-through system intended to simulate downward movement of a P solution through two different riparian soils, and determine whether ITC can provide useful information reflective of flow-through results.

## Methods and Materials

### *Investigated Soils*

Two floodplain soils from within the Illinois River watershed were sampled for use in this study. The Barren Fork Creek site (latitude: 35.90°, longitude: -94.85°) is a fourth order stream with a historical median discharge of 3.6 $m^3/s$. The study area at the Barren Fork Creek was located on the outside of a meander bend which was being actively eroded by the stream. The soils were classified as Razort gravelly loam underlain with alluvial gravel deposits. Thickness of the loam ranged from 0.3 to 2.0 m, with dry bulk densities ranging from 1.3 to 1.7 $g/cm^3$. The Clear Creek alluvial floodplain site flows into the Illinois River (latitude: 36.13°, longitude: -94.24°). Soils were loamy and silty, deep, moderately well drained to well drained. Thickness of the top loam layer ranged from 0.3 to 2.0 m, with dry bulk densities ranging from 1.5 to 1.7 $g/cm^3$. The land use in the study area was pasture and consisted of Razort gravelly loam soils. Both soils were sampled at a depth of 0 to 10 cm. Soils were air-dried and sieved to 2 mm for extraction and use in ITC experiments.

### *Soil Characterization*

All analyses were conducted in duplicate. Soil characterization consisted of (i) pH and electrical conductivity (EC; 1:1 soil:solution ratio); (ii) organic matter by combustion; (iii) sand, silt, and clay by the hydrometer method (Day, 1965); (iv) water soluble (WS) P, Al, Fe, and Ca (1:10 soil:deionized water, 1 h reaction time, filtration with 0.45 µm Millipore membrane); (v) specific surface area by gas adsorption (N2: 16 h outgassing at 160ºC) with a BET isotherm as determined by an Autosorb-1C (Quantachrome, Boynton Beach, FL); (vi) oxalate extractable P, Al, and Fe (Pox, Alox, Feox; 1:40 soil: 0.2M acid ammonium oxalate (pH 3), 2 h reaction time in the dark; McKeague and Day, 1966); and (vi) Mehlich-3 (Mehlich, 1984) P, Al, and Fe (M3-P, M3-Al, and M3-Fe: 1:10 soil:0.2 M $CH_3COOH$ + 0.25 M $NH_4NO_3$ + 0.015 M $NH_4F$ + 0.13 M $HNO_3$ + 0.001 M EDTA, 5 min reaction time, filtration with Whatman #42 paper). Extracted P, Ca, Al, and Fe were analyzed by ICP-AES. The ratio of Mehlich 3 and ammonium oxalate extractable P to (Al + Fe) (all values in mmol/kg) was expressed as:

$$[P / (Al + Fe)] * 100 \quad (1)$$

and will be referred to as M3 degree of P saturation (DPSM3) and ammonium oxalate degree of P saturation (DPSox). Note that this is exactly the same as the traditional soil degree of phosphorus saturation (DPS) calculations (Pautler and Sims, 2000) except without the empirical

constant α which is used to relate soil P sorption capacity to Alox and Feox and the denominator acts to express the effective total soil P sorption maximum. The α value was unknown, so no α value was used. Beauchemin and Simard (1999) noted that various studies have applied an α value of 0.5 to all soils, regardless of soil properties. The authors claimed that the α value is empirical and needs to be determined for each soil type and experimental conditions. In addition, Beck et al. (2004) recommended that the α value be omitted from the DPS calculation.

### *Flow-Through Sorption Experiments*

In order to test the effect of retention time (RT) and P concentration on P sorption in a flow-through setting, flow-through cells (high density polyethylene) were constructed as described in Stoner et al. (2012). A diagram of the setup is found in Fuchs et al. (2009) and Penn and McGrath (2011). Depending on the P concentration and RT utilized, some soils were mixed with acid washed, lab-grade sand (pure Si sand, 14808-60-7; Acros organics, Morris Plains, New Jersey) in order to achieve a total pore volume of 1.26 $cm^3$ (5 g of sand + soil; 50% porosity). Soils were then placed in a flow-through cell. The proportion of soil to sand varied depending on how P sorptive the material was. Less soil mass was used for more sorptive soils tested under low P inflow concentrations. The mass of soil material used in a flow through cell varied from 1 to 5 g. A suitable amount that would not result in 100 or 0% P removal for the duration of the entire experiment was typically determined by trial and error. The purpose of this was to allow a more complete picture of P breakthrough (i.e. P sorption curve). A 0.45 µm filter was placed beneath the materials and the bottom of the cell was connected to a single channel peristaltic pump (VWR variable rate "low flow" and "ultra low flow", 61161-354 and 54856-070) using plastic tubing. The desired RT (RT [min] = pore volume [mL] / flow rate [mL/min]) was achieved by varying the pump flow rate which pulled solution through the cell. Flow rates required to achieve the desired RTs of 3 and 10 min were 0.75 and 0.22 mL/min, respectively. Essentially, the RT is the amount of time required for the solution to pass through the cell. A constant head Mariotte bottle apparatus was used to maintain a constant volume of P solution on the soils. Materials were subjected to flow for 5 h in which the "outflow" from the cells was sampled at 0, 30, 60, 90, 120, 150, 180, 210, 240, 270, and 300 min. Solutions were analyzed for P by the Murphy-Riley molybdate blue method (Murphy and Riley, 1962). Discrete P sorption onto materials was calculated at each sampling time as a percentage decrease in outflow relative to inflow P concentration (i.e., source bottle). Results are presented as cumulative P sorption as a function of cumulative P addition (both in units of mg P/kg soil). Initial flow-through experiments were performed with KCl which immediately flowed through the thin layer of soil with no retardation based on measured specific conductance.

Two different P concentrations were tested: 1 and 10 mg/L using solutions made from potassium phosphate. These P concentrations correspond with the range measured in studies of runoff from high P soils (> 300 mg/kg Mehlich 3-P) or soils to which manure or chemical fertilizer P have been recently applied to the surface (Edwards and Daniel, 1993; Vadas et al., 2007). The matrix of the solution consisted of 5.6, 132, 110, 10, and 17 mg/L of Mg, Ca, S, Na, and K, respectively, using chloride and sulfate salts, followed by adjustment to pH 7. Note that ionic strength only slightly varied due to differences in P concentrations only. This matrix was chosen as it was found to be representative of agricultural runoff measured in a previous study. All flow-through RT and P concentration combinations were duplicated for each material.

### *Isothermal Titration Calorimetry Experiments*

All ITC experiments were conducted on a CSC 4200 Isothermal Titration Calorimeter (CSC Inc., Lindon, UT) at 25ºC. The ITC had a sensitivity of 0.418 µJ detectable heat effect and a "noise level" of +/- 0.0418 µJ/s (deconvoluted signal). For all soil ITC experiments, 100 mg of soil sample were placed in a 1.3 mL reaction vessel and suspended in 0.75 mL of de-ionized (DI) water. Soil titrations were replicated three times. For each experiment, a blank was determined by titration of a 0.01 M NaH2PO4 solution into de-ionized (DI) water under the same conditions employed for the actual experiment. Data produced from the blank titrations were subtracted from the sample titrations.

Two different types of titrations were conducted; 25 consecutive 10 µL titrations (300 s intervals) of P solution into the suspended soil sample, and a "single shot" titration consisting of all 250 µL of P solution. For both experiments, a 0.01 M NaH2PO4 solution was used as the titrant and soil suspensions were stirred in the reaction vessel throughout the duration of the experiment. With regard to the single shot test, after titration, change in heat was monitored for 5 h.

### *Statistical Analysis*

All values were averaged over replication. The log of the relationship between cumulative P added to soil and cumulative P sorption was tested among each set of conditions (i.e. inflow P concentration and RT) to determine whether the relationships (slope and intercept) were significantly different from each other at $P = 0.05$. The null hypothesis was that one equation could be used to describe cumulative P sorption versus cumulative P addition for both soils. This was tested by using a series of "contrast" statements in SAS (SAS, 2003) to determine whether the slope and intercept were significantly different based on soil sample.

## Results and Discussion

### *Soil properties*

General soil properties important to P retention are shown in Table 1. Soil from the Barren Fork Creek site was more acidic, and as a result, contained more water soluble Al and Fe than the Clear Creek soil. The Barren Fork Creek soil also contained more water soluble Ca. This is expected since Al, Fe, and Ca containing minerals tend to be more soluble in water as pH decreases below 7. However, ammonium oxalate extractable Al and Fe (Alox and Feox) were greater in the Clear Creek soil. Soil Al and Fe that is extractable with ammonium oxalate is considered to represent amorphous Al and Fe minerals, which typically sorb and retain the majority of soil P among near neutral and acid soils (McKeague and Day, 1966; Sakadevan and Bavor, 1998; Schoumans, 2000). The greater value for DPSox for the Barren Fork Creek soils suggests that the main P sorption sites (Alox and Feox) are more saturated with P than Clear Creek soils (Penn et al., 2006). Generally, as DPSox increases for soils, their capacity to further sorb additional P decreases, and the potential to release P to solution increases (Pautler and Sims, 2000). Evidence for this is clearly seen by the fact that the Barren Fork Creek soils possessed greater water soluble P concentrations (Table 1). However, the water soluble P concentrations are below the threshold for increased P leaching (8.6 mg/kg) as proposed by Maguire and Sims (2002).

**Table 1. Characterization of the soils collected from two different riparian sites that were used in the flow-through sorption and calorimetry studies. All values in mg/kg unless shown otherwise.**

| | Clear Creek | Barren Fork |
|---|---|---|
| pH | 6.3 | 5.8 |
| EC (uS/cm) | 68 | 132 |
| Organic matter (%) | 1.73 | 1.58 |
| Surface area ($m^2$/g) | 10.14 | 9.04 |
| Sand (%) | 16.3 | 41.3 |
| Silt (%) | 61.3 | 37.5 |
| Clay (%) | 22.5 | 21.3 |
| †WS Ca | 55 | 115 |
| WS Fe | 127 | 209 |
| WS Al | 238 | 370 |
| WS P | 2.6 | 7.1 |
| ‡$Al_{ox}$ | 904 | 707 |
| $Fe_{ox}$ | 2033 | 1955 |
| $P_{ox}$ | 92 | 170 |
| §$DPS_{ox}$ (%) | 4.25 | 8.96 |
| ¶M3-Ca | 1804 | 1698 |
| M3-Fe | 161 | 163 |
| M3-Al | 824 | 688 |
| M3-P | 2.5 | 49 |
| #$DPS_{M3}$ (%) | 0.46 | 3.1 |

† Water soluble
‡ Ammonium oxalate extractable
§ Degree of phosphorus saturation. $P_{ox}/(Al_{ox}+Fe_{ox})$; calculated on a molar basis
¶ Mehlich-3 extractable
# Degree of phosphorus saturation. M3-P/(M3-Al+M3-Fe); calculated on a molar basis

Although the soils contained appreciable amounts of Ca as indicated by the Mehlich-3 (M3) extraction, it was not very soluble based on the water extraction (Table 1). Only about 3 and 7% of M3 extractable Ca was soluble in water for the Clear Creek and Barren Fork samples, respectively. Mehlich-3 extractable Fe and Al was reflective of ammonium oxalate Al and Fe, except that ammonium oxalate extracted more than M3 solution. Sims et al. (2002) suggested values of 10 to 15% DPSM3 as a threshold to identify soils with increased risk as P sources for non-point P transport. In addition, Maguire and Sims (2002) found that there was a "break-point" value of 20% for the relationship between DPSM3 and dissolved P in leachate. Above this 20% level, the concentration of dissolved P in leached increased rapidly with increases in DPSM3. Soil organic matter (OM) was similar between soils (Table 1). Although OM is not related to P sorption in non-sandy soils with appreciable Al and Fe (Mozaffari and Sims, 1996; Zhang et al., 2005), OM can indirectly impact P sorption through interaction with Fe and Al oxides and hydroxides. This interaction between OM and Al+Fe has been shown to increase the amorphous nature of Al and Fe oxides and hydroxides, thereby increasing surface area, and potential P sorption (Saunders, 1964; Niskanen, 1990; Mozaffari and Sims, 1996). However, such interactions and the resulting amorphous nature of Fe and Al are accounted for through extraction with ammonium oxalate. This is why most studies conducted on P sorption indicate a strong correlation between P sorption and Alox, Feox, and DPSox (Khiari et al., 2000; Sims et al., 2002; Maguire and Sims, 2002; Zhang et al., 2005).

### *Phosphorus Sorption under Flow-Through Conditions*

Under flow-through conditions of constant addition of 1 mg P/L inflow solution, the longer retention time (RT), or slower flow rate, appeared to reduce P sorption for the Barren Fork soil (Figure 14a). However, this decrease in P removal with increase of RT from 3 to 10 min was not statistically significant with regard to the slope and intercept for the relationship shown in Figure 14. Table 2 provides the slope and intercept values for the relationship between log cumulative P added and cumulative P sorbed, including statistical differences. Note that the relationship between cumulative P added and cumulative P sorbed was nearly exactly the same for the 3 and 10 min RT for the Clear Creek soil (Figure 14b and Table 2). Similar results were obtained when an inflow P concentration of 10 mg P/L was used (Figure 15a and 15b), except that the slope and intercept were statistically different between the 3 and 10 min RT for the Barren Fork soil (Table 2). After application of the P sorption data set to equations developed by Stoner et al. (2012) for estimating maximum P sorption under flow-through conditions, it was apparent that the Clear Creek soil was able to sorb more P under certain flow-through conditions compared to the Barren Fork soil.

Under inflow conditions of 10 mg P/L, maximum P sorption by the Clear Creek soil was 214 and 284 mg/kg (not significantly different) at a RT of 3 and 10 min, respectively, while Barren Fork could only remove a maximum of 165 and 127 mg/kg (significantly different) at a RT of 3 and 10 min, respectively. However, under inflow conditions of 1 mg P/L, the soils would remove similar maximum amounts of P; 103 and 101 mg/kg at a RT of 3 and 10 min, respectively for Clear Creek compared to 100 and 88 mg/kg at a RT of 3 and 10, respectively for Barren Fork. Note that there was no significant difference in P removal at a 1 mg P/L inflow concentration between a 3 min and 10 min RT. The higher amount of P sorption for the Clear Creek soil is not a surprise since it possessed a lower DPSox and DPSM3, meaning that it contained a greater number of "unused" P sorption sites than the Barren Fork soil. Hooda (2000) noted that the amount of P leached was dominantly a function of the soil P saturation.

The increase in P sorption for the Barren Fork soil at the lower RT compared to the higher RT (i.e., lower flow rate) may seem counter intuitive at first. However, it does suggest that P sorption kinetics were relatively fast for this soil. While increased RT can increase P sorption in some cases, this is less likely for a scenario with fast kinetics since little time would be required for sorption to take place. The overall P removal process consists of both physical and chemical processes. As P is sorbed by the soil through precipitation, anion exchange, or ligand exchange reactions, the reactants (solution P and available sorption surfaces or ions) are "used up" (decrease) and the products (sorbed P and any resulting ions) increase. The combination of the reduction of reactants and increase in products decreases the chemical potential for further sorption reactions to occur. Simply put, a faster flow rate (lower RT) removes solution reaction products and replenishes the depleted solution reactants (i.e., inflow P) more efficiently than a slow flow rate (higher RT), thereby resulting in a greater chemical potential for further P sorption at any given point (Penn and McGrath, 2011). A similar observation was made by Stoner et al. (2012) in examination of P removal by industrial by-products under flow-through conditions.

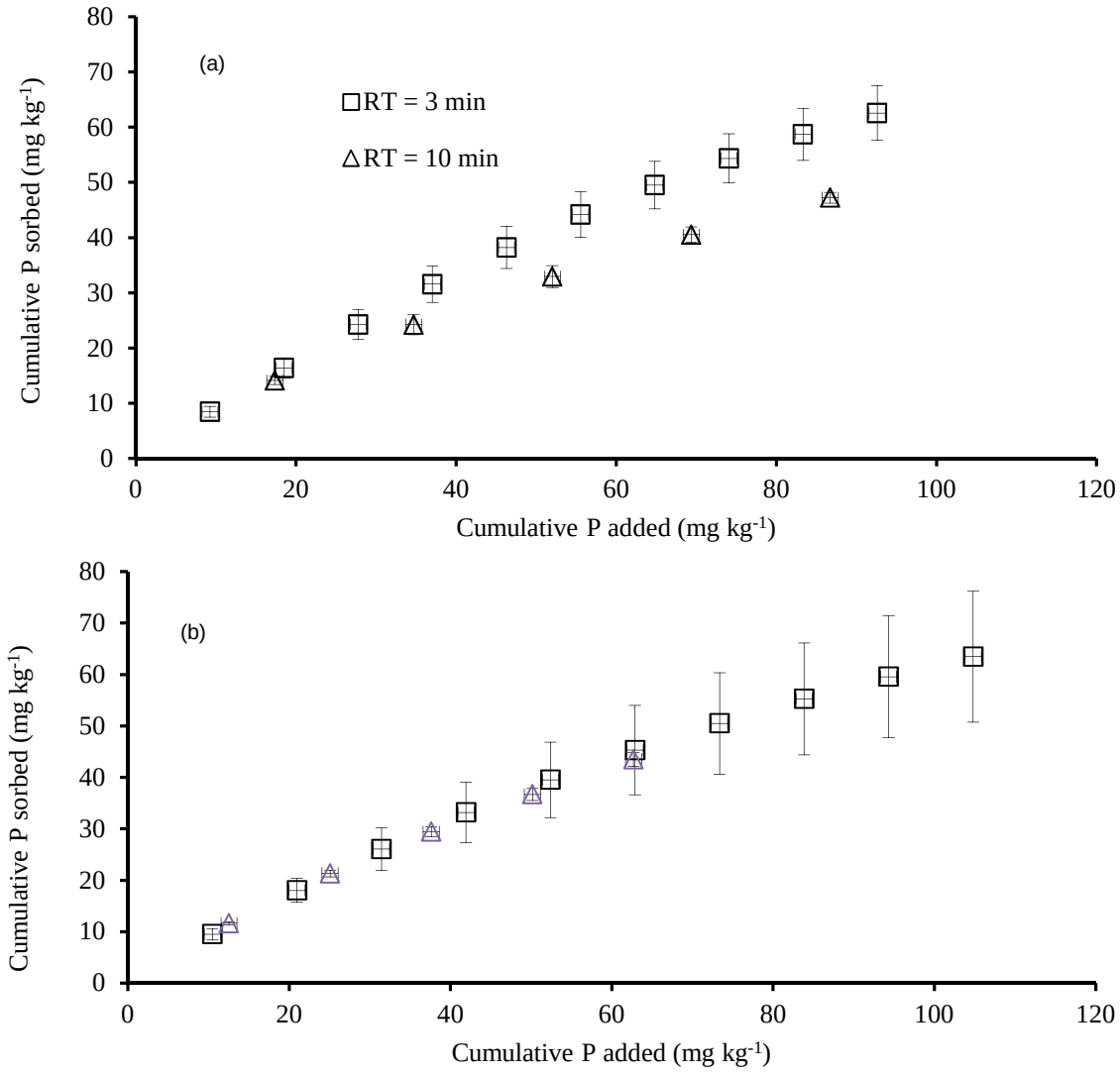


**Figure 14. Cumulative phosphorus (P) sorption onto soils in a flow-through setting with an inflow P concentration of 1 mg/L using two different retention times (RT). Soils tested were sampled from the Barren Fork (a) and Clear Creek (b) sites.**

**Table 2. Slope and intercept values for the relationship between log of cumulative phosphorus (P) added (mg/kg) and cumulative P sorbed (mg/kg) during the flow-through sorption experiments conducted at two different retention times (RT: 3 and 10 min) and and inflow P concentrations (1 and 10 mg/L).**

| | RT = 3 min | | RT = 10 min | |
|---|---|---|---|---|
| | | 1 mg P/L inflow | | |
| Soil | Slope | Intercept | Slope | Intercept |
| Barren Fork | 56.4 | -52.7 | 46.9 | -45.7 |
| Clear Creek | 55.9 | -53.6 | 44.9 | -39.4 |
| | | 10 mg P/L inflow | | |
| Barren Fork | 130.7* | -177.9* | 63.6 | -73.5 |
| Clear Creek | 149.5 | -214.5 | 144.1 | -202.2 |

* Indicates significant difference at P = 0.05 between RT 3 and 10 within soil type and inflow P concentration.

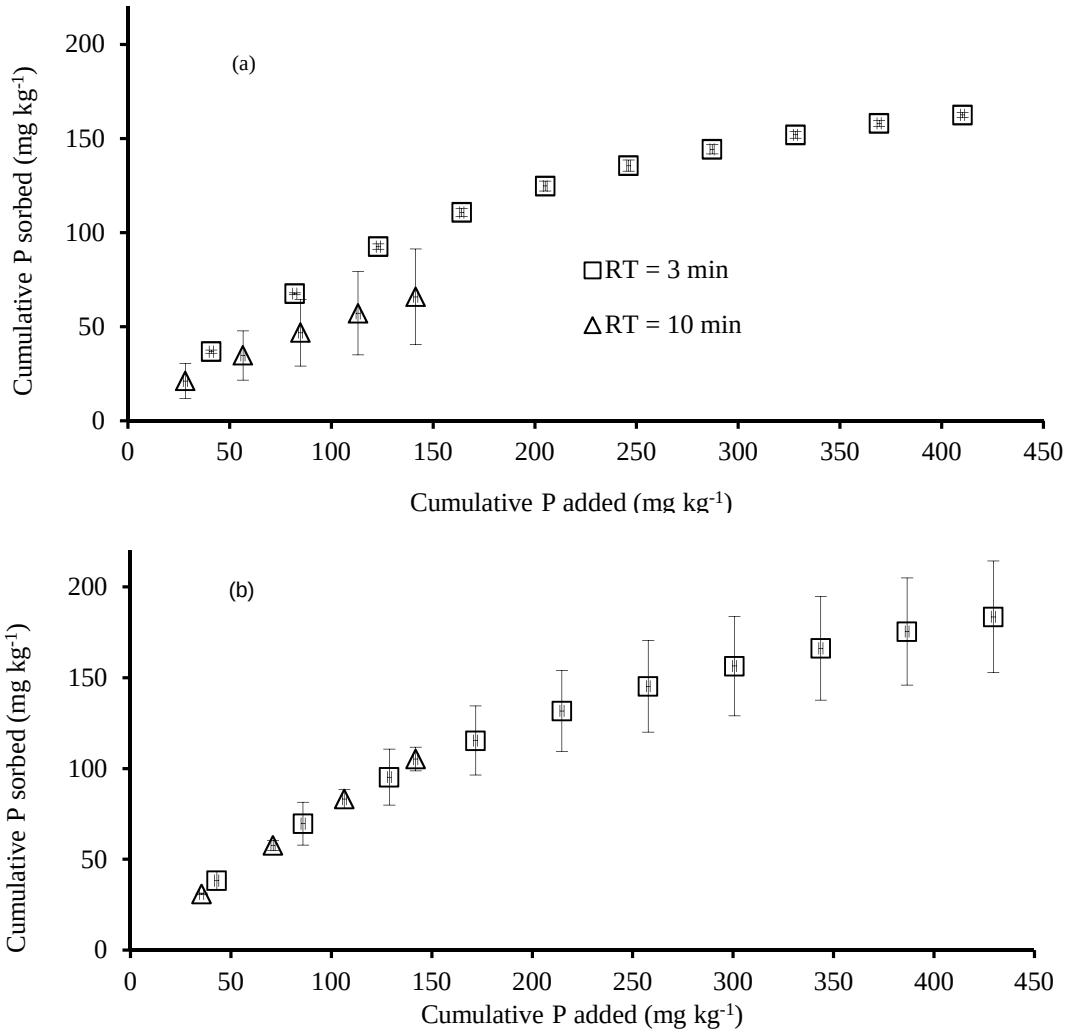


**Figure 15. Cumulative phosphorus (P) sorption onto soils in a flow-through setting with an inflow P concentration of 10 mg/L using two different retention times (RT). Soils tested were sampled from the Barren Fork (a) and Clear Creek (b) sites.**

One hypothesis to explain this phenomenon would be that at an increased flow rate, the flow in the pore space would be more turbulent, which would reduce the thickness of the low velocity boundary layer of fluid near the mineral surface. More turbulent mixing would increase the transport within the pore, i.e. from the bulk flow, through a smaller boundary layer via diffusion, and to the surface where sorption can occur. However, Reynolds numbers calculated from specific discharge during the flow through experiments and a characteristic grain size ($d_{50}$) (following Bear, 1972 and Chin et al., 2009) ranged from $2 \times 10^{-5}$ to $2 \times 10^{-4}$. These are well below the critical Reynolds number (typically ranging from 1 to 10 for flow in porous media) where flow changes from Darcian/linear flow to transitional flow, and a Reynolds number of 100 where flow has become fully turbulent. Peclet numbers (Pe) were 60 and 170 for the Barren Fork and Clear Creek sites, respectively, with Pe > 10 indicating that dispersion was negligible compared to advective transport. Although flow conditions in the flow cells were laminar

according to this analysis, it should be remembered that this is not flow through a straight conduit but through a pore space with tortuosity, dead-end pores, and a wide range of pore sizes. These flow cell data for the Barren Fork soil indicate that, even under laminar flow, higher flow rates result in faster transport of reactants from the bulk flow to the mineral surface, and/or faster transport of reaction products away from the mineral surface into the bulk flow. Either way, a higher flow rate prevented the sorption reaction from coming to a relatively "pre-mature chemical equilibrium," i.e. chemical equilibrium has been reached, but only because of limitations of the physical process. Increasing the flow rate reduces the physical limitation which allows the rate of P sorption to increase. Analogous to this is the observation that volatilization of a gas (a chemical process) can be prevented by imposing increased pressure (a physical process) on a system.

In other words, for the Barren Fork site it appears that P removal was limited by physical nonequilibrium at the pore scale. It should be noted that this process (transport from bulk flow to the mineral surface as a function of flow rate) is different than mechanical dispersion, which by definition occurs at a large enough scale to integrate the effects of many pores (Fetter, 1999).

### *Calorimetry as an Indicator of Phosphorus Sorption*

Phosphorus can sorb to soils by several mechanisms: anion exchange, ligand exchange (adsorption), and precipitation. Soils with elevated pH (> 8) and high soluble Ca concentrations are able to precipitate P as Ca phosphate minerals. However, this precipitation reaction occurs much more slowly at low pH levels compared to high pH. For soils at or below a pH of 7, P sorption dominantly occurs via ligand exchange mechanisms on the surface of amorphous Al and Fe oxide and hydroxide minerals (Violante, 2013). If there is Al and Fe in the soil solution, added P can also precipitate as Al and Fe phosphates. Under certain conditions, continued P loading to the surface of a Fe or Al oxy/hydroxide mineral can result in P removal by precipitation of Al or Fe phosphate at the surface of the Al or Fe source mineral (Ler and Stanforth, 2003; Kim and Kirkpatrick, 2004). Isothermal titration calorimetry data can be used to somewhat distinguish between these mechanisms. For example, exothermic (producing heat) reactions regarding P sorption in neutral and acid soils indicate ligand exchange mechanisms onto Al and Fe minerals and kaolinite (Rhue et al., 2002; Harvey and Rhue, 2008; Penn and Zhang, 2010; Appel et al., 2013). On the other hand, endothermic (absorbing heat) reactions indicate precipitation of Al and Fe phosphates (Penn and Warren, 2009; Rhue et al., 2002).

Figures 16 and 17 show that the heat of reaction decreases with each successive titration of P solution; this is expected since the P sorption sites are becoming saturated with each P addition. Examination of the 25 titrations of a P solution to the soils, and considering the near-neutral to acid pH of the soils, it appears that P sorption onto the Barren Fork (Figure 16a) and Clear Creek (Figure 17a) soils occurred by both ligand exchange and Al/Fe phosphate precipitation. Note that there are 25 sets of peaks; one set for each P titration.

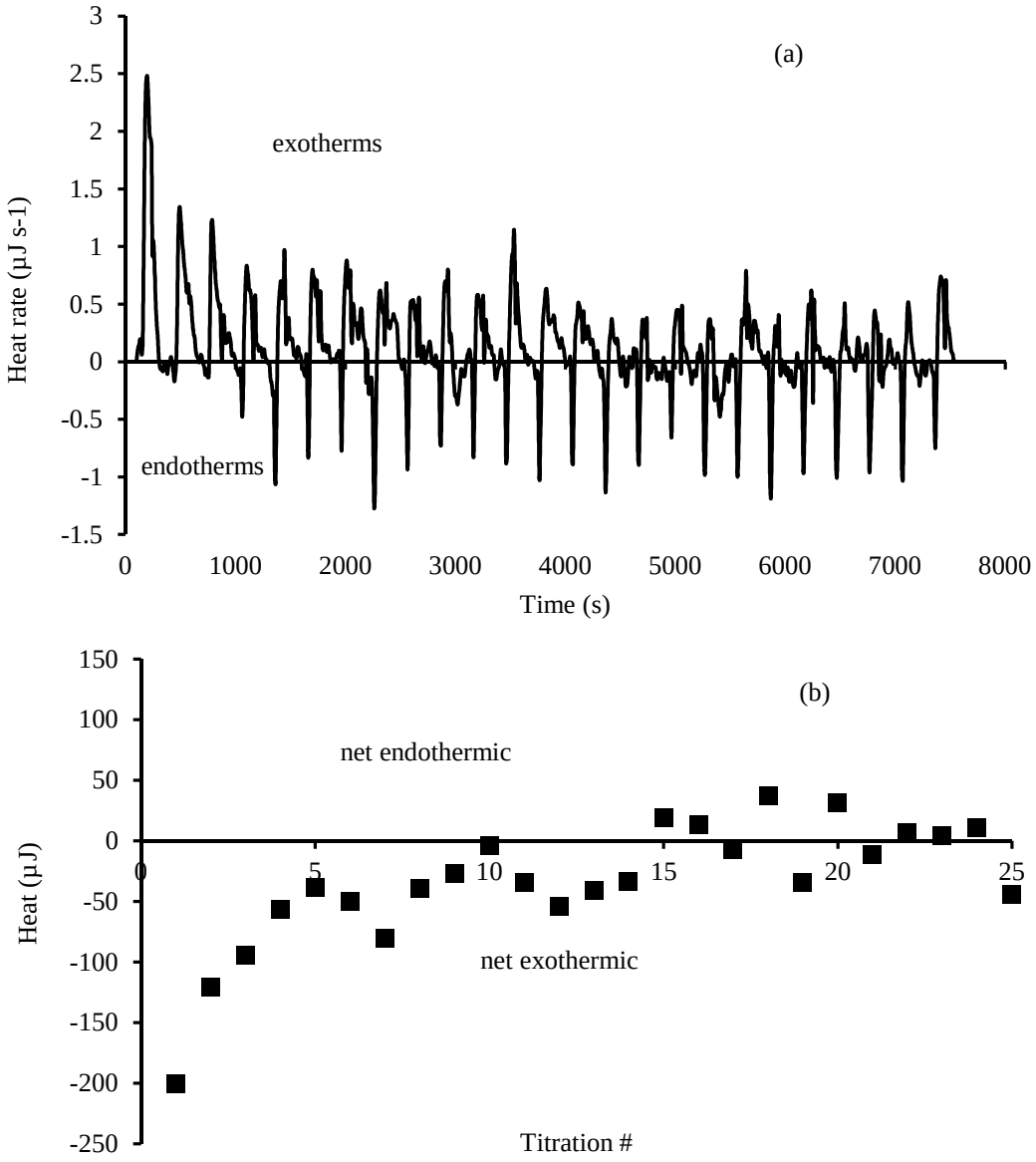


**Figure 16. Thermogram (a) for the titration of the Barren Fork soil with 0.01 mol/L NaH2PO4 using an isothermal titration calorimeter; and (b) the heat curve produced by integration of the thermogram.**

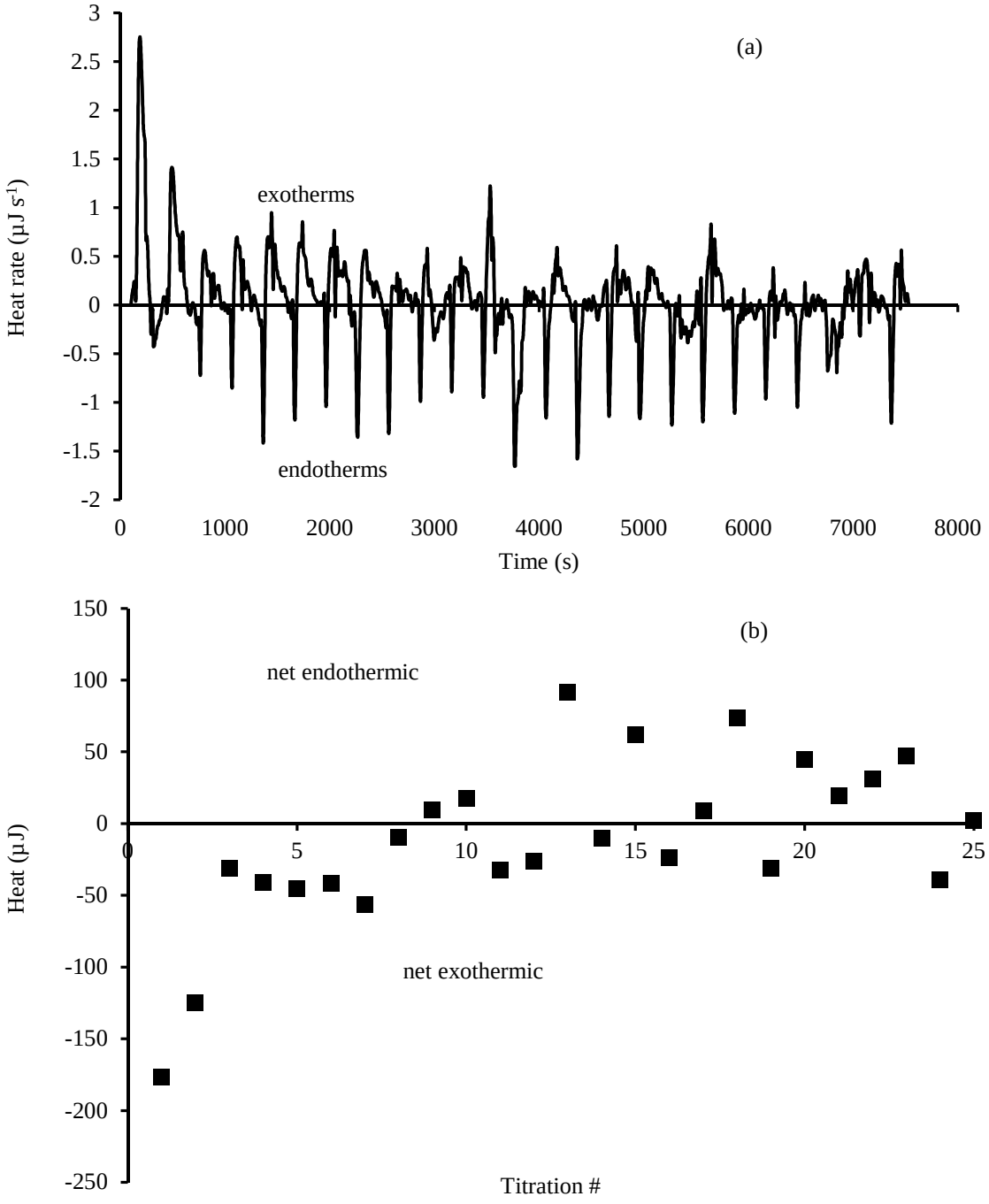


**Figure 17. Thermogram (a) for the titration of the Clear Creek soil with 0.01 mol/L NaH2PO4 using an isothermal titration calorimeter; and (b) the heat curve produced by integration of the thermogram.**

In fact, Figures 16a and 17a show that for each P addition, both an exothermic and endothermic reaction occurred. It is common for soils with pH 7 or less to display an initial exotherm immediately after titration of P, followed by a smaller endothermic peak (Penn and Zhang, 2010). However, notice that integration of each of the 25 titration peaks reveals that the net heat

release for each additional titration becomes less exothermic and more endothermic (Figures 16b and 17b). This indicates two processes. First, ligand exchange sites (i.e. terminal hydroxyls on the edges of Al/Fe oxhy/hydroxides) are becoming filled up or "saturated" with P, which decreases the chemical potential for further ligand exchange reactions; this decreases the exotherms. Second, the source Al and Fe minerals are able to slightly dissolve and produce Al and Fe for precipitation with P on the surface of the minerals; this increases the endotherms. Further evidence for precipitation of P was established by conducting a geochemical speciation of the solution using the MINTEQ2 program (Allison et al., 1991). A "sweep" was conducted to simulate the addition of P into the soil solution as performed in the calorimetry experiment; the model predicted precipitation of variscite (Al phosphate mineral). Due to the relatively high concentrations of water soluble Al and Fe measured in these soils (Table 1), it was not unexpected that added P would partially precipitate with such metals in solution. The use of calorimetry to detect simultaneous ligand exchange and precipitation reactions and general changes in mechanisms is also found in previous studies (Imai et al., 1981; Machesky et al., 1989; Partyka et al., 1989; Kabengi et al., 2006a; Penn and Warren, 2009).

A multiple linear regression equation was developed by Penn and Zhang (2010) to relate soil Alox and the heat of the first titration to P sorption in a batch isotherm which added 500 mg P/kg soil. Application of the heat of the first titration (Figures 16 and 17) and Alox (Table 1) into this equation yielded a prediction of P sorption of 167 and 177 mg P/kg for the Barren Fork and Clear Creek soils, respectively. Note that these predicted P sorption values are similar to cumulative P sorption values under flow-through conditions at P loading values approaching 500 mg/kg (Figure 15).

Examination of the single P titration to the soils provided valuable information regarding the degree of, and kinetics of P sorption. Figure 18 indicates that the degree of P sorption for the Clear Creek soil was greater than the Barren Fork soil as evidenced by the area under the peak. Several studies have related total heat release to the degree of P sorption (Imai et al., 1981; Miltenburg and Golterman, 1998; Harvey and Rhue, 2008). The greater heat release from P titration of Clear Creek compared to Barren Fork soil is supported by the larger amount of P sorption measured in the flow-through experiments (Figures 14 and 15). Note that overall P sorption was net exothermic even though both exothermic and endothermic reactions were occurring, suggesting that ligand exchange was the most dominant P removal mechanism as supported by Figures 16 and 17. Observation of the single titration peaks also showed that P removal reactions by the Barren Fork soil were faster than Clear Creek (Figure 18).

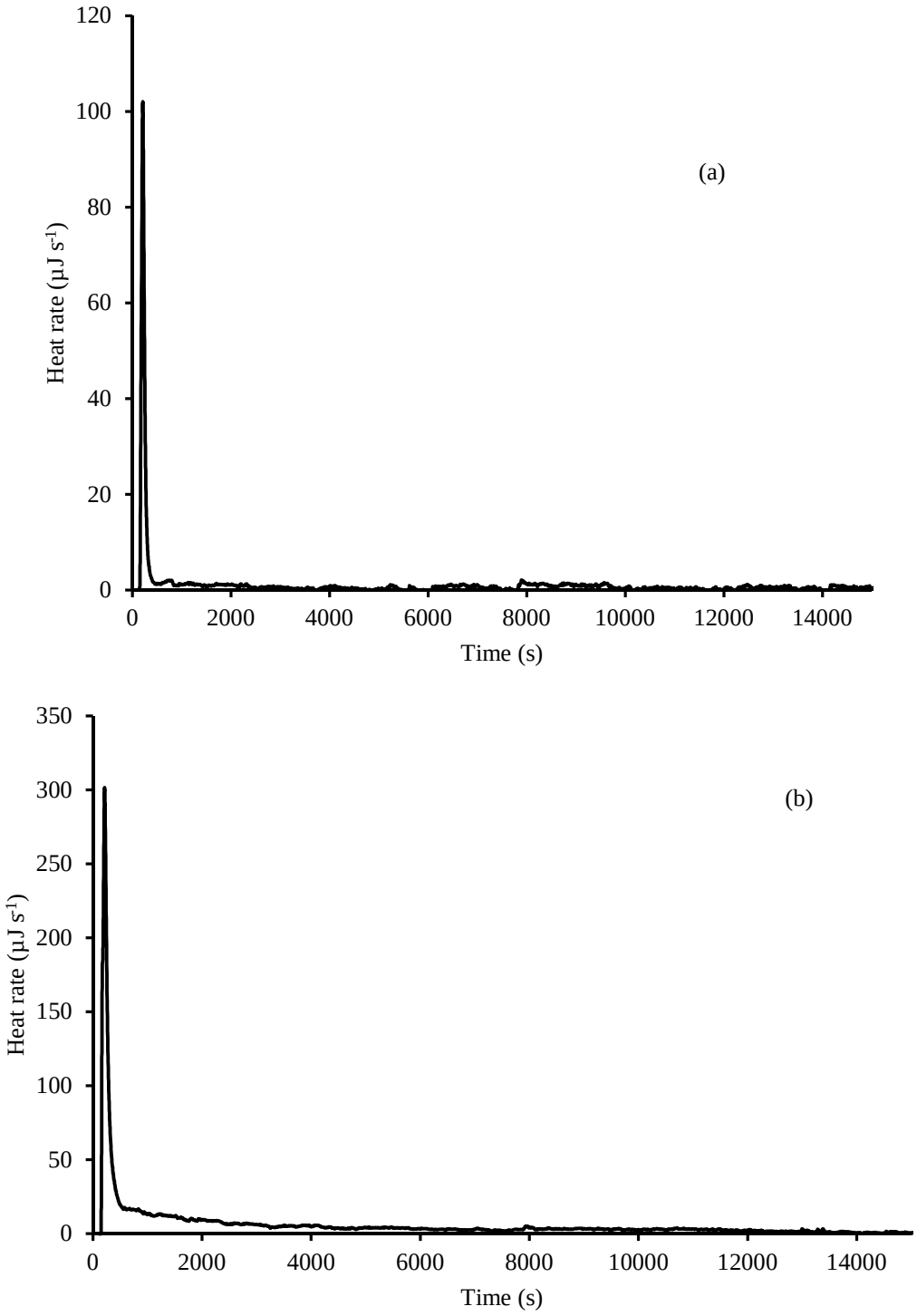


**Figure 18. Thermogram for a single titration of 250 µL of 0.01 mol/L NaH2PO4 into 0.1 g of soil sampled from the Barren Fork (a) and Clear Creek (b) sites. Peaks above zero indicate exothermic reactions. Titration made at 100 s.**

For example, the heat production rate after P addition to the Barren Fork soil returned to equilibrium in approximately 4 minutes (Figure 18a). However, the broad peak for the Clear Creek soil suggests that P sorption was not completed until at least 50 minutes, although much of the reaction occurred within 10 minutes (Figure 18b). While P sorption reactions (chemical process) indeed require time to occur, transport kinetics for sorbate from liquid to solid (soil) must also be considered. For example, Aharoni and Sparks (1991) describe sorbate transport processes in a solid-liquid system with several scenarios: transport of sorbate in the soil solution, transport across a liquid film at the solid-liquid interface, transport in a liquid-filled micropore, and diffusion of a sorbate at the soil surface or into a micropore. The "slow burn" (Rhue et al., 2002) displayed by the Clear Creek soil has been observed in other studies (Kabengi et al., 2006b; Harvey and Rhue, 2008). Since both soils were dominated by ligand exchange chemical mechanisms which are extremely fast (Sposito, 1994), a possible explanation for the long "slow burn" for P sorption in the Clear Creek soil is that after the initial P sorption reactions occurred on the surfaces of minerals, further P sorption occurred only after the slow physical transport and diffusion of P into micropores (micropore scale physical nonequilibrium). This suggests that for Clear Creek, the overall P removal process was appreciably limited by the kinetics of a physical process (transport of sorbate from liquid to solid) rather than a chemical process. It is typical for removal of a sorbate by soil to be limited by physical processes due to the presence of a porous solid phase (Sparks, 1989). Essentially, P sorption reactions were able to occur much faster than the physical processes which deliver phosphate to the soil surface. A possible explanation for why this "slow burn" was observed in the Clear Creek sample and not the Barren Fork might be that either the Barren Fork soils did not possess the same type of inner-porosity, or such zones were already occupied with P due to the higher initial soil P concentrations (Table 1). Since the soils consisted of the same soil type, had similar surface area (Table 2), and because Barren Fork had twice the P saturation as Clear Creek, the explanation is likely the latter. A similar "slow burn" diffusion preceded by a fast reaction was observed by Penn et al. (2010).

The difference between P sorption kinetics becomes more apparent when comparing the distribution of the area under the peaks of Figure 18. For Barren Fork, nearly 100% of the reaction occurred within 3 min. Contrast this to the Clear Creek sample in which only 50% of the 10 min reaction was completed within 3 min. In addition, about 31% of the total reaction occurred after 10 minutes, which suggests that additional retention time beyond 10 minutes for the Clear Creek soil will improve P sorption. This supports the results of the flow-through P sorption experiments that suggested that the Barren Fork soil sorbed P faster than the Clear Creek soil.

## Implications

Isothermal titration calorimetry provided non-detailed background information with regard to the degree of, mechanisms, and kinetics of P sorption onto soils when evaluated based on characterization data and flow-through P sorption experiments. Both single titrations and 25 consecutive titration calorimetry experiments predicted the greater P sorption capacity of the Clear Creek compared to Barren Fork soil. In fact, P sorption under flow-through conditions was well predicted using an equation previously developed by Penn and Zhang (2010), which utilized heat values from calorimetry and soil Alox concentrations.

Calorimetry data also provided information on P sorption mechanisms. Both soils in this study displayed thermal patterns typical of P sorption by ligand exchange mechanisms onto Al and Fe oxides and hydroxides, followed by a lesser degree of Al and Fe phosphate precipitation. Knowledge of these mechanisms is important since the manner in which P is held can have an impact on the resistance to P desorption. The impact of chemical conditions on P desorption will also vary depending on the mechanism in which P is held. For example, P bound onto Fe and Al is typically more stable than P bound onto Ca (McDowell et al., 2002; Penn et al., 2011), and sorption of P by Ca phosphate precipitation is usually more sensitive to RT than sorption by ligand exchange reactions (Sposito, 1994).

Perhaps most important, calorimetry proved to be a useful tool in regard to providing an initial assessment of kinetics and therefore the impact of RT on P removal. In contrast to a batch isotherm, the rate of P sorption in a flow through system depends on transport of products and reactants as well as the kinetics of sorption.

This study demonstrated that soils which appear similar based on routine characterization can differ greatly in regard to P sorption behavior under flow-through conditions. Isothermal titration calorimetry was a quick and inexpensive method to initially assess P sorption behavior among different soil samples. The calorimetry approach presented in this study can help to provide soil-specific information on the risk of P inputs to leaching (i.e., degree of P sorption) under different conditions (i.e., flow rate or RT), and potential for desorption (P sorption mechanisms).

## (D) Plot-Scale Studies - Berm Infiltration/Leaching Technique (Heeren, Fox, Storm, 2013, A berm infiltration method for conducting leaching tests at various spatial scales, *Journal of Hydrologic Engineering*, In press)

The berm was constructed of four sections of 15 cm vinyl hose attached to four $90^{o}$ elbows constructed from 15 cm steel pipe (Figure 19). Each elbow had an air vent and one elbow had a gate valve with a garden hose fitting for water. The vinyl hoses were secured to the elbows with stainless steel hose clamps and sealed with silicone sealant. The berms were then partially filled with water to add weight, but excess pressure was avoided to ensure the vinyl did not separate from the elbows.

Plots were located on relatively level areas in an attempt to maintain uniform water depths. Larger plots required shallower slopes to ensure that the entire plot could be inundated without overflowing the berm. The vinyl hose was placed in a shallow trench (3 to 5 cm) cut through the surface thatch layer to minimize lateral flow at the surface. A thick bead of liquid bentonite was also placed on the inside and outside of the berm to create a seal between the berm and the soil. High-density polyethylene tanks, 4.9 and 0.76 $m^3$, were used for the 3 m by 3 m and the 1 m by 1 m plots, respectively, to mix water and a potassium chloride tracer, Rhodamine WT, and a phosphorus solution. Tanks were instrumented with automated water level data loggers with an accuracy of 0.5 cm (HoboWare U20, Onset Computer Corp., Cape Cod, MA) to monitor water depth (pressure) and temperature at one minute intervals. An additional water level data logger was used to monitor atmospheric pressure. Logger data were processed with HoboWare Pro

software, which adjusted for changes in atmospheric pressure and water density. Tank water depth over time was used to calculate flow rate with a volumetric rating curve.

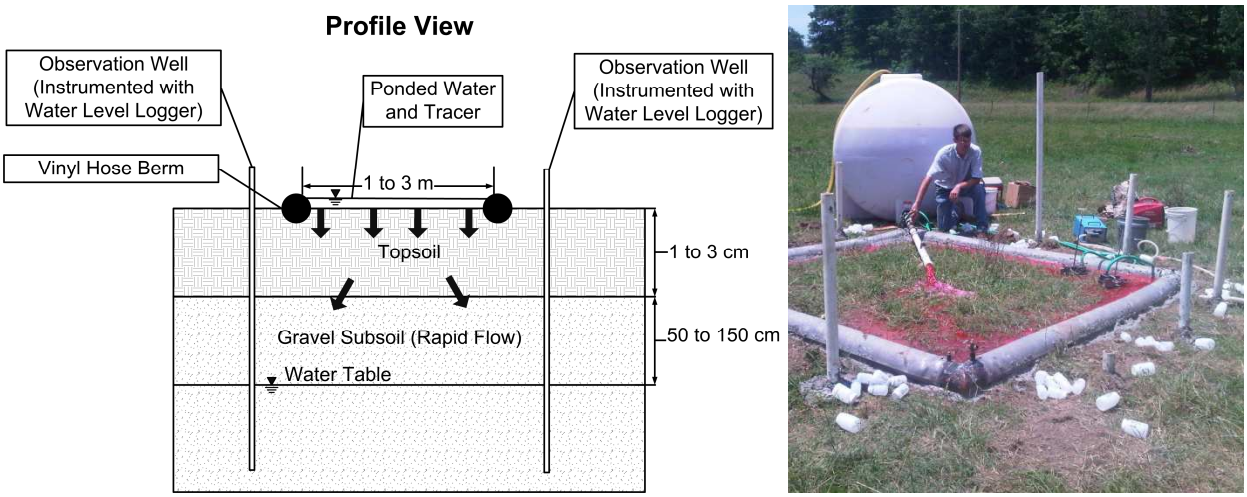


**Figure 19. Berm infiltration method, including vinyl berms to contain water-tracer solution and observation wells for collecting groundwater samples: design (left) and implementation at the Pumpkin Hollow floodplain site in eastern Oklahoma (right).**

A combination of 5.1 cm diameter Polyvinyl chloride (PVC) pipe with a manual gate valve and vinyl garden hoses with float valves were used to deliver gravity fed water from the tanks to the plots. For low flow rates, one to two garden hoses with float valves were sufficient. When higher flow rates were required to achieve the desired constant head, flow was dominated by the larger PVC pipe and the garden hoses with float valves were relatively ineffective. For these cases a fine-adjustment gate valve was required to manually control the flow rate to achieve a relatively constant head in the plots. When a tank was nearly empty, flow was temporarily stopped while water and tracer was added to the tank. Chloride was used as a conservative tracer and Rhodamine WT as a visual tracer with injection concentrations 20 to 30 times background levels. Phosphorus was also injected into the plot. Depth in each plot area was monitored with a water level data logger. Heads were maintained between 3 and 10 cm across the plots.

A Geoprobe Systems drilling machine (6200 TMP, Kejr, Inc., Salina, KS), which has been found to be effective in coarse gravel soils (Heeren et al., 2011; Miller et al., 2011), was used to install four to twelve observation wells around each plot. Boreholes were sealed with liquid bentonite to avoid water leaking down the hole. Observation wells were instrumented with water level data loggers. Reference water table elevations, obtained with a water level indicator and laser level data for each well, were then calculated. Water table elevation data had an accuracy of 1 cm. Low flow sampling with a peristaltic pump was used to collect water samples from the top of the water table, which ranged from 50 to 150 cm below ground surface.

Porous media flow from hypothetical 1 m by 1 m infiltration plots were simulated using HYDRUS-3D (Šimůnek et al., 2006) for three different soil types: sand, loam, and silt. This

method was not expected to be used on soils finer than silt. HYDRUS is a finite element model for simulating two- and three-dimensional movement of water, heat, and multiple solutes in variably saturated media (Šimůnek et al., 2006; Akay et al., 2008). The HYDRUS code numerically solves the Richards equation for saturated-unsaturated water flow (Šimůnek et al., 2006).

The finite element grid consisted of triangular prism elements spaced equally every 25 cm in the horizontal, lateral, and vertical directions. The simulation domain consisted of a 1 m by 1 m constant head infiltration plot centered within a 10 m by 10 m area with a 3-m deep soil profile (Figure 20). All cells on the surface of the simulation domain outside the infiltration plot were no-flux boundaries. A constant head boundary condition was used to simulate the infiltration plot with constant heads ranging from 2.54 to 15.24 cm. The initial water table depth was varied between simulations, which included depths of 1.0, 2.0, and 2.5 m below ground surface. Below the water table, a no flux boundary condition was specified for the shell and bottom of the simulation domain to simulate the presence of a regional groundwater system. Above the water table, the shell boundary condition was a possible seepage face (Figure 20). At the water table depth, observation nodes were added to the simulation domain located at various distances (0 to 450 cm) away from the edge of the infiltration plot.

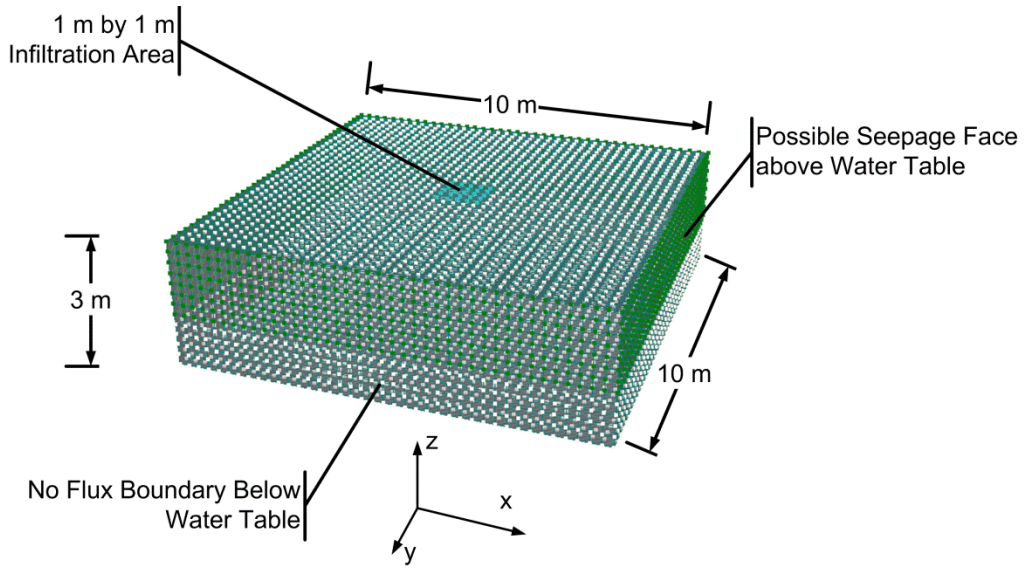


**Figure 20. Simulation domain for HYDRUS-3D modeling of hypothetical infiltration experiments with a 1 m by 1 m infiltration plot.**

The van Genuchten-Mualem model (van Genuchten, 1980) was used to describe the water retention, $\theta(h)$, and conductivity, $K(h)$, functions for the assumed homogeneous soil matrix:

$$\theta(h) = \begin{cases} \theta_r + \dfrac{\theta_s - \theta_r}{\left[1 + |\alpha h|^n\right]^m} & h < 0 \\ \theta_s & h \geq 0 \end{cases} \quad (2)$$

$$K(h) = K_s S_e^l \left[1 - (1 - S_e^{1/m})^m\right]^2 \qquad m = 1 - 1/n, \quad n > 1 \quad (3)$$

where $S_e = (\theta - \theta_r)/(\theta_s - \theta_r)$ is the effective saturation; $\alpha$ (1/L), $n$, and $l$ are empirical parameters; $\theta_s$ is the saturated water content ($L^3/L^3$); $\theta_r$ is the residual water content ($L^3/L^3$); and $K_s$ (L/T) is the saturated hydraulic conductivity. Hydraulic parameters for the sand, loam, and silt soils were acquired from the soil catalog in HYDRUS, derived from Carsel and Parrish (1988), in order to represent average values for these different textural classes (Table 3).

HYDRUS simulations were conducted to determine the time at which a detectable water table rise, defined as 1 cm, was observed in the observation nodes. This information was used to correlate the response time in observation wells installed next to the infiltration plot relative to the soil type, head in the infiltration plot, distance the observation well was installed from the infiltration plot edge, and the water table depth.

**Table 3. Soil properties for the sand, loam, and silt soils simulated by HYDRUS-3D for the hypothetical 1 m by 1 m infiltration experiments. Soil properties were from the soil catalog for the textural classes in HYDRUS.**

| Soil Type | Residual Water Content, $\theta_r$ ($cm^3/cm^3$) | Saturated Water Content, $\theta_s$ ($cm^3/cm^3$) | $\alpha$* (1/cm) | $n$* | Saturated Hydraulic Conductivity, $K_s$ (cm/min) | Pore-Connectivity Parameter, $l$ |
|---|---|---|---|---|---|---|
| Sand | 0.045 | 0.430 | 0.145 | 2.68 | 0.495 | 0.5 |
| Loam | 0.078 | 0.430 | 0.036 | 1.56 | 0.017 | 0.5 |
| Silt | 0.034 | 0.460 | 0.016 | 1.37 | 0.004 | 0.5 |

*Empirical constants.

As an example, infiltration rates measured at Pumpkin Hollow ranged from 5 to 70 cm/hr, indicating considerable heterogeneity in the infiltration rates of the floodplains due to the occurrence of gravel outcrops. These data were higher than the U.S. Natural Resources Conservation Service (NRCS) Adair County, Oklahoma Soil Survey (NRCS, 2012), indicating the need for larger scale field measurements of infiltration rate. The NRCS Soil Survey (NRCS, 2012) estimated permeability of the limiting layer to be in the range of 1.5 to 5 cm/hr for the Razort gravelly loam. This method was successful in quantifying high infiltration rate soils (i.e., gravels) even for large 3 m by 3 m plots, and lower infiltration rates could be easily measured. Larger plot sizes may require excessively large tanks, and thus continuous pumping and dosing to inject tracers directly into the pump hose may provide a better alternative for adequate mixing.

Figure 21 shows the relationship between flow rate and the time to empty the tank, which can be used to aid the design of infiltration experiments. For example, one of the 3 m by 3 m plots had a quasi-steady state infiltration rate of 6.3 cm/hr, which required an average flow rate of 9.5 L/min. According to Figure 21, the tank will need to be refilled every 8 hr for a 4.9 $m^3$ tank. Actual times to empty the tank after quasi-steady state was reached were 6.5, 6.0, and 8.0 hr at Pumpkin Hollow for example, which is consistent with the fact that refills were performed before the tank was completely empty.

A constant head assumption was considered valid if the water depth in the infiltration plot was within 1.5 cm of the mean depth at least 85% of the time. All experiments met this requirement (Figure 22). Float valves were reliable and effective, allowing the system to run automatically for several hours at a time. Manual gate valves required attentive monitoring in order to be effective. Observed response times based on chloride detection in groundwater wells (located 0.5 m from the edge of the berm) ranged from 18 minutes (coarse gravel outcrop) to more than 32 hours. All plots had at least some wells where chloride was never detected above background levels (duration of experiments ranged from 3 to 32 hours), again indicating significant heterogeneity within the floodplain soils.

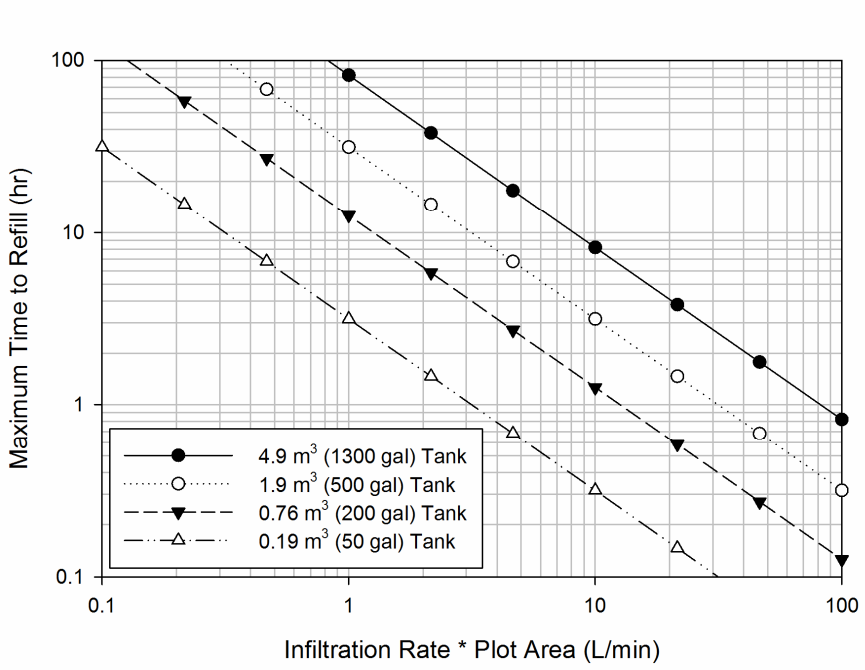


**Figure 21. Relationship between expected infiltration flow rate and time to empty water tank for different size water tanks.**

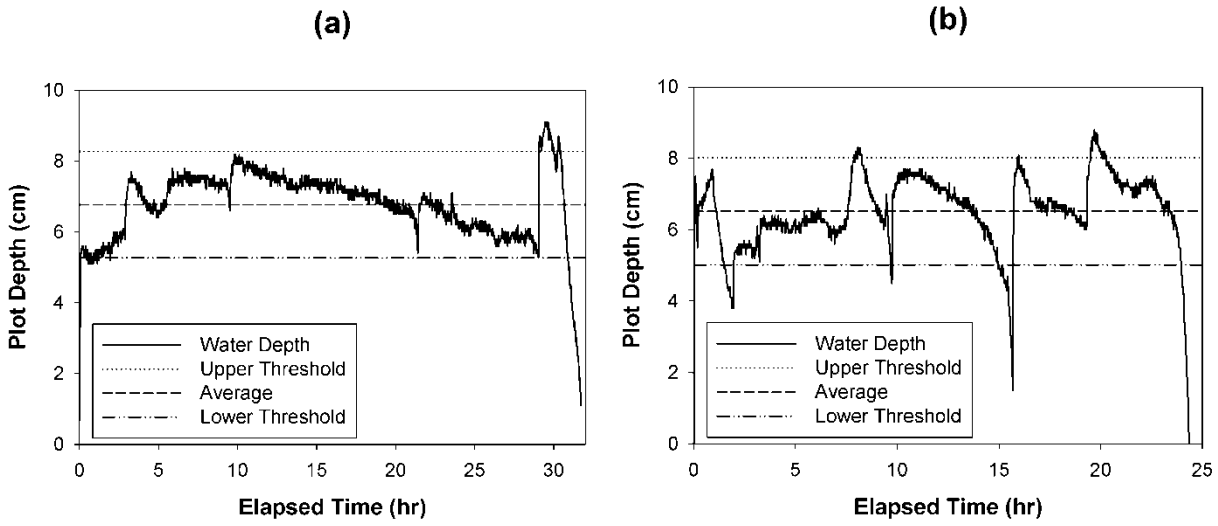


**Figure 22. Measured plot water depth over time for a 1 m by 1 m plot with flow controlled primarily by an automatic float valve (a) and for a 3 m by 3 m plot with flow controlled primarily by a manual gate valve (b). Water depths were within 1.5 cm of the mean depth 92% (left) and 89% (right) of the time, meeting the prescribed requirements for constant head infiltration.**

Modeled response times using HYDRUS-3D were more dependent on water table depth than distance from the plot edge. In sand and coarser soils (Figure 23), response times were predicted to be less than 200 minutes (approximately 3 hrs), even with a deep water table (250 cm) and observation wells installed as much as 4 m from the edge of the infiltration plot. For silt and finer soils, experiments would need to be conducted for multiple days when sampling from a groundwater table 200 cm below ground surface (Figure 23).

This research successfully demonstrated an innovative method for quantifying infiltration rates and leaching in highly conductive gravelly soils at the plot scale, maintaining a constant head at least 85% of the time during experiments. Guidelines have been provided for future infiltration experiments. The berm infiltration method allows investigations of various plot sizes and was demonstrated to be capable of measuring infiltration rates ranging from 5 to 70 cm/hr. Larger plot sizes may require continuous pumping and tracer injection directly into the pump hose instead of using tanks. Numerical modeling indicated that experimental times in homogeneous soils were more dependent on water table depth than distance from the plot edge, especially for coarser soils. Experimental durations may be less than 200 minutes in sand and coarser soils to multiple days for silt and finer soils.

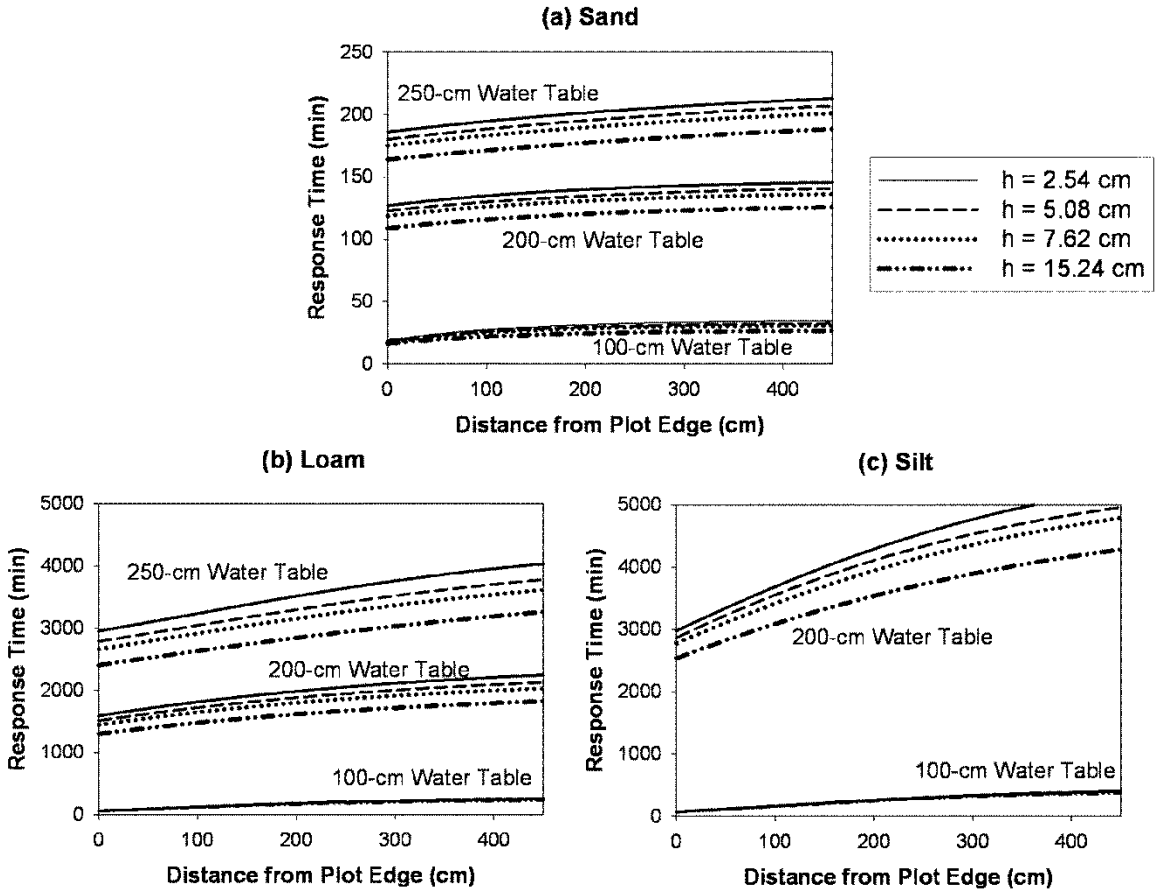


**Figure 23. HYDRUS-3D predicted response times in observation wells installed next to infiltration plots as a function of soil type, head in the infiltration plot (h), distance the observation well was installed from the infiltration plot edge, and the depth to water table.**

## (E) Impact of Measurement Scale on Infiltration in Gravel-Dominated Alluvial Floodplains (Heeren, Fox, Storm, Haggard, Penn, and Halihan, 2013, Impact of measurement scale on infiltration and phosphorus leaching in Ozark floodplains, ASABE Paper No. 131621213, St. Joseph, Mich.: ASABE.)

Relatively few studies on infiltration and P leaching have been done at the plot scale where infiltration and transport may be controlled by heterogeneity present at various scales (Nelson et al., 2005). In many riparian floodplains, gravel outcrops and macropores are present. Infiltration is often assumed to be uniform at the field scale, but this neglects the high spatial variability common in anisotropic, heterogeneous alluvial-floodplain soils (Heeren et al., 2013b). Accounting for spatial variability in infiltration rates is important not only for watershed flow and transport models, but also for management of variable rate irrigation (Evans et al., 2012) which can account for in-field heterogeneity in soil properties. Easton (2013) used geostatistics to study spatial trends in infiltration rate on a hillslope and found that “methods of measuring the

infiltration rate of a soil differ in first order statistical measures (mean and variance), but not substantially in second order statistical measures (spatial structure)."

Gravel outcrops and macropores can significantly affect infiltration and leaching in these floodplains. For water movement through soil, macropores have been shown to have a large impact on flow and solute transport (Thomas and Phillips, 1979; Fox et al., 2004; Djodjic et al., 2004; Akay and Fox, 2007; Gotovac et al., 2009). Infiltration is often assumed to be uniform (piston flow) at the field scale, but this neglects the high spatial variability common in anisotropic, heterogeneous alluvial-floodplain soils.

As the scale of measurement increases, physical properties of a porous media like soil tend to have decreasing spatial variability until a representative elementary volume (REV) is reached (Bear, 1972; Brown et al., 2000). The REV is bounded by a minimum ($V_{min}$) and maximum ($V_{max}$) volume. For measurement volumes less than $V_{min}$, the measured property fluctuates rapidly in space due to the influence of individual pores. For measurement volumes above $V_{max}$, "additional morphological structures allow the property to drift to new values, which results in large field variability" (Brown et al., 2000). Increasing the diameter of double ring infiltrometers has been found to reduce the variability of measured infiltration rates (Sisson and Wierenga, 1981; Lai and Ren (2007). However, whether double ring infiltration can be scaled up to the plot or field scale has not been well established. Massman (2003) observed that hydraulic conductivities measured with flood tests in infiltration basins were up to two orders of magnitude higher or lower than hydraulic conductivities determined from air conductivity or estimated from grain size parameters. It was hypothesized that as the scale of measurement increases, measured infiltration rate and hydraulic conductivity of the topsoil will increase due to large but infrequent macropores, and that the spatial variability will decrease, until an REV is attained. Therefore, the overarching objective of this line of research was to characterize P leaching to alluvial aquifers in the coarse gravel floodplains of the Ozark ecoregion, while the specific objective of this paper was to quantify infiltration and hydraulic conductivity across a range of scales (point to 100 $m^2$) to evaluate the effect of measurement scale. Accurately understanding infiltration is essential for understanding P transport.

## Methods

### *Floodplain Sites*

The alluvial floodplain sites were located in the Ozark ecoregion of northeastern Oklahoma and northwestern Arkansas (Figure 2). The Ozark ecoregion of Missouri, Arkansas, and Oklahoma is approximately 62,000 $km^2$ and is characterized by gravel bed streams and cherty soils in the riparian floodplains. The erosion of carbonate bedrock (primarily limestone) by slightly acidic water has left a large residuum of chert gravel in Ozark soils, with floodplains generally consisting of coarse chert gravel overlain by a mantle (1 to 300 cm) of gravelly loam or silt loam. The alluvium is spatially heterogeneous, resulting in preferential flow pathways which are hypothesized to be ancient buried gravel bars (Heeren et al., 2010). Similar hydrogeologic conditions exist near gravel bed streams in their associated alluvial floodplains worldwide.

Vertical electrical resistivity profiles were collected at the floodplain sites to characterize the heterogeneity of the unconsolidated floodplain sediments. Electrical resistivity imaging (ERI) data were collected using a SuperSting R8/IP Earth Resistivity Meter (Advanced GeoSciences

Inc., Austin, Tex.) with 56-electrode arrays. The profiles typically employed electrode spacings of 1 to 1.5 m with an associated depth of investigation of approximately 13 m, which included the vadose zone, alluvial aquifer, and bedrock. The resistivity sampling with the SuperSting R8/IP, and subsequent inversion utilized a proprietary routine devised by Halihan et al. (2005), which produced higher resolution images than conventional techniques.

The Barren Fork Creek site (Figure 24, latitude: 35.90°, longitude: -94.85°) was immediately downstream of the Eldon Bridge U.S. Geological Survey (USGS) gage station 07197000. With a watershed size of 845 $km^2$, the Barren Fork Creek site was a fourth order stream with a historical median discharge of 3.6 $m^3$ $s^{-1}$. The study area at the Barren Fork Creek was located on the outside of a meander bend which was being actively eroded by the stream (Midgley et al., 2012). The soils were classified as Razort gravelly loam underlain with alluvial gravel deposits. Thickness of the loam ranged from 0.3 to 2.0 m, with dry bulk densities ranging from 1.3 to 1.7 g $cm^{-3}$. Soil hydraulic studies on these soil types have shown that subtle morphological features can lead to considerable differences in soil water flow rates (Sauer and Logsdon, 2002; Sauer et al., 2005).

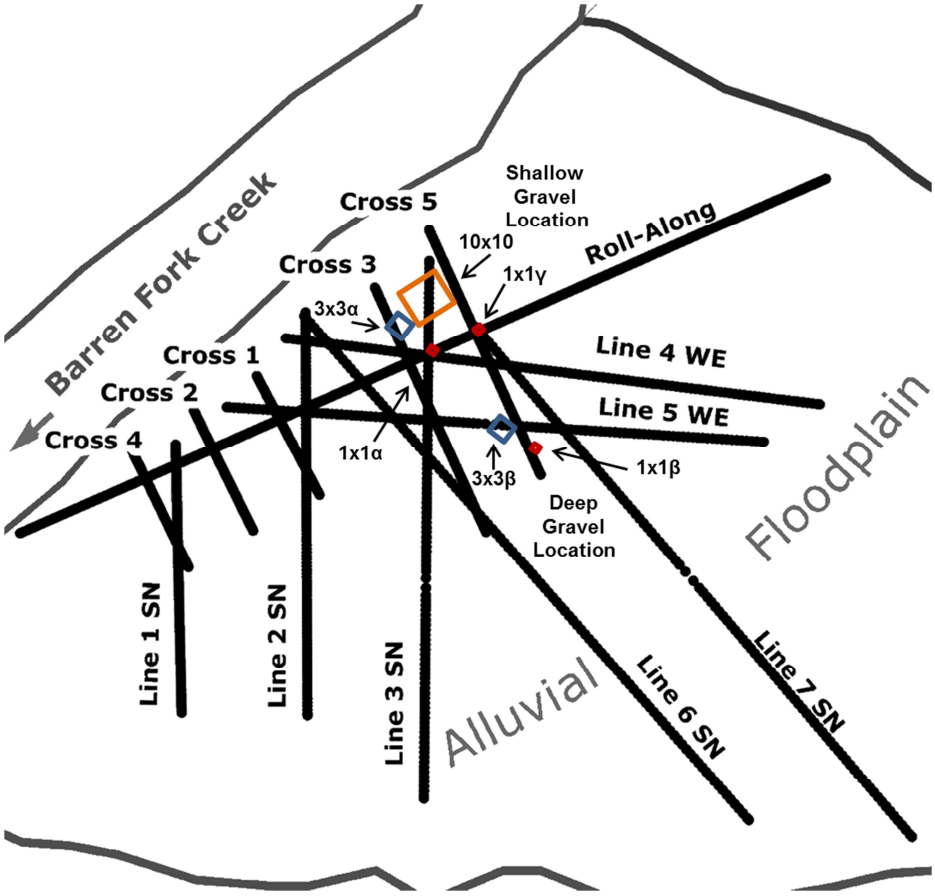


**Figure 24. Barren Fork Creek floodplain site, including locations of plots for infiltration experiments (labeled according to plot size in m). Thick black lines are locations of electrical resistivity profiles (Miller, 2012; Appendix A), which were used to select plot locations. For orientation, north is up. The floodplain is bounded by the Barren Fork Creek to the northwest, a small tributary to the northeast, and a bluff to the south. Figure adapted from Miller (2012).**

The Pumpkin Hollow floodplain site (Figure 25) was also located in the Ozark ecoregion of northeastern Oklahoma (latitude: 36.02°, longitude: -94.81°). A small tributary of the Illinois River, Pumpkin Hollow Creek was a first order ephemeral stream in its upper reaches. The entire floodplain was 120 to 130 m across at the research site, with an estimated watershed area of 15 $km^2$. The land use at the site was pasture for cattle. The Pumpkin Hollow field site was a combination of Razort gravelly loam and Elsah very gravelly loam, although infiltration experiments were limited to the Razort gravelly loam soils. Topsoil thickness ranged from 0 to 3 cm, and bulk densities of the cohesive material were between 1.3 and 1.5 g $cm^{-3}$.

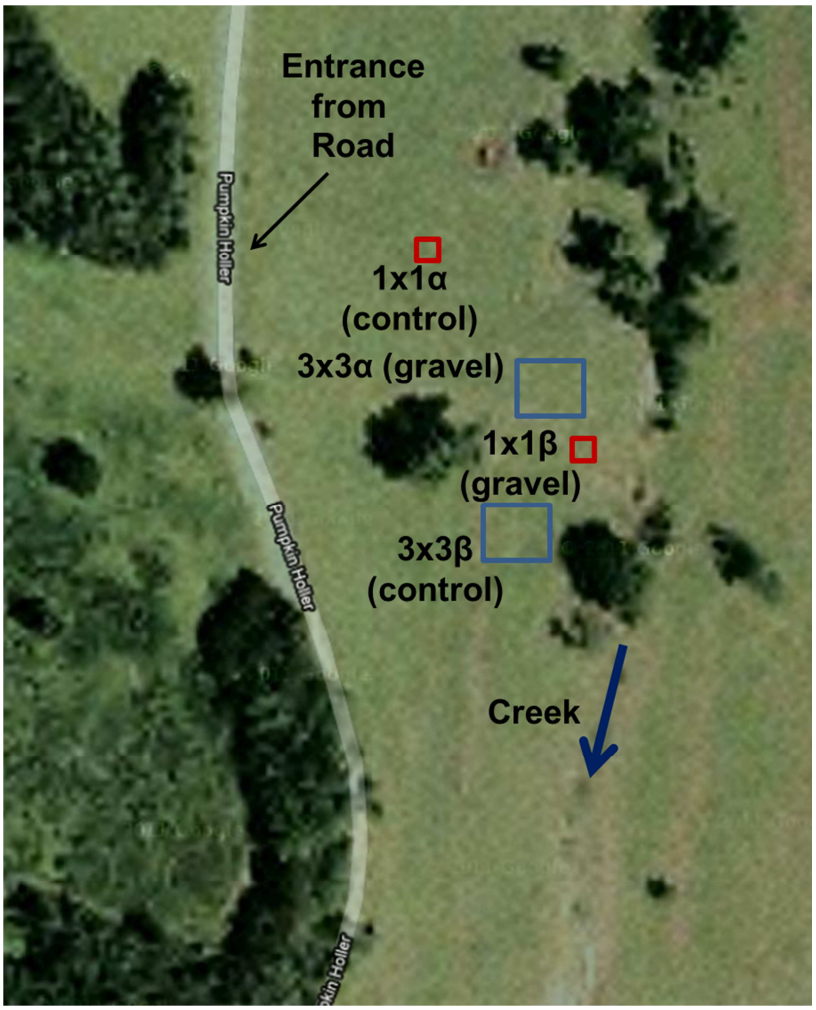


**Figure 25. Pumpkin Hollow floodplain site, including locations of plots for infiltration experiments (labeled according to plot size in m). For orientation, north is up. The floodplain is bounded by Pumpkin Hollow Creek to the east and a bluff to the west. Background electrical resistivity profiles (not shown) were located just south of the plot locations (Miller, 2012; Appendix A).**

The Clear Creek alluvial floodplain site (Figure 26) was located just west of Fayetteville, AR in the Arkansas River Basin and flows into the Illinois River (latitude: 36.13°, longitude: -94.24°). The total drainage area was 199 $km^2$ for the entire watershed. Land use in the basin was 36%

pasture, 34% forest, 27% urban and 3% other. Soils were loamy and silty, deep, moderately well drained to well drained (U.S. EPA, 2009), and generally contained less chert or gravel than the Barren Fork Creek or Pumpkin Hollow floodplain sites. Thickness of the top loam layer ranged from 0.3 to 2.0 m, with dry bulk densities ranging from 1.5 to 1.7 g $cm^{-3}$. A fourth order stream with a flow of approximately 0.5 $m^3$ $s^{-1}$ at the study site, the area of the watershed above that point was 101 $km^2$. The land use in the study area was pasture and consisted of Razort gravelly loam soils.

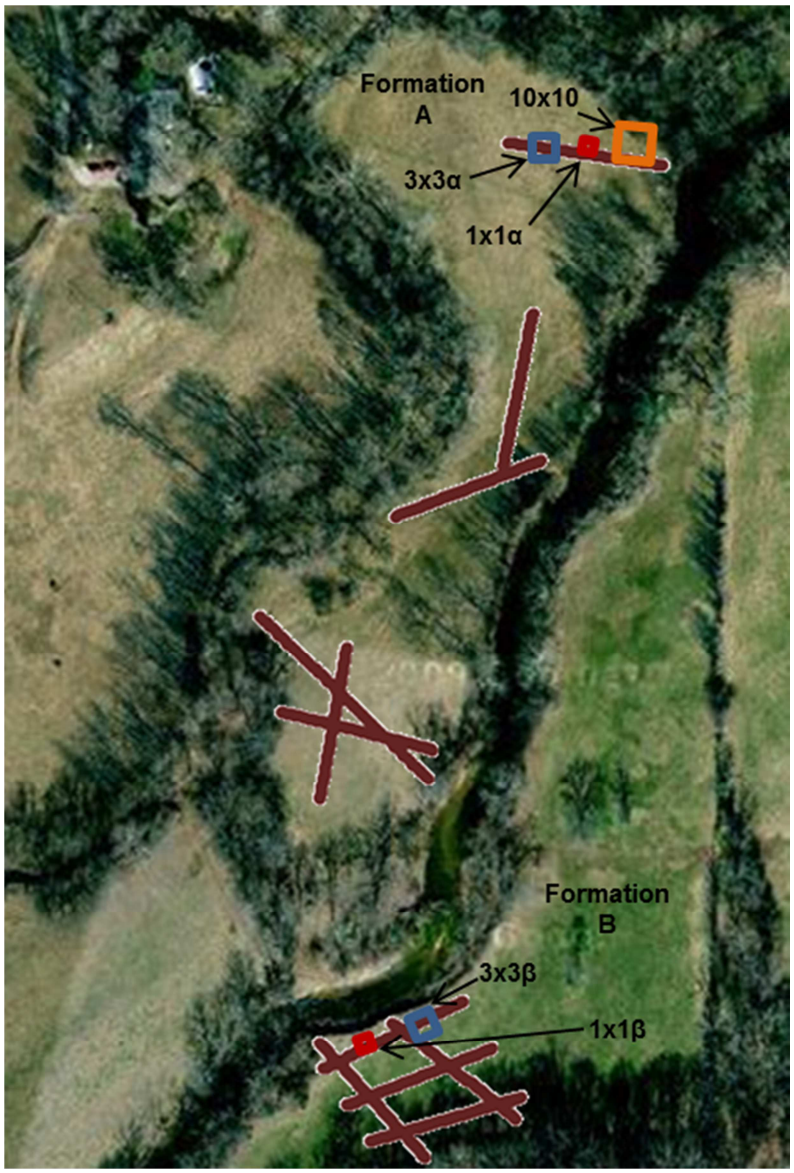


**Figure 26. Clear Creek floodplain site, including locations of plots for infiltration experiments (labeled according to plot size in m). Thick maroon lines are locations of electrical resistivity profiles (Heeren, 2012; Appendix A), which were used to select plot locations. For orientation, north is up. Within the floodplain, Formation A is bounded by Clear Creek to the east and a small overflow channel to the north and west, and Formation B is bounded by Clear Creek to the north and a bluff to the south.**

### *Infiltration Plots*

Measuring infiltration rates and/or leaching of solutes at a plot scale is difficult, especially for high hydraulic conductivity soils, without innovative field methods. In this research, the berm method (Heeren et al., 2013a) was used to confine infiltration plots and maintain a constant head of water, with plot sizes ranging from 1 m by 1 m to 10 m by 10 m. Four to six infiltration experiments were performed at each site with plots selected to represent a range of infiltration rates at each floodplain site (Figures 24 to 26, Table 4). Plots were located on relatively level areas in order to minimize the variation in water depth across the plot. Larger plots were required to have smaller slopes to ensure that the entire plot could be inundated without overflowing the berm.

**Table 4. Infiltration experiments at three alluvial floodplain sites in the Ozark ecoregion.**

| Floodplain Site | Date | Plot | Area ($m^2$) | Treatment | Duration (hr) | "Steady State" Infiltration ($q$) (cm $hr^{-1}$) | Limiting Layer Depth ($d$) (cm) | Average Head ($h$) (cm) | Hydraulic Gradient ($i$) (cm $cm^{-1}$) | Hydraulic Conductivity ($K_{eff}$) (cm $hr^{-1}$) |
|---|---|---|---|---|---|---|---|---|---|---|
| Pumpkin Hollow | 5/4/11 | 1x1α | 1 | Control | 32 | 5.3 | 99 | 6.8 | 1.07 | 5.0 |
| Pumpkin Hollow | 5/5/11 | 3x3α | 9 | Gravel Outcrop | 2.8 | 18 | 46 | 5.4 | 1.12 | 16 |
| Pumpkin Hollow | 6/1/11 | 1x1β | 1 | Gravel Outcrop | 4.3 | 74 | 36 | 3.2 | 1.09 | 68 |
| Pumpkin Hollow | 6/2/11 | 3x3β | 9 | Control | 24 | 6.3 | 58 | 6.5 | 1.11 | 5.7 |
| Barren Fork | 6/30/11 | 1x1α | 1 | Shallow gravel | 22 | 10 | 92 | 5.8 | 1.06 | 9.6 |
| Barren Fork | 6/30/11 | 3x3α | 9 | Shallow gravel | 22 | 13 | 110 | 3.1 | 1.03 | 12 |
| Barren Fork | 7/13/11 | 1x1β | 1 | Deep gravel | 46 | 6.8 | 134 | 4.7 | 1.04 | 6.6 |
| Barren Fork | 7/13/11 | 3x3β | 9 | Deep gravel | 48 | 3.0 | 145 | 6.4 | 1.04 | 2.9 |
| Barren Fork | 5/7/12 | 10x10 | 60* | Shallow gravel | 4 | 13 | 107 | 3.0 | 1.03 | 13 |
| Barren Fork | 6/6/12 | 1x1γ | 1 | Shallow gravel | 86 | 14 | 113 | 9.0 | 1.08 | 13 |
| Clear Creek | 4/12/11 | 1x1α | 1 | Formation A | 41 | 5.6 | 57 | 1.8 | 1.03 | 5.4 |
| Clear Creek | 4/12/11 | 3x3α | 9 | Formation A | 41 | 3.3 | 76 | 1.8 | 1.02 | 3.2 |
| Clear Creek | 7/27/11 | 1x1β | 1 | Formation B | 48 | 1.3 | 137 | 6.3 | 1.05 | 1.2 |
| Clear Creek | 7/27/11 | 3x3β | 9 | Formation B | 45 | 0.8 | 210 | 7.2 | 1.03 | 0.7 |
| Clear Creek | 5/21/12 | 10x10 | 100 | Formation A | 52 | 0.6 | 84 | 6.0 | 1.07 | 0.6 |

*Pump capacity was not sufficient to keep the entire infiltration gallery inundated.

Each berm was constructed of four sections of 15 cm vinyl hose which were attached to $90^0$ steel elbows and surrounded the infiltration gallery. A shallow trench (3 to 5 cm) was cut through the thatch layer and a thick bead of liquid bentonite was used to create a seal between the berm and the soil.

High density polyethylene tanks (4.9 $m^3$ and 0.76 $m^3$) were used to mix stream water and solutes. A combination of 5.1-cm diameter PVC with manual valves and garden hoses with float valves were used to deliver water (gravity fed) from the tanks to the plots. When a tank was nearly empty, flow was temporarily stopped while the tank was refilled and solutes were added and mixed. The largest plot sizes (10 m by 10 m) required continuous pumping and solute injection directly into the pump hose using Dosatron® injectors (D8R, Dosatron®, Clearwater, FL) instead of using tanks for mixing. Constant heads in the plots were maintained (Heeren et al., 2013a) between 3 and 10 cm. Depth to the water table ranged from 50 cm at the Pumpkin Hollow site up to 350 cm at the Clear Creek site.

### *Soil Cores and Particle Size Analysis*

During the installation of the observation wells with a Geoprobe Systems (Salina, KS) 6200 TMP (Trailer-mounted Probe) direct-push drilling machine, which has been shown to be effective in coarse gravel aquifers (Miller et al., 2011), soil core samples were collected at known depths using a dual-tube core sampler with a 4.45 cm opening. The sampler opening (size) limited the particle size that could be sampled and large cobbles occasionally clogged the sampler resulting in incomplete cores for that depth interval. Direct push cores were recovered from one to four wells per plot.

A subset of the soil core samples were dry sieved with a sieve stack ranging from 2 to 12.5 mm for a particle size analysis. Samples preparation included disaggregation with a rubber-tipped pestle when necessary. If particles were retained on the 12.5 mm sieve, a measurement of the “b” axis (longest intermediate axis perpendicular to the long “a” axis) of the largest particle was utilized as the sieve size that 100% of the sample would pass through because that dimension largely controls whether a particle will pass a particular sieve (Bunte and Abt, 2001).
A complete textural analysis was desired for surface soil samples from one soil core per plot. Following the procedure developed by Miller (2012), the particle size distribution (PSD) of the mass retained on the finest sieve (2 mm) “was determined using a Cilas 1180 Particle Size Analyzer (Cilas USA, Madison, WI), which calculated the ratio of particle sizes based on the obscurance of a laser beam. The Cilas 1180 measured the relative volume for particle size ranges of a representative sample. The PSD of the fine fraction was calculated by multiplying the percent distribution from the sample by the total volume of the fine dry-sieved fraction.”

### *Double Ring Infiltrometer Soil Hydraulic Conductivity*

While this research was driven by infiltration and leaching, the best way to compare data across scales was to convert infiltration data to effective saturated hydraulic conductivity ($K_{eff}$) of the top soil layer. In most cases (at the Ozark floodplain sites) this was a layer of silt loam which was overlying coarse gravel.

In order to represent a scale in between the plot scale and the point scale, a double ring infiltrometer (ELE 25-0660, ELE International, Loveland, CO), with an outer ring diameter of 60

cm and an inner ring diameter of 30.5 cm (infiltration area of 0.07 $m^2$), was used at the Barren Fork Creek site. Tests were performed at two locations: near the "shallow gravel" plots and near the "deep gravel" plots. The shallow gravel location was an area where a high hydraulic conductivity zone (a buried gravel bar) came close to the soil surface, with only 0.3 to 1 m of silt loam. At the deep gravel location, 1.0 to 1.3 m of silt loam capped the coarse gravel layer. During the constant head double ring experiments (12 to 55 min), the wetting front (total infiltration of 0.6 cm) did not proceed past the top silt loam layer of soil. With the double ring infiltrometer, flow from the inner ring was assumed to be one dimensional. Therefore, the data was fit to the following well known one dimensional transient solution (Philip, 1957; Lai & Ren, 2007):

$$I = St^{\frac{1}{2}} + At \tag{4}$$

where $I$ is cumulative infiltration (L), $S$ is sorptivity (L $T^{-1/2}$), $t$ is the elapsed time from initiation of infiltration (T), and $A$ is a constant (L $T^{-1}$). An example is shown in Figure 27. The $A$ term was taken to be the effective saturated hydraulic conductivity ($K_{eff}$). Water depth (around 10 cm) is not included in this equation, but its effect is accounted for in the sorptivity term along with matric potential effects. For the experiment at the deep gravel location, the first three points were treated as outliers and it was assumed that the experiment started on the 4th data point (seven minutes after initiation).

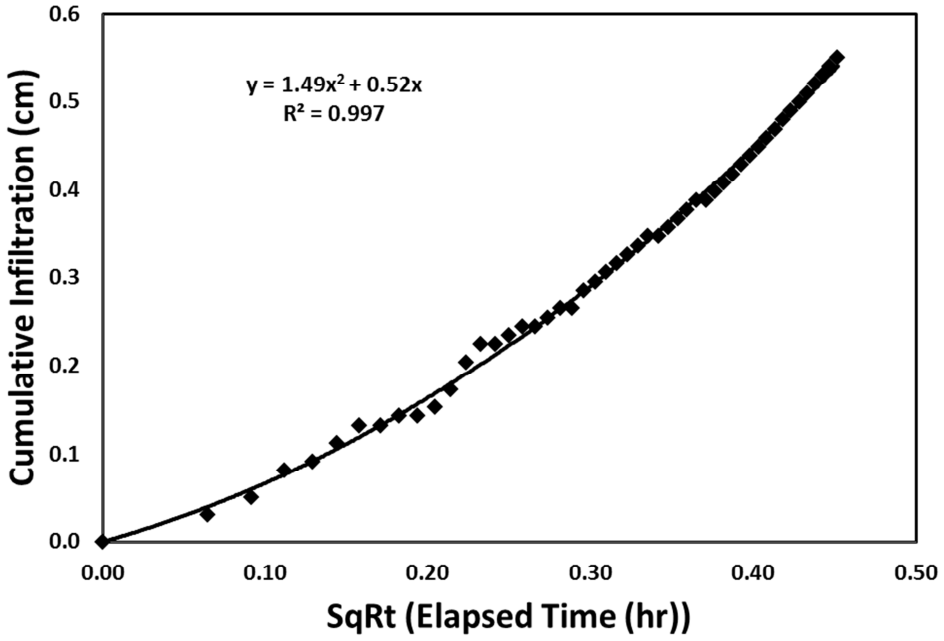


**Figure 27. Double ring infiltrometer data from the shallow gravel location at the Barren Fork Creek site, resulting in an effective saturated hydraulic conductivity of 1.5 cm hr 1 and a sorptivity of 0.52 cm $hr^{-1/2}$.**

### *Plot Scale Soil Hydraulic Conductivity*

A brief survey of the literature was performed to determine the best method to determine $K_{eff}$ from plot scale constant head infiltration rate data. Transient solutions are available for early

time infiltration data (e.g. Philip, 1957; equation 4) for one dimensional infiltration. A quadratic equation can be fit to the data in order to determine two parameters: $K_{eff}$ and sorptivity, the latter of which accounts for both capillary action and depth of the water above the soil surface (head). This approach worked well for double ring infiltrometer experiments at the Barren Fork Creek site with a high level of precision of measurements at the beginning of infiltration and a limited depth of total infiltration, since the equation assumes a homogenous semi-infinite medium. For the longer duration (3 to 52 hr) plot scale experiments, though, the depth of infiltration often exceeded the top layer of soil, violating the homogeneous assumption in these equations. Also, it was difficult to get precise transient early time data when accounting for measurement error and the change in storage of water above the soil surface during plot scale experiments.

The second major category of equations for predicting $K_{eff}$ from infiltration data is steady state equations (Bodhinayake et al., 2004). Most of the plots were run long enough to achieve quasi-steady state conditions, with total infiltration often greatly exceeding the depth of the top layer of soil. Without transient data, more parameters are needed for these solutions (ponded depth, geometry to account for two dimensional (radial) effects, etc.). However, a good solution for our situation, with two distinct soil layers, was not found.

Therefore, we developed our own solution applying Darcy's law specifically to the top layer of soil for steady state infiltration under a constant head. Since edge effects were considered small compared to the large area of the infiltration gallery at the plot scale, one dimensional vertical flow was assumed at the plot scale. Equation 5 is for infiltration into a lower conductivity layer underlain by a higher conductivity layer:

$$q = K_{eff} i = K_{eff}(1 + \frac{h}{d}) \quad (5)$$

where $q$ is the steady state infiltration rate (L $T^{-1}$), $K_{eff}$ is the effective saturated hydraulic conductivity (L $T^{-1}$), $i$ is the hydraulic gradient (L $L^{-1}$), $h$ is the spatial and temporal average depth of water in the infiltration gallery (L), and $d$ is the depth of the top layer of soil. The first term in the parentheses represents the hydraulic gradient due to gravity, which is unigradient. The second term is the gradient due to the change in pressure head over the length of flow. Water pressure at the soil surface is the hydrostatic pressure head associated with the spatially and temporally averaged depth of water in the plot. As water flows from a restrictive layer of soil into a more conductive layer, an inverted water table will form at the bottom of the restrictive layer, indicating a pressure head of zero at the bottom of the top layer of soil. It is acknowledged that the one dimensional flow assumption is a limitation of this approach when considering the heterogeneity and anisotropy of these complex alluvial deposits (Fox et al., 2011).

For 1 m by 1 m and 3 m by 3 m plots, $q$ was determined based on flow rates from the mixing tanks. The tanks were instrumented with automated water level data loggers with an accuracy of 0.5 cm (HoboWare U20, Onset Computer Corp., Cape Cod, MA) to monitor water depth (pressure) and temperature at one minute intervals. An additional water level data logger was used to monitor the atmospheric pressure. Logger data were processed with HoboWare Pro software, which adjusted for changes in atmospheric pressure and water density. Measured tank water depth over time was used to calculate the flow rate using a volumetric rating curve. For the 10 m by 10 m plots, flow was estimated based on the frequency of cycles in the Dosatron®

injectors (D8R, Dosatron®, Clearwater, FL). The *h* was determined from automated water level data loggers (HoboWare U20, Onset Computer Corp., Cape Cod, MA) placed in the plots along with manual measurements of water depth.

The *d* of the silt loam layer was determined from soil cores within and near the plots. The Barren Fork Creek site had a distinct layer change from silt loam to coarse gravel. The Pumpkin Hollow site was highly heterogeneous, and it was sometimes difficult to identify the bottom of a restrictive layer. In some cases (e.g. gravel outcrops), the majority of the flow would have been lateral flow above a restrictive layer. With these limitations in mind, the results were termed *effective* saturated hydraulic conductivity ($K_{eff}$). While not precise, this method allowed us to compare values for a soil property that varies across orders of magnitude.

### *Point Scale Soil Hydraulic Conductivity*

Point scale $K_{eff}$ were estimated based on a topsoil sample from one soil core per plot, as described above. Using the PSD determined by sieving and the Cilas Particle Size Analyzer, $K_{eff}$ was estimated by Retention Curve (RETC) with the van Genuchten equation using the Mualem assumption (van Genuchten et al., 1991). RETC requires the percent sand, silt, and clay according to the USDA soil classification, which defines clay as particles less than 2 µm. Since the Cilas Particle Size Analyzer only measured down to 3.9 µm, a minor amount of extrapolation was required to extend the PSD to 2 µm. In order to best account for this source of uncertainty, both a low and high clay content were estimated for each sample. RETC was utilized for both clay contents, and the average of the two $K_{eff}$ was taken to be the $K_{eff}$ for that sample. Since RETC only utilized sand, silt and clay percentages, one of the limits of this method is that it does not account for the gravel content of a soil sample.

### *Tension Infiltrometers*

After the plot infiltration experiments, mini-disk infiltrometers (Decagon Devices, Pullman, WA) were used inside the plots (after the soil profile had dried) to measure soil matrix infiltration. Tension infiltrometers are designed to measure unsaturated soil infiltration rates by exposing water that is under tension (negative pressure) to the soil surface. Water must flow from a higher potential to a lower potential. Therefore, water under tension infiltrated into the soil matrix, which had a more negative capillary pressure. However, the water did not infiltrate into the macropores, which had a less negative capillary pressure. Since the macropores remained dry, flow was restricted to the soil matrix with the infiltration rate equivalent to matrix infiltration. Saturated infiltration from the plot scale experiments represented total infiltration from both matrix and macropores. Macropore infiltration was estimated by subtracting the matrix infiltration from the total infiltration.

Suction levels of 1, 3, and 6 cm, spanning the ability of the infiltrometer, were used. Equivalent radii were calculated for each suction level with the capillary rise equation (Scott, 2000):

$$h = \frac{2\sigma \cos\theta}{r\rho_w g} = \frac{0.15}{r} \tag{6}$$

where *h* is the capillary rise or suction (L), $\sigma$ is the surface tension of water (F/L), $\theta$ is the contact angle, *r* is the equivalent radius (L), $\rho_w$ is the density of water ($M/L^3$), and $g$ is the acceleration

due to gravity ($L/T^2$). The $\theta$ was assumed to be zero and $\sigma$ was assumed to be 72.8 mN/m (for water at $20^0$C). The unit conversion coefficient of 0.15 arises for $h$ and $r$ in cm.

In order to enable the comparison between suction level and pore geometry, the following conceptual model was used. The soil pore space was conceptualized as circular tubes (not necessarily vertical) with a distribution of radii. Each pore was considered either activated (saturated) or dry. For a given suction level, the infiltration is limited to pores with radii less than or equal to the radius corresponding to the suction level. A comparison between plot infiltration data (all pores activated) and tension infiltrometer was used to differentiate between matrix and macropore flow. The simplification in this conceptualization is that it neglects flow in a thin film along a pore wall when that pore is unsaturated. Accounting for thin film flow in macropores would increase their contribution; therefore, this approach gives a conservative estimate of the impact of macropores. Soils pores have been classified as macropores (greater than 75 μm), mesopores (30 to 75 μm), and micropores (5 to 30 μm) (SSSA, 2008). In this research, macropores were defined as pore spaces with equivalent diameters of 500 μm (i.e. 6 cm capillary pressure) or more due to limitations of the infiltrometer.

The unsaturated hydraulic conductivity was calculated from the tension infiltrometer results using the method of Zhang (1997). Readings were taken until the infiltrometer reservoir was depleted (14 to 121 minutes), which was sufficient to fit the hydraulic conductivity and sorptivity to the cumulative infiltration versus time data.

## Results and Discussion

### *Barren Fork Creek*

Calculated $K_{eff}$ varied widely across sites and within sites, ranging from 0.5 to 68 cm $hr^{-1}$. At the Barren Fork Creek site, estimated $K_{eff}$ of the top layer of soil based on double ring infiltrometer experiments were 1.5 cm $hr^{-1}$ and 0.5 cm $hr^{-1}$ for the shallow gravel and deep gravel, respectively (Figure 24). While the shallow gravel location had a smaller layer of silt loam soil, the thickness of the limiting layer should not have an effect on short duration (12 to 55 min) double ring infiltrometer experiments. In effect, the double ring infiltrometer not only measures a smaller horizontal area than plot scale infiltration experiments, it also measures the effective hydraulic conductivity for a shallower depth of soil.

During plot scale infiltration experiments at the Barren Fork Creek site, hydraulic gradients ranged from 1.03 to 1.08 cm $cm^{-1}$ (Figure 24, Table 4). Infiltration rates ranged from 3.0 to 6.8 cm $hr^{-1}$ for the deep gravel plots and from 10 to 14 cm $hr^{-1}$ for the plots with shallow gravel. The calculated $K_{eff}$ data were similar, ranging from 2.9 to 6.6 cm $hr^{-1}$ for the deep gravel plots and from 9.6 to 13 cm $hr^{-1}$ for the shallow gravel plots. The pattern of higher $K_{eff}$ in the shallow gravel location compared to the deep gravel location held for both double ring infiltrometer data and plot scale data, although the magnitude of the $K_{eff}$ measured at the plot scale was an order of magnitude greater than $K_{eff}$ measured by the double ring infiltrometer. This may be due to (1) measuring at a different scale (area as well as depth of soil), (2) differences in procedure (short versus long duration), (3) using a different equation (transient versus steady-state), or (4) the double ring infiltrometer being more faithful to the one dimensional flow assumption.

Data from the plot scale and double ring experiments were compared to point scale estimates of $K_{eff}$ and the estimated permeability of the limiting layer reported by the U.S. Natural Resources Conservation Service (NRCS) for Cherokee County, Oklahoma (NRCS, 2012), which ranged from 1.5 to 5 cm $hr^{-1}$ for the Razort gravelly loam soils at the floodplain sites (Figure 28). Five out of the six plot scale data were higher than the maximum predicted by the NRCS soil survey, as well as the point scale estimates. It is also noted that the point scale estimates do not capture the variability in $K_{eff}$ shown in the plot scale data, which may be partly due to the fact that point scale estimates do not account for variability in soil structure. Within the plot scale, increasing plot size did not seem to have a strong impact on $K_{eff}$ or reduce spatial variability in $K_{eff}$. Especially for the shallow gravel formation, the plot scale (1 m by 1 m to 10 m by 10 m) appears to be within the REV.

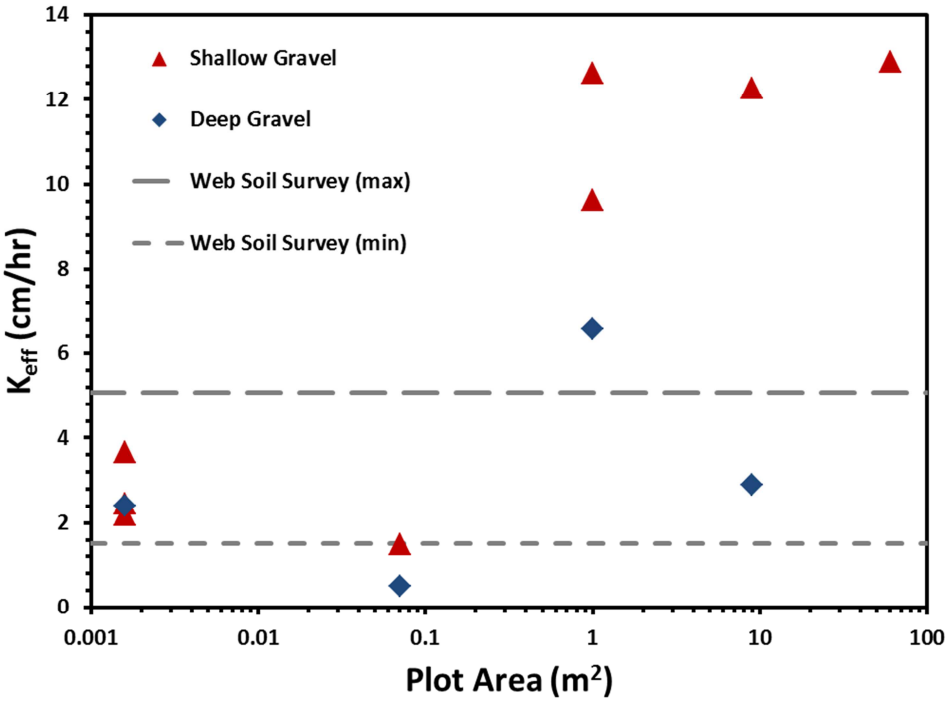


**Figure 28. Effective saturated hydraulic conductivity (Keff) data for the Barren Fork Creek floodplain site, including both point scale estimates and plot scale infiltration experiments. Double ring infiltrometer data is also included (infiltration area of 0.07 $m^2$). The expected range of infiltration rates based on the permeability of the limiting layer reported in the Natural Resources Conservation Service Soil Survey (NRCS, 2012) is shown by the dashed lines.**

In order to analyze spatial variability in the soil properties at the Barren Fork Creek site, geostatistics were performed on electrical resistivity data (Miller, 2012) which have been correlated to hydraulic conductivity (Miller et al., 2013; Miller, 2012). The geostatistical program GS+ (Gamma Design Software, LLC, Plainwell MI) was used to analyze the top (approximately 0.0 to 0.2 m below ground surface) and the second (approximately 0.2 to 0.5 m below ground surface) layers of log-transformed electrical resistivity (Ω-m). While the top layer would be closer to where the infiltration occurs, the second layer of electrical resistivity was more reliable and would usually still be within the silt loam at the Barren Fork site. Both

isotropic and anisotropic variograms were created, although the anisotropic variograms did not reveal strong directional patterns in either layer. This is in contrast to previous research which did find strong directional patterns in the deeper gravel subsoil (Miller, 2012), likely related to ancient gravel bars and abandoned stream channels. Results from the exponential isotropic model (Figure 29) showed greater variability in the top layer but a similar pattern for both layers. The range ($A_0$), beyond which data were not autocorrelated, was 27 m and 20 m for the top and second layers, respectively. These $A_0$ data may indicate the approximate scale of the $V_{max}$, where the REV ends and $K_{fs}$ begins to drift due to changing geomorphic formations. The $A_0$ from the Barren Fork Creek site were comparable to Easton (2013), who reported $A_0$ from 17 m to 34 m for infiltration rates on an Arkport fine sandy loam soil hillslope (11% average slope). An interesting comparison, though, is that Easton (2013) found the nugget to be zero in most cases for infiltration rate, where the Barren Fork Creek site had a non-zero nugget for the electrical resistivity.

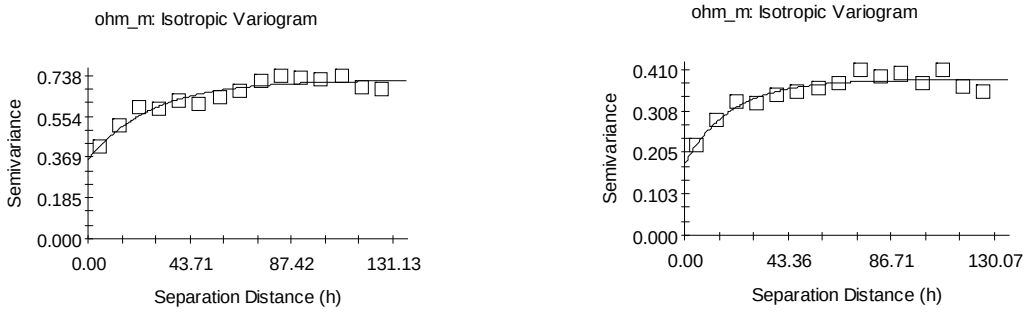


**Figure 29. Variorums for the Barren Fork Creek site based on the top (approximately 0.0 to 0.2 m below ground surface) layer (left) and the second (approximately 0.2 to 0.5 m below ground surface) layer (right) of log-transformed electrical resistivity data. The x-axis is separation distance in m.**

### *Pumpkin Hollow*

Plots at the Pumpkin Hollow field site were located in gravel outcrops and control locations (Figure 25). Gravel outcrops in the floodplain appeared to be gravel splays from a recent high flow event (on the order of a 50 year recurrence interval) rather than an exposed buried gravel bar. Soils were heterogeneous, even within a small area of a given floodplain (Figure 30). A 10 m by 10 m plot was not performed at the Pumpkin Hollow site because of insufficient water supply in the small ephemeral creek.

During the plot scale infiltration experiments, estimated hydraulic gradients ranged from 1.07 to 1.12 cm cm$^{-1}$ with calculated $K_{eff}$ ranging from 5.0 to 5.7 cm hr$^{-1}$ for the control plots and from 16 to 68 cm hr$^{-1}$ for the gravel outcrop plots (Table 4). This wide range indicates considerable heterogeneity in infiltration processes at the Pumpkin Hollow floodplain due to the occurrence of gravel outcrops. This range is remarkable considering the close proximity of the plots. For example, the 1x1β and 3x3β beta plots (Figure 25) were approximately 10 m apart and had $K_{eff}$ values of 68 and 5.7 cm cm$^{-1}$, respectively. The very high conductivity gravel outcrops achieved quasi-stead state flow quickly, resulting in relatively short (less than 5 hr) plot infiltration experiments.

Plot scale data were analyzed along with point scale calculations of $K_{eff}$ and estimates from NRCS (NRCS 2012) (Figure 31). Both point scale data and NRCS soil survey data severely underestimated the capacity of the gravel outcrops to infiltrate water. This difference indicates the need for larger scale field measurements of infiltration rate and $K_{eff}$. For example, soil survey measurements may represent a typical soil pedon but miss gravel outcrops or large macropores which may be infrequent but have a disproportionate impact on infiltration. The agreement between the point scale data and the NRCS estimates (for both the Pumpkin Hollow and the Barren Fork Creek sites) supports the idea that the NRCS data may be more representative of hydrological processes at a small scale rather than a plot or field scale.

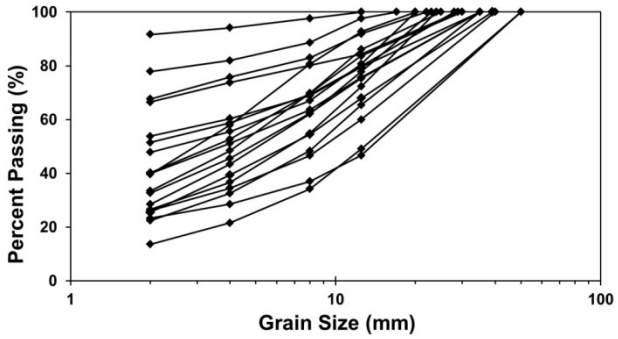


**Figure 30. Particle size distributions of Pumpkin Hollow soil core samples.**

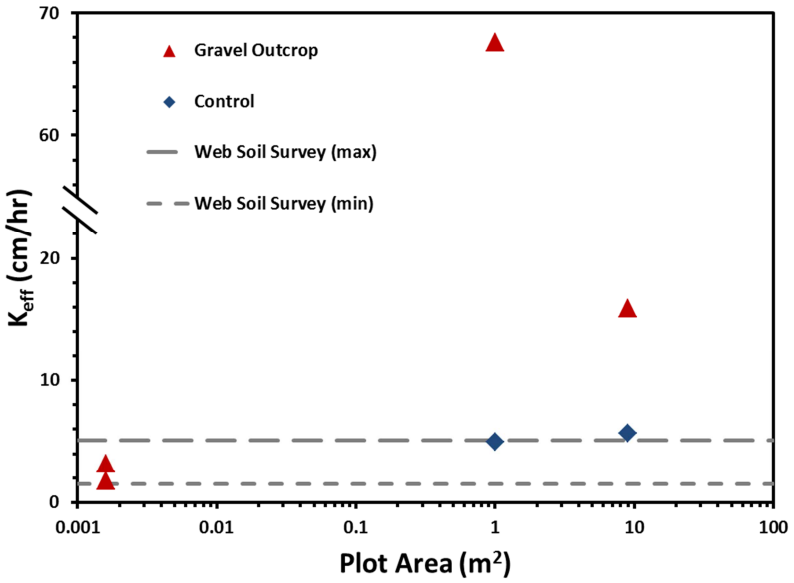


**Figure 31. Effective saturated hydraulic conductivity (Keff) data for the Pumpkin Hollow floodplain site, including both point scale estimates and plot scale infiltration experiments. The expected range of infiltration rates based on the permeability of the limiting layer reported in the Natural Resources Conservation Service Soil Survey (NRCS, 2012) is shown by the dashed lines.**

### *Clear Creek*

Infiltration plots at the Clear Creek floodplain site were located in two unique geomorphic formations (Figure 26). "Formation A," located on the west side of the creek, was very similar to the alluvial deposits at the Barren Fork Creek site with an apparently uniform layer of silt loam (0.5 to 1.0 m) above the gravel. Unlike the Barren Fork Creek site, the gravel in Formation A did contain a buried soil horizon with potential for a perched water table. "Formation B," located on the east side of the creek, was very gravelly at the surface but had enough fines mixed in to result in low infiltration rates. The streambank profile at Formation B is 3.5 m tall, with a very thick limiting layer ranging from 2.1 to 2.4 m (Table 4). At this location Clear Creek is a bedrock stream, with the water table in the alluvial aquifer being essentially at bedrock (determined by auger refusal with the Geoprobe drilling machine) during baseflow conditions.

Plot scale infiltration rates were lower than the other sites, ranging from 0.7 to 5.6 cm $hr^{-1}$ (Table 4). The correlating $K_{eff}$ data (0.6 to 5.4 cm $hr^{-1}$) were compared to the point scale data and estimates from NRCS (NRCS 2012) (Figure 32). At the Clear Creek site, $K_{eff}$ from all three data sources were comparable. However, similar to the other sites, the point scale estimates failed to capture the spatial variability in $K_{eff}$ present in these floodplains. There was a negative correlation between $K_{eff}$ and plot size at the Clear Creek site (similar to the gravel outcrop plots at the Pumpkin Hollow site). This could be due to the large variability in the data, making it difficult to discern the significance of the trend with limited data points. Additional infiltration plots would have enabled more rigorous statistics, but the effort required for plot scale infiltration experiments made a large sample size prohibitive.

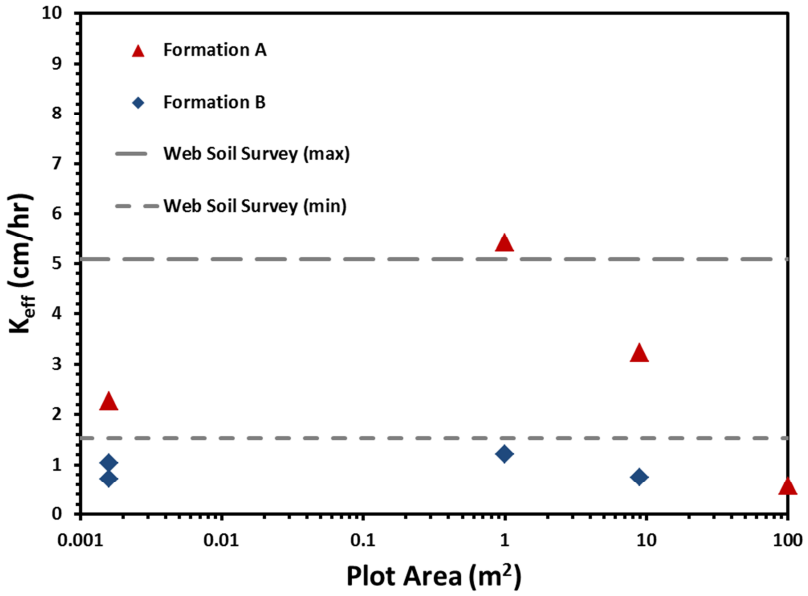


**Figure 32. Effective saturated hydraulic conductivity (Keff) data for the Clear Creek floodplain site, including both point scale estimates and plot scale infiltration experiments. The expected range of infiltration rates based on the permeability of the limiting layer reported in the Natural Resources Conservation Service Soil Survey (NRCS, 2012) is shown by the dashed lines.**

### *Impact of Macropores*

Tension infiltrometers confirmed the importance of macropore flow. Matrix infiltration (in pore space less than or equal to 500 μm) was quantified with a tension of 6 cm and was one to two

orders of magnitude lower than saturated infiltration rates (Figure 33). Macropore flow accounted for approximately 99% of the total infiltration at the Barren Fork Creek site, 85% to 87% at the Clear Creek site, and 97% to 99% at the Pumpkin Hollow site.

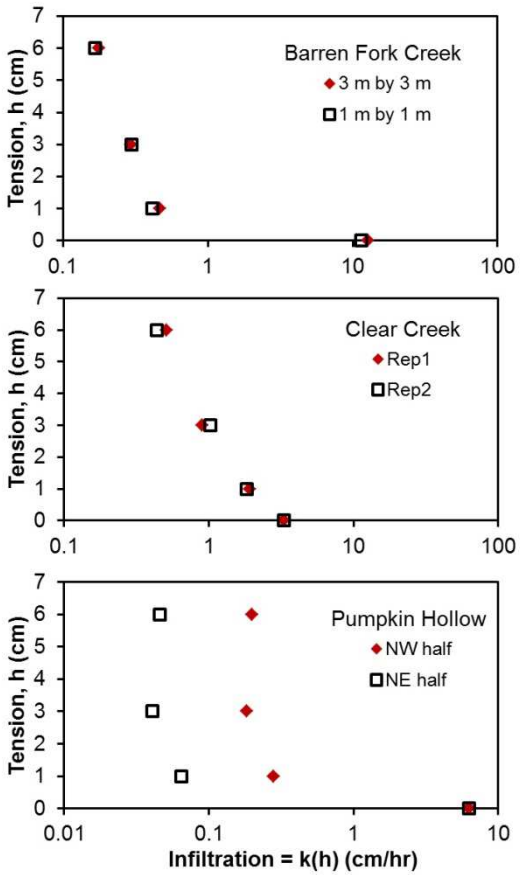


**Figure 33. Infiltration rates based on infiltration plots for saturated infiltration (h = 0 cm) and unsaturated hydraulic conductivity (k) calculated from tension infiltrometer data. Locations included gravel outcrop plots at the Barren Fork Creek site, the 3 m by 3 m control plot at the Clear Creek site, and the 3 m by 3 m control plot at the Pumpkin Hollow site.**

Observed large macropores (greater than 1 cm) did not have as much impact on infiltration as expected. For example, a 4 to 5 cm diameter macropore was observed in the 10 m by 10 m plot at the Barren Fork Creek site. Subsequent excavation revealed that the macropore descended vertically to a depth of 1.0 m, into the gravel layer, before proceeding laterally 15 cm (Figure 34). Infiltration into this single macropore was quantified to be 27.4 L $min^{-1}$ with head of 3.4 cm (the maximum achieved during the plot scale infiltration test), and up to 56.2 L $min^{-1}$ with a head of 20 cm. However, a head of 0.4 cm, designed to better simulate natural rainfall conditions, resulted in a flow of only 1.3 L $min^{-1}$. As the diameter of a macropore increases, it has a larger capacity to transport water, but at some critical diameter this capacity surpasses typical rainfall rates and flow into the macropore becomes supply limited. Macropores larger than this critical diameter do not have a larger flow rate and, assuming a typical soil pore size distribution, are less frequent. It is hypothesized that there is a dominant diameter, less than the critical diameter, which is the pore size responsible for the most infiltration, because it is large enough to have

significant flow but small enough to occur frequently. In fact, this pore size range occurs frequently enough that it can be characterized sufficiently by 1 m by 1 m plots, explaining in part why they are included in the REV.

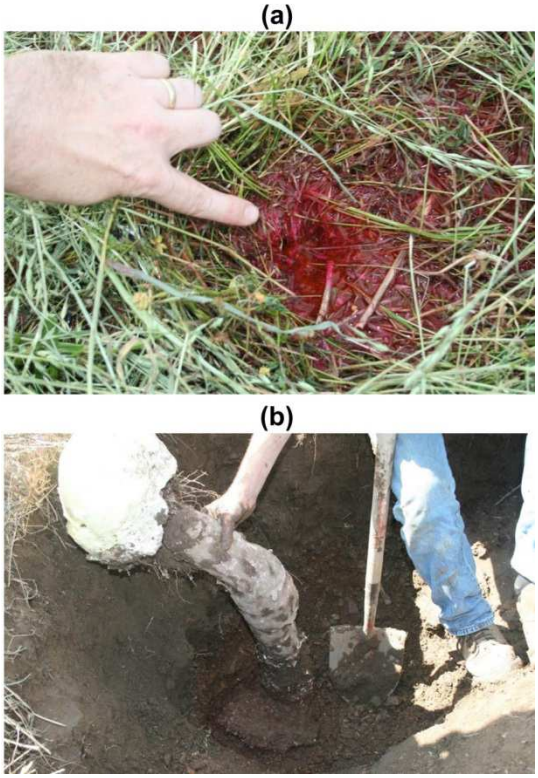


**Figure 34. Large macropore at the Barren Fork Creek site observed during plot scale infiltration experiment (a) and subsequently filled with expandable foam and excavated (b).**

### *Research Implications*

It was hypothesized that as the scale of measurement increases, measured infiltration rate and hydraulic conductivity of the topsoil will increase due to an increased likelihood of having a very large but infrequent macropore in a large plot size, and that the spatial variability will decrease, until an REV is attained (Bear, 1972; Brown et al., 2000). At all sites the $K_{eff}$ did increase until the plot scale was reached (1 m by 1 m), but $K_{eff}$ did not consistently increase or decrease as the plot scale increased from 1 m by 1 m to 10 m by 10 m. While spatial variability in $K_{eff}$ decreased as the scale increased from 1 m by 1 m to 3 m by 3 m at the Pumpkin Hollow and Clear Creek sites, the spatial variability actually increased at the Barren Fork site as the scale of measurement increased from 1 m by 1 m to 3 m by 3 m. More specifically, the $K_{eff}$ were relatively constant within the plot scale for the shallow gravel formation (Barren Fork), the control plots (Pumpkin Hollow), and Formation B (Clear Creek). Therefore, it was concluded that the plot scale (1 $m^2$ to 100 $m^2$) is generally within the REV for geomorphic formations in these alluvial floodplains. Beyond the REV, the $K_{eff}$ is expected to drift as different geomorphic formations are encountered.

In order to best characterize infiltration processes at the field scale, plot scale infiltration tests are recommended over double ring infiltrometer tests or point scale estimates. Also, since the 1 m by 1 m plot size is already within the REV, 1 m by 1 m plots are recommended. While a decrease in spatial variability can be observed for larger plot sizes at the Pumpkin Hollow and Clear Creek sites, the level of difficulty in doing plot scale infiltration measurements increases significantly at the 3 m by 3 m and especially the 10 m by 10 m scales. Instead of investing in larger plot sizes, more will be gained from investing in a higher number of 1 m by 1 m plots in order to accurately determine the mean $K_{eff}$ for a field. Plots should ideally be randomly located and at least 27 m apart (based on $A_0$ for the Barren Fork site) in order to sample different geomorphic formations. In order to evaluate the number of plots necessary, the standard error of the mean was calculated according to Steel and Torrie (1980) for each floodplain site:

$$SE = \frac{s}{\sqrt{n}} \tag{7}$$

where *SE* is the standard error of the mean, *s* is the standard deviation, and *n* is the number of plots. The *SE* is a measure of how close a sample mean is to the population mean. While $K_{eff}$ data tend to be more lognormally distributed, parametric statistics could be calculated with the small number of samples and give an indication of the level of site characterization achieved for a range of sample sizes (Table 5). For example, if three plot scale infiltration experiments were performed at each site, the standard error of the mean would be 25% of the mean at the Barren Fork Creek site, 73% of the mean at the Pumpkin Hollow site, and 53% of the mean at the Clear Creek site. The Pumpkin Hollow site would be the most difficult to characterize with a low number of plots due to the high level of heterogeneity present.

**Table 5. Statistics for effective saturated hydraulic conductivity (Keff) derived from plot scale infiltration experiments, including mean, standard deviation, and coefficient of variation, for each floodplain site. Hypothetical standard errors were calculated to evaluate the level of site characterization achieved for a range of sample sizes.**

| | Barren Fork Creek | Pumpkin Hollow | Clear Creek |
|---|---|---|---|
| Measured Data | | | |
| n | 6 | 4 | 5 |
| Mean (cm $hr^{-1}$) | 9.5 | 24 | 2.2 |
| Standard Deviation (cm $hr^{-1}$) | 4.0 | 30 | 2.1 |
| Coefficient of Variation (cm $hr^{-1}$) | 0.4 | 1.3 | 0.9 |
| Hypothetical | | | |
| n | | Standard Error of the Mean (cm $hr^{-1}$) | |
| 1 | 4.0 | 30 | 2.1 |
| 2 | 2.9 | 21 | 1.5 |
| 3 | 2.3 | 17 | 1.2 |
| 4 | 2.0 | 15 | 1.0 |
| 5 | 1.8 | 13 | 0.9 |
| 6 | 1.6 | 12 | 0.8 |

## Conclusions

Effective saturated hydraulic conductivity ($K_{eff}$) data, based on plot scale infiltration rates, were highly heterogeneous, and reached 68 cm $hr^{-1}$ on one gravel outcrop. Point scale estimates of $K_{eff}$ were significantly lower than plot scale $K_{eff}$, and also failed to capture the variability of $K_{eff}$

within a field site. The estimated permeability of the limiting layer reported by the U.S. Natural Resources Conservation Service (NRCS) Soil Survey was consistent with point scale estimates of $K_{eff}$, but was lower than plot scale $K_{eff}$ at most sites. While this research doesn't answer the question of scale impacts on infiltration definitively, the results do indicate that the scale effect should be considered. Plot scale infiltration tests are recommended over double ring infiltrometer tests or point scale estimates, although only small plots (1 m by 1 m) are necessary. For silt loam soils, infiltration was dominated by rapid macropore flow. Tension infiltrometers showed that macropore flow accounted for approximately 85% to 99% of the total infiltration. This research highlighted the difference between the conceptual infiltration model of a diffuse wetting front characterized by Richards Equation and actual infiltration in field conditions.

## (F) Plot-Scale Studies - Quantification and Heterogeneity of Phosphorus Leaching in Alluvial Floodplains (Heeren, Fox, Storm, Haggard, Penn, and Halihan, 2013, Impact of measurement scale on infiltration and phosphorus leaching in Ozark floodplains, ASABE Paper No. 131621213, St. Joseph, Mich.: ASABE.)

### A Legal Perspective on Excess Phosphorus in the Ozarks

*Arkansas et al. v. Oklahoma et al.*, 503 U.S. 91 (1992), was the first lawsuit addressing excess P loading to surface waters in the Ozark ecoregion. This case reached the U.S. Supreme Court certiorari after the Court of Appeals for the Tenth Circuit. Justice Stephens delivered the opinion for the unanimous court. *Arkansas v. Oklahoma* focused on point source pollution of the Illinois River and the application of the 1972 Clean Water Act (CWA). In particular, a Waste Water Treatment Plant (WWTP) in Fayetteville, Ark., had obtained a U.S. Environmental Protection Agency (EPA) issued permit to discharge into a tributary of the Illinois River, although Oklahoma water quality standards allowed no degradation of the Illinois River. A significant finding was that the Supreme Court upheld the EPA in requiring an upstream state to meet downstream water quality standards, based on § 401(a)(2) of the CWA (33 U.S.C. §1341(a)(2)). Even if the CWA were silent on this, according to Justice Stephens, the EPA would be justified by the Chevron Doctrine (*Chevron U.S.A. Inc. v. Natural Resources Defense Council, Inc.*, 467 U.S. 837, 842-845 (1984)). The findings of *Arkansas v. Oklahoma* continues to have a bearing on water quality in the IRW today. Total Maximum Daily Load (TMDL) standards are being developed for the IRW and will have an impact on upstream sources in Arkansas (Pryor et al., 2011).

Progress has been made in cleaning the IRW, with the Illinois River being declared a scenic river by the state of Oklahoma. Initially the EPA recommended a P standard of 0.01 mg $L^{-1}$, but Arkansas was concerned about a very low P standard limiting opportunities for growth since the Fayetteville–Springdale–Rogers Metropolitan Area is one of the fastest growing areas in the nation (Soerens et al., 2003). Based on published data by Clark et al. (2000), the P standard was established at 0.037 mg $L^{-1}$, which is the standard set for Oklahoma Scenic Rivers (OWRB, 2010). Communities in Arkansas and Oklahoma have invested more than $225 million to improve water quality (Pryor et al., 2011). Flow adjusted total phosphorus (TP) concentrations in the Illinois River near the state line (Watts, Okla.) have been decreasing since about 2002

(Haggard, 2010), which matches a known change in WWTP effluent discharge. Engle (2008) also reported reductions in WWTP loads since 2003. Also, the feasibility of water quality trading in the IRW has been evaluated (Bastian, 2011), concluding that at least five of the seven success factors for water quality trading exist in the IRW. Water quality trading, which is being advocated by the EPA (U.S. EPA, 2003), is a market based approach to solving water quality problems and has been to shown to provide significant benefits where water quality trading is feasible (Ribaudo, 2008; Yandle, 2008; Pittman, 2011; Lee and Douglas-Mankin, 2011).

In *City of Tulsa v. Tyson Foods et al.* (2003, U.S. District Court for the Northern District of Oklahoma), the city of Tulsa, Okla., filed suit against the poultry industry and the city of Decatur, whose WWTP receives most of its waste from a poultry processing plant (Soerens et al., 2003). This dispute was over the Eucha watershed which is also in the Ozark ecoregion and provides roughly half of the water supply for the city of Tulsa. The water quality in Lake Eucha had deteriorated significantly, including taste and odor problems that were attributed to algal production (Blackstock, 2003). The poultry industry has grown tremendously in the last few decades in the Ozark ecoregion of northeastern Oklahoma and northwestern Arkansas and has been a great economic benefit to local communities (Soerens et al., 2003). The poultry waste, known as poultry litter, is a valuable fertilizer and is often land applied to pastures and hay fields. However, excess poultry litter application can result in high soil P levels, resulting in high P levels in rainfall runoff to streams. Storm et al. (2001) found that anthropogenic non-point sources, including poultry litter, were responsible for 73% of the P load to Lake Eucha. Engle (2008) found that on a watershed scale mass balance of P, much more P is imported than exported. These imports are largely associated with feed for the poultry industry. While concerned with the WWTP for the city of Decatur, Okla., *Tulsa v. Tyson* was focused primarily on non-point sources of P. The lawsuit was settled in 2003 with agreements regarding the management of nutrients (including poultry litter) in the watershed, including a P index specific to the Eucha watershed mandated by the court (DeLaune et al., 2006).

At least two interesting things came out of this case. The first issue regarded the admissibility of scientific models for expert witness (Blackstock, 2003). Storm et al. (2001) presented data from the Soil and Water Assessment Tool (SWAT) model, which was used to evaluate P sources and loads in the watershed. The court applied the Daubert test for admissibility of scientific evidence, which includes four factors: capability of empirical testing, publication in a peer-reviewed journal, error rate, and acceptance in the scientific community. The court found most of the SWAT results admissible, making it the first court case to use SWAT results as scientific evidence (Blackstock, 2003).

The second issue was the application of the 1980 Comprehensive Environmental Response, Compensation, and Liability Act (CERCLA) to agriculture (Warren, 2003). In *City of Tulsa v. Tyson Foods et al.*, poultry litter was considered a hazardous substance under CERCLA. This is significant because “CERCLA provides for strict liability for any person found responsible for depositing hazardous substances in such a way as to endanger human health or safety.” The court held that a watershed could be considered a “facility”, but failed to hold poultry companies liable for “arranging” the disposal of poultry waster (Warren, 2003).

In the ongoing litigation of *Oklahoma ex rel. Edmondson v. Tyson Foods et al.* (filed June 13, 2005), Oklahoma Attorney General Drew Edmondson sued 11 poultry companies. Oklahoma sought both monetary damages and injunctive relief under CERCLA (McBride, 2011) in the Tulsa federal court. Storm et al. (2010) found that 13% of the total P load in the Illinois River was directly from poultry litter, and 11% from elevated soil P levels. U.S. District Judge Gregory Frizzell found that the Cherokee Nation was a required party and dismissed the monetary claims of the suit for lack of standing. This was upheld by the Tenth Circuit (McBride, 2011), meaning that Tyson likely escaped paying damages and leaving Oklahoma limited to the pursuit of an injunction. Judge Frizzell later ruled that poultry litter is not a solid waste, but the Attorney General has appealed and the Tenth Circuit Court of Appeals (Denver, Colo.) will hear the case.

## Phosphorus Transport Mechanisms

Considerable research has been performed on properties of point soil samples, and some research has been done on transport in undisturbed soil columns (Ulen, 1999; Maguire and Sims, 2002; Djodjic et al., 2004). However, relatively few studies on both infiltration and transport have been done at the plot scale where infiltration and transport may be controlled by heterogeneity present at various scales (Nelson et al., 2005).

For example, research is currently limited in understanding the potential significance of connectivity between phosphorus (P) in surface runoff and groundwater and nutrient movement from the soil to groundwater in watersheds with cherty and gravelly soils (Fox et al., 2011; Heeren et al., 2011; Mittelstet et al., 2011). While optimum crop growth requires a range of P above 0.2 mg/L, preventing surface water enrichment generally requires P to be below 0.03 mg/L (Pierzynski et al., 2005). In fact, surface waters in the Ozark ecoregion in particular may have a threshold closer to 0.01 mg/L (D.E. Storm, 2012, personal communication). While surface runoff is considered to be the primary transport mechanism for P (Gburek et al., 2005), the potential for P leaching is commonly estimated based on point-measurements of soil test phosphorus (STP) or measurements of the sorption capability of disturbed soil samples representing the soil matrix. However, in many riparian floodplains, gravel outcrops and macropores are present (Heeren et al., 2011). These gravel outcrops can lead to extremely high infiltration rates, some of which are reported to be on the order of 10 cm/min (Sauer and Logsdon, 2002; Saur et al., 2005). In fact, infiltration of P-laden water during high flow discharges that exceed bankfull events can infiltrate in the floodplain subsoil and migrate back to the streams. Djodjic et al. (2004) performed experiments on P leaching through undisturbed soil columns, and stressed the need to consider larger-scale leaching processes due to soil heterogeneity. They stated that the "water transport mechanism through the soil and subsoil properties seemed to be more important for P leaching than soil test P value in the topsoil. In one soil, where preferential flow was the dominant water transport pathway, water and P bypassed the high sorption capacity of the subsoil, resulting in high losses."

A common best management practice in riparian floodplains is riparian buffers or vegetative filter strips (VFS), utilized to reduce sediment, nutrient, and pesticide loading to nearby surface water bodies (Popov et al., 2005; Reichenberger et al., 2007; Sabbagh et al., 2009). Reduced transport occurs through contact between dissolved phase solutes with vegetation in the filter strip, and/or by reducing flow velocities to the point where eroded sediment particles can settle out of the water. In floodplains with significant heterogeneity such as macroporosity and chert or

gravel soils, the effectiveness in preventing loading to nearby streams and rivers may be less than originally anticipated if a significant transport pathway occurs into the shallow groundwater and then bypasses the filtering capacity of the VFS. The impact of such heterogeneous infiltration and leaching is not known at this time.

Several studies have been conducted to investigate subsurface P transport at alluvial floodplain sites in the Ozark ecoregion. Injection tests were performed which showed preferential flow paths and physical non-equilibrium in the coarse gravel vadose and phreatic zones (Fuchs et al., 2009; Heeren et al., 2010). Preferential flow paths were interpreted to be buried gravel bars (Miller, 2012; Miller et al., 2013; Heeren et al., 2010). Long-term flow and transport monitoring was performed at two floodplain sites, showing aquifer heterogeneity and large scale bank storage of stream water, as well as large scale, stage-dependent transient storage of P in the alluvial aquifer (Heeren et al., 2011; Heeren et al., 2013b). Redox conditions were not expected to be a concern for characterizing P fate and transport because of the lack of anaerobic conditions due to the high porosity and excessive drainage of both the soil and subsurface materials in Ozark floodplains. For example, dissolved oxygen (DO) of the groundwater at the Barren Fork Creek site (measured with a ProODO DO meter, YSI Inc., Yellow Springs, Ohio) ranged from approximately 8 mg $L^{-1}$near the creek to 4 mg $L^{-1}$ up to 100 m from the creek (Heeren, 2012). Subsurface P transport rates in the alluvial aquifers were quantified and found to be significant compared to surface runoff P transport rates on well managed pastures (Mittelstet et al., 2011).

## Methods

### *Alluvial Floodplain Sites*

The Barren Fork Creek site (latitude: 35.90°, longitude: -94.85°) was immediately downstream of the Eldon Bridge U.S. Geological Survey (USGS) gage station 07197000. With a watershed size of 845 $km^2$, the Barren Fork Creek site was a fourth order stream with a historical median discharge of 3.6 $m^3 s^{-1}$. The study area at the Barren Fork Creek was located on the outside of a meander bend which was being actively eroded by the stream (Midgley et al., 2012). The soils were classified as Razort gravelly loam underlain with alluvial gravel deposits. Thickness of the loam ranged from 0.3 to 2.0 m, with dry bulk densities ranging from 1.3 to 1.7 g $cm^{-3}$. The Barren Fork Creek site was a hay field and had not received fertilizer for several years. Soil hydraulic studies on these soil types have shown that subtle morphological features can lead to considerable differences in soil water flow rates (Sauer and Logsdon, 2002). Fuchs et al. (2009) described some of the soil and hydraulic characteristics of the Barren Fork Creek floodplain site, including estimates of hydraulic conductivity for the gravel subsoil between 140 and 230 m $d^{-1}$ based on falling head trench tests. Heeren et al. (2010) performed a tracer injection into a PFP, identified as a buried gravel bar, at the Barren Fork Creek site. Local transient storage and physical nonequilibrium was observed as evidenced by the elongated tails of breakthrough curves in some observation wells due to physical heterogeneity in the aquifer materials.

The Pumpkin Hollow floodplain site was also located in the Ozark ecoregion of northeastern Oklahoma (latitude: 36.02°, longitude: -94.81°). A small tributary of the Illinois River, Pumpkin Hollow Creek was a first order ephemeral stream in its upper reaches. The entire floodplain was 120 to 130 m across at the research site, with an estimated watershed area of 15 $km^2$. The land use at the site was pasture for cattle. The Pumpkin Hollow field site was a combination of Razort gravelly loam and Elsah very gravelly loam, although infiltration experiments were limited to the

Razort gravelly loam soils. Topsoil thickness ranged from 0 to 3 cm, and bulk densities of the cohesive material were in the range of 1.3 to 1.5 g $cm^{-3}$.

The Clear Creek alluvial floodplain site was located just west of Fayetteville, AR in the Arkansas River Basin and flows into the Illinois River (latitude: 36.13°, longitude: 94.24°). The total drainage area was 199 $km^2$ for the entire watershed. Land use in the basin was 36% pasture, 34% forest, 27% urban and 3% other. Soils were loamy and silty, deep, moderately well drained to well drained (U.S. EPA, 2009), and generally contained less chert or gravel than the Barren Fork Creek or Pumpkin Hollow floodplain sites. A fourth order stream with a flow of approximately 0.5 $m^3$ $s^{-1}$ at the study site, the area of the watershed above that point was 101 $km^2$. The land use in the study area was pasture and consisted of Razort gravelly loam soils. Thickness of the top loam layer ranged from 0.3 to 2.0 m, with dry bulk densities ranging from 1.5 to 1.7 g $cm^{-3}$.

Background soil P levels were characterized with the Mehlich III soil test P (STP) method. At each site, 25-30 samples were collected from random locations in a large area around the infiltration plots. Each sample was collected with a STP coring tool from the top 15 cm of topsoil. Samples were all added to a bucket, mixed thoroughly, and three representative samples (i.e., three replicates) were taken from the bucket and delivered to Oklahoma State University Soil, Water, and Forage Analytical Laboratory (SWFAL) for testing. The Barren Fork Creek and Pumpkin Hollow Creek sites had STPs of 33 and 120 mg $kg^{-1}$, respectively. The Clear Creek site had an STP of 32 mg $kg^{-1}$ in "Formation A" on the west side of the creek (Table 6).

Topsoil samples from both the Clear Creek and Barren Fork Creek sites were analyzed with flow-through P sorption isothermal titration calorimetry (ITC) experiments (see earlier section). Results showed that the dominant P sorption reaction was ligand exchange onto Al/Fe oxides/hydroxides, with a lesser degree of precipitation, and that P removal for both soils was limited by physical nonequilibrium instead of chemical nonequilibrium (sorption kinetics).

### *Soil Cores and Chemical Analysis*

Soil core samples were collected with a Geoprobe Systems (Salina, KS) 6200 TMP (Trailer-mounted Probe) direct-push drilling machine using a dual-tube core sampler with a 4.45 cm opening. The sampler opening (size) limited the particle size that could be sampled from the coarse gravel subsoil and large cobbles occasionally clogged the sampler resulting in incomplete cores for that depth interval.

Before phosphorus injection experiments, background soil cores were collected during the installation of the observation wells from one to four wells per plot. After an experiment was complete, an additional two to four soil cores were collected from within the plot in order to document the change in the soil profile (e.g. soil P levels) due to the infiltration of P laden water. Geoprobe soil coring typically began at the soil surface and proceeded to or past the water table (0.5 to 3.5 m below ground surface). After the 10 m by 10 m plots, a hand soil sampler (0 to 45 cm) was used in order to take a higher number of samples across the plot.

In the lab soil cores were sliced into approximately 15 cm samples representing different vertical horizons. All soils were air-dried and sieved with a 2 mm sieve prior to analysis. Soil pH and electrical conductivity (EC) were determined with a 1:1 soil to de-ionized water solution, stirred

with a glass rod and equilibrated for 30 minutes. All soil samples (approximately 670) were analyzed for soluble Al, Fe, Ca, Mg, and Mn oxide content for characterization of P sorption and retardation potential. Water extractions for water soluble (WS) P, Al, Fe, Ca, Mg, and Mn were conducted by shaking air dried soil with de-ionized water (soil:solution ratio of 1:10) end over end for 1 h, followed by centrifuging (2500 rpm at 5 min) and filtration with 0.45 µm Millipore membrane. Extracted Al, Fe, Ca, Mg, and Mn were analyzed by inductively coupled plasma atomic emission spectroscopy (ICP-AES).

Oxalate extractable P, Al, Fe, and Mg ($P_{ox}$, $Al_{ox}$, $Fe_{ox}$, $Mg_{ox}$; 1:40 soil: 0.2M acid ammonium oxalate (pH 3), 2 h reaction time in the dark; McKeague and Day, 1966) were determined for all "topsoil" (approximately the top 10-15 cm of the soil core) samples ($n$ = 64). The P, Ca, Mg, K, Al, and Fe from ammonium oxalate extractions were measured using ICP-AES. Amorphous Al and Fe are considered to be the most reactive soil fraction in regard to P sorption. The ratio of ammonium oxalate extractable P to (Al + Fe) (all values in mmol $kg^{-1}$) was expressed as:

$$DPS_{ox} = \left[\frac{P_{ox}}{Al_{ox}+Fe_{ox}}\right] 100\% \quad (8)$$

where $DPS_{ox}$ is the ammonium oxalate degree of P saturation. Note that this is exactly the same as the traditional soil degree of phosphorus saturation (DPS) calculations (Pautler and Sims, 2000) except without the empirical constant α which is used to relate soil P sorption capacity to $Al_{ox}$ and $Fe_{ox}$ and the denominator acts to express the effective total soil P sorption maximum. The α value was unknown, so no α value was used. Beauchemin and Simard (1999) noted that various studies have applied an α value of 0.5 to all soils, regardless of soil properties. The authors claimed that the α value is empirical and needs to be determined for each soil type and experimental conditions. In addition, Beck et al. (2004) recommended that the α value be omitted from the DPS calculation.

Nine P adsorption isotherms were performed on background vadose zone samples from each geomorphic formation at each site, from various depths, and across a range of textures. The P adsorption isotherms were conducted by adding different levels of P (0.0, 0.5, 1.0, 10, and 20 mg P/L) to two gram soil samples, equilibrating for 24 hr (shaking), and measuring P in the equilibrated, centrifuged, and filtered samples by ICP-AES. Using a linear least squares model, data were fit to the Langmuir equation (Šejna et al., 2011):

$$q = \frac{bK_L C_{eq}}{1+K_L C_{eq}} = \frac{k_s C_{eq}}{1+K_L C_{eq}} \quad (9)$$

where $q$ is the mass sorbed (mg P / kg soil), $b$ is traditionally understood to be the maximum sorption (mg P / kg soil), $K_L$ is traditionally understood to be the sorption affinity (L water / mg P), $C_{eq}$ is the equilibrium solution P concentration (mg P / L water), and $k_s$ is the initial slope of the curve (at low $C_{eq}$) of the isotherm (L water / kg soil).

### *Berm Installation and Hydraulics*

Measuring infiltration rates and/or leaching of solutes at a plot scale is difficult, especially for high hydraulic conductivity soils, without innovative field methods. In this research, the berm method (Heeren et al., 2013a) was used to confine infiltration plots and maintain a constant head

of water, with plot sizes ranging from 1 m by 1 m to 10 m by 10 m. Four to six infiltration experiments were performed at each site with plots selected to represent a range of infiltration rates at each floodplain site (Table 6). Plots were located on relatively level areas in order to minimize the variation in water depth across the plot. Larger plots were required to have smaller slopes to ensure that the entire plot could be inundated without overflowing the berm.

**Table 6. Infiltration experiments at three alluvial floodplain sites in the Ozark ecoregion.**

| Site | Date | Plot Size | Geomorphic Formation | Duration (h) | Infiltration (cm/hr) | Total Wells | Wells containing: $Cl^-$ | Wells containing: RhWT[a] | Wells containing: DP[a] |
|---|---|---|---|---|---|---|---|---|---|
| Clear Creek | 4/12/11 | 1x1 | Formation A | 41 | 5.6 | 4 | --[b] | 4 | 0 |
| Clear Creek | 4/12/11 | 3x3 | Formation A | 41 | 3.3 | 8 | --[b] | 4 | 1 |
| Clear Creek | 7/27/11 | 1x1 | Formation B | 48 | 1.3 | 8 | 0 | 0 | 0 |
| Clear Creek | 7/27/11 | 3x3 | Formation B | 45 | 0.8 | 12 | 0 | 0 | 0 |
| Clear Creek | 5/21/12 | 10x10 | Formation A | 52 | 0.6 | 14 | 5 | -- | 0 |
| Pumpkin Hollow | 5/4/11 | 1x1 | Control | 32 | 5.3 | 8 | 3 | 3 | 3 |
| Pumpkin Hollow | 5/5/11 | 3x3 | Gravel outcrop | 2.8 | 18 | 12 | 5 | 9 | 5 |
| Pumpkin Hollow | 6/1/11 | 1x1 | Gravel outcrop | 4.3 | 74 | 4 | 4 | 4 | 1 |
| Pumpkin Hollow | 6/2/11 | 3x3 | Control | 24 | 6.3 | 12 | --[c] | 0 | 0 |
| Barren Fork | 6/30/11 | 1x1 | Shallow gravel | 22 | 10 | 5 | 5 | 5 | 2 |
| Barren Fork | 6/30/11 | 3x3 | Shallow gravel | 22 | 13 | 12 | 10 | 10 | 3 |
| Barren Fork | 7/13/11 | 1x1 | Deep gravel | 46 | 6.8 | 4 | 1 | 1 | 0 |
| Barren Fork | 7/13/11 | 3x3 | Deep gravel | 48 | 3.0 | 12 | 5 | 5 | 0 |
| Barren Fork | 5/7/12 | 10x10 | Shallow gravel | 4 | 13 | 14 | 13 | -- | 5 |
| Barren Fork | 6/6/12 | 1x1 | Shallow gravel | 86 | 14 | 7[d] | 2 | 2 | 0 |

[a] RhWT = Rhodamine WT; DP = Dissolved phosphorus.
[b] Chloride added but not sufficiently above background concentrations in the stream and groundwater.
[c] Not measured.
[d] Four wells were located around the plot. Three additional wells were located approximately 5 to 10 m downgradient based on transient electrical resistivity data after infiltration commenced.

Each berm was constructed of four sections of 15 cm vinyl hose which were attached to $90^0$ steel elbows and surrounded the infiltration gallery (Figure 35). A shallow trench (3 to 5 cm) was cut through the thatch layer and a thick bead of liquid bentonite was used to create a seal between the berm and the soil.

High density polyethylene tanks (4.9 $m^3$ and 0.76 $m^3$) were used to mix stream water and solutes. A combination of 5.1-cm diameter PVC with manual valves and garden hoses with float valves were used to deliver water (gravity fed) from the tanks to the plots. When a tank was nearly empty, flow was temporarily stopped while the tank was refilled and solutes were added and mixed. The largest plot sizes (10 m by 10 m) required continuous pumping and solute injection directly into the pump hose using Dosatron® injectors (D8R, Dosatron®, Clearwater, FL) instead of using tanks for mixing. Constant heads in the plots were maintained (Heeren et al., 2013a) between 3 and 10 cm. Depth to the water table ranged from 50 cm at the Pumpkin Hollow site up to 350 cm at the Clear Creek site.

Chloride ($Cl^-$) was used as a conservative (nonsorbing) tracer. Target tracer concentrations were 100 to 200 mg/L KCl (correlating to 48 to 95 mg/L $Cl^-$), depending on background EC levels. The RhWT was a slightly-sorbing dye and was introduced into the plots at concentrations of 10 to 100 mg/L. The RhWT was regarded as a slightly sorbing solute since the soils were expected to have organic matter contents of less than 2%, resulting in a minor amount of Rhodamine WT sorption. The RhWT served as a visual indicator of hydraulic connectivity in the observation wells.

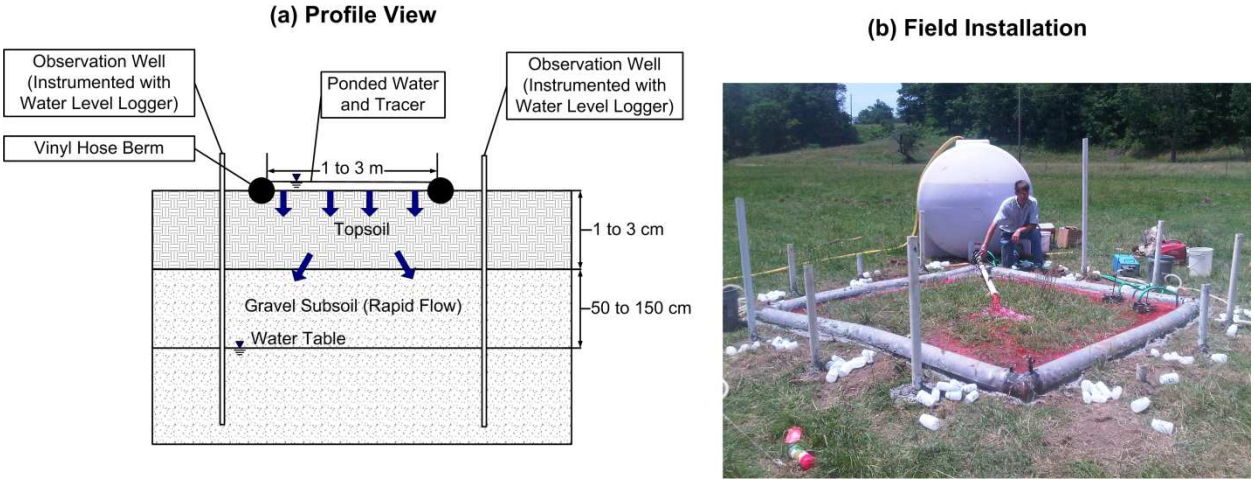


**Figure 35. Berm infiltration method, including vinyl berms to contain water-solute solution and observation wells for collecting groundwater samples: (a) design and (b) implementation at the Pumpkin Hollow floodplain site.**

Phosphorus (highly sorbing) concentrations of 3 to 10 mg/L (corresponding to 10 to 32 mg/L as phosphate) were used to represent poultry litter application rates (typically used as a fertilizer source in the Ozark ecoregion) in the range of 2 to 8 Mg/ha (1 to 3 ton/acre). Previous research (Kleinman et al., 2002; DeLaune et al., 2004; Schroeder et al., 2004) has observed dissolved reactive phosphorus in the range of 5 to 40 mg/L in runoff from recently applied poultry litter in the range of 2 to 14 Mg poultry litter per hectare.

Phosphorus concentrations were achieved by adding phosphoric acid ($H_3PO_4$), which deprotonated to $H_2PO_4^-$ and $HPO_4^{2-}$ in the slightly acidic solution. The inflow water in the plot was sampled throughout the experiment to verify these concentrations. The source stream water was also sampled over time to quantify its P contribution. Redox conditions were not expected to be a concern for characterizing P fate and transport because of the lack of anaerobic conditions due to the high porosity and excessive drainage of both the soil and subsurface materials in Ozark floodplains. For example, dissolved oxygen (DO) of the groundwater at the Barren Fork Creek site (measured with a ProODO DO meter, YSI Inc., Yellow Springs, Ohio) ranged from approximately 8 mg/L near the creek to 4 mg/L up to 100 m from the creek.

In general, the P concentration in the groundwater samples were expected to decrease relative to input P concentration due to sorption as the water infiltrates down through the soil profile.

Without considering macropore and/or gravel outcrop infiltration, P would be expected to only minimally, if at all, travel through the soil matrix. Comparisons in the breakthrough curves, peak concentrations, and the time to reach the peak concentration in the monitoring wells between the $Cl^-$, RhWT and P concentrations, which possess different sorption properties, were made to indicate differences in sorptive rates.

### *Monitoring with Electrical Resistivity*

Vertical electrical resistivity profiles were collected at the floodplain sites during the infiltration/leaching experiments (Figure 36). Electrical resistivity was utilized to characterize the heterogeneity of the unconsolidated floodplain sediments, as well as locate the infiltrating plume of water and solutes by detecting changes in pore water. Electrical resistivity imaging (ERI) is based on measuring the electrical properties of near-surface earth materials (McNeill, 1980), which vary with grain size, pore-space saturation, pore water solute content, and electrical properties of the minerals. The electrical behavior of earth materials is controlled by Ohm's law, in which current is directly proportional to voltage and inversely proportional to resistance. Generally, electrical current travels readily in solute-rich pore water and poorly in air. In addition, cations adsorbed to soil particle surfaces reduce resistivity. Clay particles have a large surface area per volume and thus have generally lower resistivity (1 to 100 Ω-m) compared to sands or gravels (10 to 800 Ω -m), which are lower than limestone bedrock (McNeill, 1980). ERI data were collected using a SuperSting R8/IP Earth Resistivity Meter (Advanced GeoSciences Inc., Austin, Tex.) with 28-electrode arrays. The profiles employed electrode spacings of 0.5 m with an associated depth of investigation of approximately 3 m, which included the vadose zone as well as the top of the water table. The resistivity sampling with the SuperSting R8/IP, and subsequent inversion utilized a proprietary routine devised by Halihan et al. (2005), which produced higher resolution images than conventional techniques. The ERI resistivity data were interpolated into grids and contoured using Surfer 8 (Golden Software, Inc., Golden, CO). Inverted and interpolated resistivity data were termed “ERI profiles” as opposed to “ERI pseudosections”, which were the raw resistivity measurements as collected in the field. Differencing was used to display the percent difference in resistivity between the background image and images collected during the infiltration experiments.

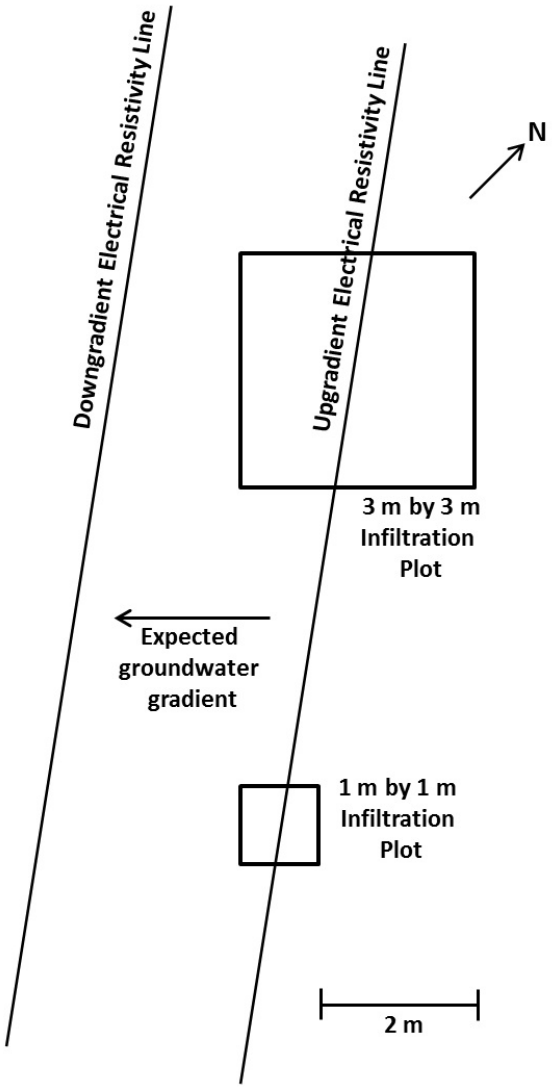


**Figure 36. Electrical resistivity design for the deep gravel plots at the Barren Fork Creek site.**

### *Observation Wells and Sample Analysis*

Suction cup lysimeters were not used because of the difficulty of installation in gravelly soils, risk of creating preferential flow paths in vadose zone, and low likelihood of intercepting macropores. Since there are not currently any effective techniques for taking measurements from underneath a given plot in these gravelly soils, observation wells were installed every 0.5 to 2 m around the perimeter of the plots to collect groundwater samples (Figure 35). When a confining layer was present (based on soil cores), shallow observation wells were installed with alternating wells designed specifically to sample from the vadose zone (where perched water was expected) and the remaining observation wells designed specifically to sample from the phreatic zone.

A Geoprobe Systems drilling machine (6200 TMP, Kejr, Inc., Salina, KS), which has been found to be effective in coarse gravel soils (Heeren et al., 2011; Miller et al., 2011), was used to install

four to twelve observation wells around each plot. Boreholes were sealed with liquid bentonite to avoid water and solutes leaking down the borehole. Low flow sampling with a peristaltic pump was used to collect water samples from the top of the water table (Heeren et al., 2011). Sampling intervals were adjusted based on EC meter readings (to detect elevated levels of $Cl^-$) and visual observations of RhWT with the goal of having enough data points to characterize the breakthrough curve.

Well and plot water samples, as well as background stream and groundwater samples, were stored and transported on ice and were tested for both P and $Cl^-$ at the AWRC Water Quality Laboratory on the University of Arkansas campus. The soluble reactive phosphorus (SRP) samples were filtered within 24 hours of sampling using 0.45 µm filters and acidified with sulfuric acid. The SRP was determined colorimetrically with the modified ascorbic acid method (EPA Method 365.2; Murphy and Riley, 1962) with a spectrophotometer (DU 720, Beckman Coulter, Indianapolis, IN, minimum detection limit of 0.002 mg/L). Autoclave per-sulfate digestions (APHA 4500 PJ) were performed on unfiltered total phosphorus (TP) samples in order to dissolve any particulate or organic P. The TP (minimum detection limit of 0.01 mg/L) was then determined colorimetrically with the modified ascorbic acid method. The $Cl^-$ concentrations were determined with ion chromatography (minimum detection limit of 0.16 mg/L). The RhWT samples were analyzed at Oklahoma State University with a Trilogy laboratory fluorometer (Turner Designs, Inc., Sunnyvale, CA, minimum detection limit of 0.01 mg/L).

Automated water level loggers (HoboWare, Onset Computer Corp., Cape Cod, MA, water level accuracy of 0.5 cm) were used to monitor water levels at one minute intervals in the observation wells, plots, and tanks, from which flow rates were calculated. An additional logger was used to monitor atmospheric pressure. Logger data were processed with HoboWare Pro software, which accounted for changes in atmospheric pressure as well as changes in water density due to temperature.

## Results and Discussion

### *Soil Chemical Properties*

All isotherms (Table 7) were performed on soil samples from observation well installation, i.e. on soil samples that were collected before the P injection experiment occurred at that location. The equilibrium P concentration (EPC) is the solution P concentration where zero net P sorption or desorption occurs. Therefore when the solution surrounding a soil or sediment is greater than its respective EPC, the sediment is expect to sorb P. If the solution P concentration is less than the EPC, then the material is expected to desorb P. The EPC, estimated as the x-intercept of the relationship between solution P concentration and sorbed P, ranged from 0.38 to 3.09 mg $L^{-1}$ (Table 7). The P injection solutions typically had a P concentration around 3 mg $L^{-1}$; therefore P sorption was expected to occur with P desorption occurring only minimally.

Both water soluble extractions and ammonium oxalate extractions (Table 8) were performed on all topsoil samples (approximately the top 10-15 cm of the soil core). Soil cores were taken during well installation (before the infiltration experiments) and inside the plot (after the infiltration experiments) in order to compare soil P concentrations before and after the injection of P laden water.

**Table 7. Soil physical and chemical properties for samples selected for phosphorus adsorption isotherms.**

| Floodplain Site | Plot | Borehole | Depth (cm) | Geomorphic Formation* | Soil type | 8 mm sieve (% retained) | EPC ($mg\ L^{-1}$) | $K_L$ ($L\ mg^{-1}$) | b ($mg\ kg^{-1}$) | $k_s$ ($L\ kg^{-1}$) |
|---|---|---|---|---|---|---|---|---|---|---|
| *Soil Physical Characteristics and Isotherms* | | | | | | | | | | |
| Barren Fork | 1x1α | Well B | 64-83 | Shallow gravel | Silt loam, some gravel | 6 | 0.94 | 0.006 | 1213 | 7.3 |
| Barren Fork | 3x3α | Well K | 142-163 | Shallow gravel | Sandy gravel | 43 | 1.08 | 0.002 | 1285 | 2.6 |
| Barren Fork | 1x1β | Well C | 74-90 | Deep gravel | Silt loam | 0 | 0.77 | 0.037 | 319 | 11.8 |
| Pumpkin Hollow | 3x3α | Well T | 0-17 | Outcrop | Silt loam, some gravel | 6 | 0.73 | 0.014 | 527 | 7.4 |
| Pumpkin Hollow | 1x1β | Well D | 78-105 | Outcrop | Gravel, some sand | 53 | 0.69 | 0.035 | 268 | 9.4 |
| Pumpkin Hollow | 3x3β | Well J | 40-80 | Control | Gravelly silt loam | 26 | 0.71 | 0.039 | 263 | 10.2 |
| Clear Creek | 1x1α | Well C | 156-175 | Formation A | Gravel, some sand | 56 | 3.09 | 0.004 | 2237 | 8.9 |
| Clear Creek | 3x3α | Well I | 39-63 | Formation A | Silt loam, some gravel | 5 | 0.38 | 0.083 | 253 | 21.0 |
| Clear Creek | 3x3β | Well "O" | 64-83 | Formation B | Silt loam | -- | 1.70 | 0.003 | 1525 | 4.6 |

| Floodplain Site | Plot | Borehole | Depth (cm) | pH | EC ($\mu S\ cm^{-1}$) | Water Soluble P ($mg\ kg^{-1}$) | Al ($mg\ kg^{-1}$) | Fe ($mg\ kg^{-1}$) | Ca ($mg\ kg^{-1}$) | Mg ($mg\ kg^{-1}$) | Mn ($mg\ kg^{-1}$) |
|---|---|---|---|---|---|---|---|---|---|---|---|
| *Soil Chemical Properties* | | | | | | | | | | | |
| Barren Fork | 1x1α | Well B | 64-83 | 6.3 | 26 | 2.8 | 799 | 113.1 | 74 | 18 | 2.7 |
| Barren Fork | 3x3α | Well K | 142-163 | 6.4 | 10 | 2.7 | 321 | 89.4 | 17 | 10 | 1.7 |
| Barren Fork | 1x1β | Well C | 74-90 | 6.4 | 23 | 2.3 | 381 | 106.7 | 64 | 16 | 2.2 |
| Pumpkin Hollow | 3x3α | Well T | 0-17 | 6.5 | 148 | 5.5 | 250 | 116 | 102 | 22 | 1.5 |
| Pumpkin Hollow | 1x1β | Well D | 78-105 | 7.3 | 37 | 3.2 | 419 | 184 | 65 | 24 | 3.3 |
| Pumpkin Hollow | 3x3β | Well J | 40-80 | 6.9 | 37 | 2.1 | 209 | 97 | 35 | 12 | 1.0 |
| Clear Creek | 1x1α | Well C | 156-175 | 6.8 | 10 | 7.6 | 2561 | 586.7 | 64 | 61 | 1.1 |
| Clear Creek | 3x3α | Well I | 39-63 | 6.2 | 35 | 1.4 | 139 | 55.4 | 19 | 6 | 1.0 |
| Clear Creek | 3x3β | Well "O" | 64-83 | 6.2 | 13 | 5.6 | 331 | 163.4 | 20 | 17 | 1.5 |

**Table 8. Soil chemical properties for the topsoil (approximately the top 10-15 cm of the soil core) at each plot location for both before and after the water and solute infiltration experiments. Data include electrical conductivity (EC) and the Degree of P Saturation (DPS), which was calculated based on the molar concentrations of the ammonium oxalate extract.**

| Floodplain Site | Plot | P Injection | n | pH | EC ($\mu S\ cm^{-1}$) | Water Soluble ($mg\ kg^{-1}$) | | | | | | Ammonium Oxalate ($mg\ kg^{-1}$) | | | | DPS (%) |
|---|---|---|---|---|---|---|---|---|---|---|---|---|---|---|---|---|
| | | | | | | P | Al | Fe | Ca | Mg | Mn | P | Al | Fe | Mg | |
| Barren Fork Creek | 1x1α | Before | 2 | 6.3 | 97 | 4.6 | 192 | 40 | 41 | 9 | 1.3 | 223 | 621 | 2,050 | 101 | 12.0 |
| | | After | 1 | 6.3 | 325 | 7.5 | 71 | 39 | 123 | 18 | 2.4 | 300 | 604 | 2,296 | 160 | 15.3 |
| | 3x3α | Before | 2 | 6.5 | 139 | 5.2 | 321 | 66 | 39 | 12 | 2.0 | 246 | 704 | 2,535 | 102 | 11.1 |
| | | After | 3 | 6.5 | 134 | 4.9 | 198 | 52 | 51 | 10 | 1.0 | 269 | 643 | 2,373 | 129 | 13.1 |
| | 1x1β | Before | 2 | 6.0 | 129 | 3.3 | 108 | 35 | 81 | 11 | 2.2 | 223 | 714 | 2,691 | 140 | 9.7 |
| | | After | 2 | 6.4 | 91 | 3.8 | 209 | 57 | 38 | 10 | 0.8 | 233 | 669 | 2,765 | 90 | 10.1 |
| | 3x3β | Before | 2 | 6.1 | 112 | 3.0 | 95 | 42 | 86 | 11 | 1.3 | 230 | 674 | 2,647 | 119 | 10.3 |
| | | After | 2 | 6.3 | 139 | 1.8 | 202 | 43 | 32 | 7 | 1.0 | 204 | 570 | 2,388 | 90 | 10.3 |
| | 1x1γ | Before | 1 | 6.9 | 235 | 6.7 | 157 | 37 | 40 | 9 | 1.3 | 248 | 630 | 2,476 | 154 | 11.9 |
| | | After | 4 | 6.7 | 213 | 20.7 | 155 | 75 | 86 | 14 | 1.4 | 321 | 509 | 1,902 | 96 | 19.6 |
| | 10x10 | Before | 1 | 6.1 | 93 | 5.7 | 90 | 45 | 87 | 14 | 2.8 | 246 | 706 | 2,486 | 176 | 11.2 |
| | | After | 6 | 6.1 | 97 | 6.8 | 137 | 67 | 65 | 14 | 2.2 | 252 | 687 | 2,424 | 148 | 11.8 |
| Pumpkin Hollow | 1x1α | Before | 2 | 6.3 | 87.2 | 11.1 | 212 | 100 | 66 | 19 | 3.9 | 163 | 604 | 1,252 | 106 | 11.8 |
| | | After | 1 | 6.5 | 159 | 15.5 | 206 | 105 | 89 | 24 | 3.5 | 268 | 582 | 1,676 | 187 | 16.8 |
| | 3x3α | Before | 2 | 6.8 | 102.3 | 5.2 | 353 | 168 | 98 | 26 | 4.4 | 129 | 582 | 1,439 | 87 | 8.6 |
| | | After | 2 | 7.0 | 88.5 | 4.0 | 251 | 129 | 87 | 20 | 3.0 | 56 | 286 | 764 | 43 | 7.2 |
| | 1x1β | Before | 3 | 6.4 | 99.6 | 5.8 | 197 | 119 | 89 | 19 | 4.9 | 160 | 601 | 8,846 | 105 | 7.7 |
| | | After | 1 | 6.2 | 182 | 3.6 | 152 | 74 | 104 | 16 | 4.4 | 179 | 627 | 1,740 | 100 | 10.6 |
| | 3x3β | Before | 1 | 6.8 | 43 | 2.2 | 203 | 92 | 55 | 14 | 1.4 | 89 | 649 | 986 | 64 | 6.9 |
| | | After | 2 | 6.2 | 318.5 | 11.5 | 157 | 76 | 123 | 19 | 2.4 | 240 | 712 | 1,399 | 145 | 15.0 |
| Clear Creek | 1x1α | Before | 1 | 5.4 | 242 | 1.9 | 73 | 32.5 | 38 | 9 | 0.8 | 196 | 630 | 1,724 | 114 | 11.7 |
| | | After | 2 | 6.0 | 107.1 | 3.4 | 61.6 | 28.5 | 37 | 7 | 1.0 | 247 | 855 | 1,918 | 114 | 12.0 |
| | 3x3α | Before | 2 | 5.4 | 306.1 | 3.8 | 62.5 | 27.9 | 89 | 18 | 1.8 | 276 | 804 | 1,767 | 221 | 14.9 |
| | | After | 2 | 5.5 | 240.2 | 1.3 | 68.8 | 31.6 | 65 | 11 | 0.8 | 235 | 767 | 1,929 | 146 | 12.1 |
| | 1x1β | Before | 1 | 5.8 | 101 | 9.2 | 55 | 32.0 | 42 | 7 | 3.3 | 280 | 900 | 1,054 | 92 | 17.3 |
| | | After | 2 | 6.5 | 120.4 | 7.0 | 122.3 | 67.9 | 39 | 8 | 3.0 | 427 | 1064 | 1,757 | 102 | 19.5 |
| | 3x3β | Before | 3 | 5.9 | 79.0 | 13.0 | 51.2 | 25.7 | 36 | 8 | 3.2 | 455 | 1120 | 1,213 | 141 | 22.9 |
| | | After | 2 | 6.5 | 137.4 | 8.5 | 528.0 | 301.7 | 42 | 39 | 2.0 | 515 | 1042 | 1,250 | 118 | 27.2 |
| | 10x10 | Before | 2 | 5.9 | 48.1 | 3.3 | 137.1 | 79.2 | 46 | 11 | 3.1 | 196 | 740 | 1,998 | 114 | 9.8 |
| | | After | 5 | 6.1 | 122.9 | 5.9 | 92.7 | 48.8 | 71 | 9 | 3.0 | 251 | 737 | 2,139 | 113 | 12.4 |

### *Water Levels*

Infiltrating water either reached the water table before moving laterally or lateral movement in the vadose zone was induced by a confining layer. Water table elevations in phreatic zone wells were used to discern the presence of a groundwater mound (Figure 37). Sharp decreases indicate the times when fluid samples were collected and the rate of recovery of the piezometric surface gives a qualitative indication of hydraulic conductivity.

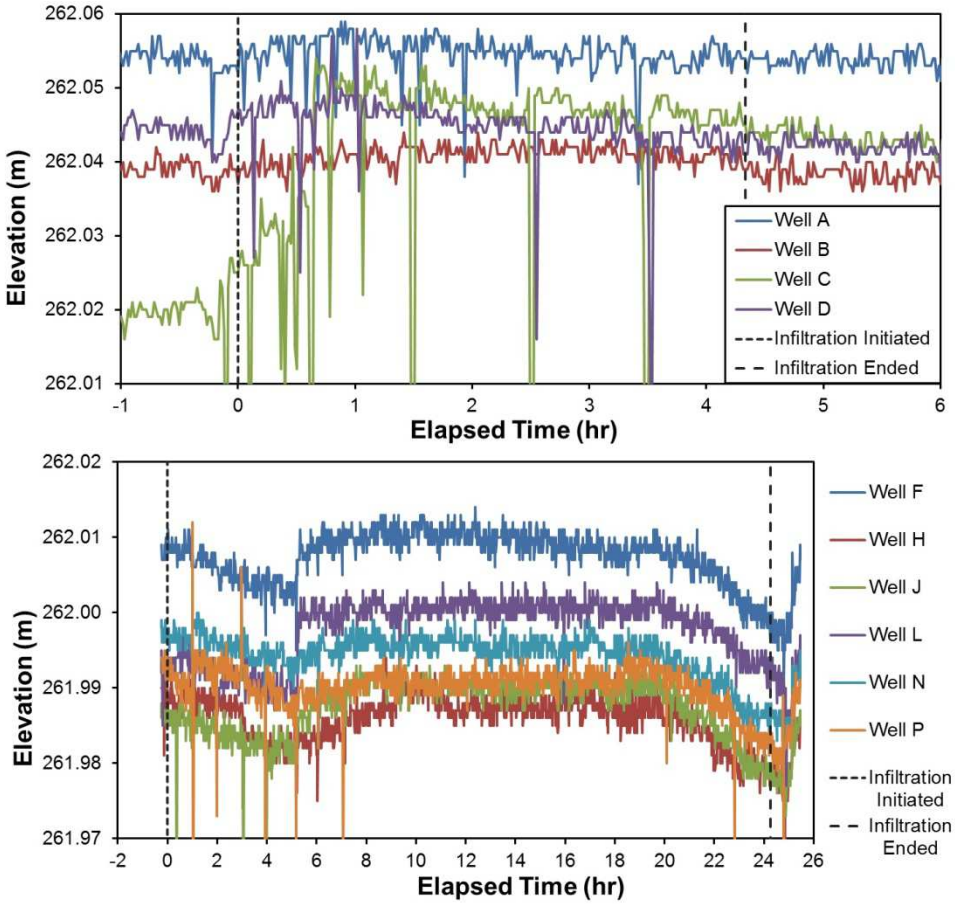


**Figure 37. Water levels in phreatic zone observation wells of the 1 m by 1 m gravel outcrop infiltration plot (June 1, 2011) and the of 3 m by 3 m control infiltration plot (June 2, 2011) at the Pumpkin Hollow floodplain site.**

### *Transport*

Rhodamine WT and $Cl^-$ were observed in no wells in some plots to all wells in other plots, while detection of P ranged from no wells to nearly half of the wells for a given plot (Table 6). Response times ranged from 18 min to greater than 48 hr. Infiltration and leaching appear to correlate weakly to topsoil thickness and stream order.

For each solute, the concentration ratio ($C_r = C / C_0$) between the concentration in the well ($C$) and the concentration injected into the plot ($C_0$) was used to examine breakthrough curves (BTCs) (Figure 38). Concentration ratios began at background levels (near zero) and generally increased with time, approaching unity for $Cl^-$ in some cases. Within a well, the $Cl^-$

(conservative) BTC generally began first, followed by RhWT (slightly sorbing), and finally P (highly sorbing) (Figure 38, Table 9).

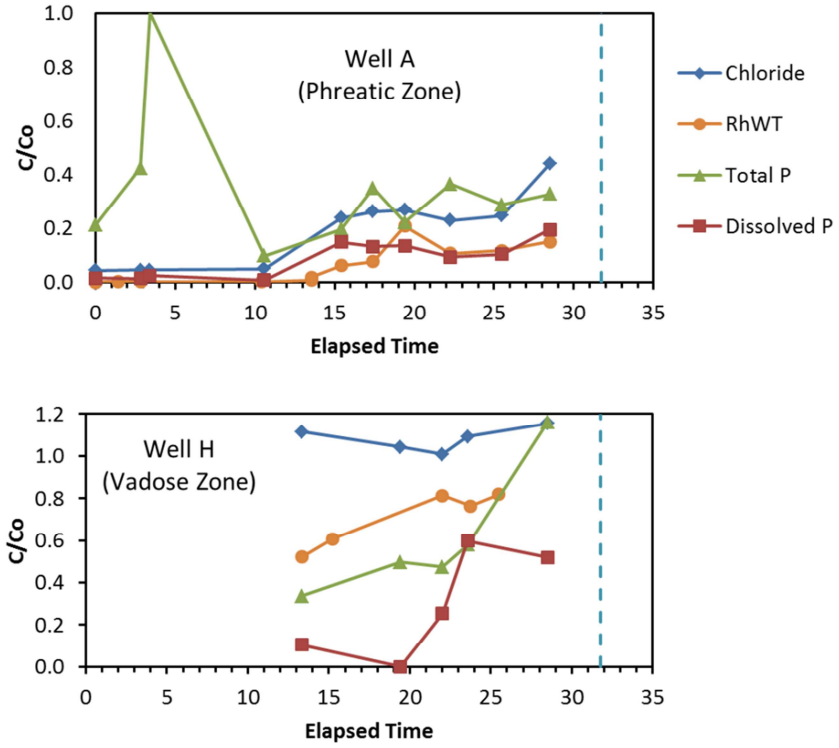


**Figure 38. Concentration ratio ($C/C_o$) for two of the observation wells for the Pumpkin Hollow gravel outcrop 1 m by 1 m (top, May 4, 2011) and 3 m by 3 m (bottom, May 5, 2011) infiltration experiments.**

For observation wells in the vadose zone, sample collection was not possible until a sufficient level of water had perched, at which point concentrations were usually high (Figure 38, Table 9). In vadose zone wells, dilution was expected to be limited to displaced water from the unsaturated zone, so the $C_r$ of a conservative tracer should be near 100%.

For the Barren Fork Creek shallow gravel plots (June 30, 2011), the RhWT and $Cl^-$ concentrations increased by the second sample after the start of the experiment, which was approximately two hours after initiating the leaching. In fact, slight increases in concentrations of both RhWT and $Cl^-$ were observed after the first sample in some wells, which was taken approximately thirty minutes to one hour after the start of the experiment. Groundwater concentrations reached approximately 50% of the injected $Cl^-$ concentration at a breakthrough time less than two hours from the initiation of infiltration. Samples were collected from the water table approximately 300 cm below the surface, meaning the $Cl^-$ had an advective transport rate, or pore velocity, up to 150 cm/hr. Combining measured infiltration rates of 11 to 13 cm/hr with an estimated porosity of 0.5 results in a pore velocity of only 24 cm/hr assuming uniform matrix flow. This indicates the importance of macropore flow, transporting water and solutes an order of magnitude faster than the average soil infiltration rate at the Barren Fork Creek site.
During the May 5, 2011, infiltration experiment at Pumpkin Hollow (3 m by 3 m outcrop), RhWT was observed in the stream approximately 15 m from infiltration plot in less than 1.7 hr

after initiation infiltration. The $C_r$ of RhWT in the stream near the seep face reached 0.02 (Table 9).

**Table 9. Transport data by well for the 1 m by 1 m (May 4, 2011, control, 32 hr duration, 5.3 cm/hr infiltration) and 3 m by 3 m (May 5, 2011, gravel outcrop, 2.8 hr duration, 18 cm/hr infiltration) plots at the Pumpkin Hollow floodplain site.**

| | | | Detection Time (hr) | | | Time to Peak (hr) | | | Peak Concentration Ratio | | |
|---|---|---|---|---|---|---|---|---|---|---|---|
| Plot | Well | Zone | $Cl^-$ | RhWT[a] | DP[a] | $Cl^-$ | RhWT | DP | $Cl^-$ | RhWT | DP |
| 1x1 | A | Phreatic | 15 | 14 | 15 | >29 | 19 | >29 | 0.44 | 0.21 | 0.19 |
| | B | Vadose | -- | 14 | -- | 29 | >29 | >29 | 1.04 | 0.35 | 0.21 |
| | C | Phreatic | >29 | >29 | >29 | >29 | >29 | >29 | -- | -- | -- |
| | D | Vadose | remained dry | | | | | | | | |
| | E | Phreatic | >29 | >29 | >29 | >29 | >29 | >29 | -- | -- | -- |
| | F | Vadose | remained dry | | | | | | | | |
| | G | Phreatic | >29 | 26 | >29 | >29 | 26 | >29 | -- | 0.001 | -- |
| | H | Vadose | 13 | 13 | 13 | 29 | >26 | 24 | 1.16 | 0.82 | 0.60 |
| 3x3 | I | Vadose | 0.7 | 0.5 | 0.8 | 1.4 | 0.8 | 0.8 | 0.51 | 0.49 | 0.03 |
| | J | Phreatic | >3.1 | 0.7 | >3.1 | >3.1 | 0.8 | >3.1 | -- | 0.0003 | -- |
| | K | Vadose | remained dry | | | | | | | | |
| | L | Phreatic | >3 | 0.7 | >3 | >3 | 1.1 | >3 | -- | 0.004 | -- |
| | M | Vadose | remained dry | | | | | | | | |
| | N | Phreatic | 0.6 | 0.6 | 0.6 | 1.5 | 0.8 | 0.8 | 0.58 | 0.28 | 0.06 |
| | O | Vadose | -- | 0.7 | -- | 1.0 | 1.0 | >1.0 | 0.67 | 0.36 | 0.14 |
| | P | Phreatic | >2.9 | 0.7 | >2.9 | >2.9 | 2.9 | >2.9 | -- | 0.01 | -- |
| | Q | Vadose | 1.1 | 0.6 | 1.1 | 2.2 | >1.8 | >3.0 | 0.75 | 0.32 | 0.30 |
| | R | Phreatic | >2.9 | >2.9 | >2.9 | >2.9 | >2.9 | >2.9 | -- | -- | -- |
| | S | Vadose | 0.8 | -- | 0.8 | 0.8 | 1.1 | 1.6 | 0.80 | 0.40 | 0.13 |
| | T | Phreatic | >2.9 | >2.9 | >2.9 | >2.9 | >2.9 | >2.9 | -- | -- | -- |
| | Seep | Stream | -- | -- | >2.9 | 2.3 | 2.3 | >2.9 | 0.08 | 0.02 | -- |

[a] RhWT = Rhodamine WT; DP = Dissolved phosphorus.

Spatial variability in flow and transport data was significant. Advection along the regional groundwater gradient generally resulted in higher concentrations on the down-gradient side of the plots (Figure 39). The soils in the alluvial floodplain were extremely heterogeneous, which corroborates previous research (Miller et al., 2010; Heeren et al., 2011). Even wells only 1 m apart showed significant variation in $Cl^-$ (Figure 39).

At the Pumpkin Hollow 3 m by 3 m control plot (June 2, 2011), 1.5 m of infiltration occurred over 24 hr. With a shallow water table (0.9 to 1.0 m below ground surface), the infiltrating water must have moved laterally beyond the wells (0.5 m from the edge of the plot), especially when considering porosity. Yet, RhWT was never observed in any of the 12 observation wells, with observation wells in the phreatic zone spaced from 2 to 3 m apart. Either the flow must have been occurring at a small enough scale to flow between the well spacing, or RhWT sorption to organic matter was sufficient to reduce concentrations to below the minimum detection limit (over three orders of magnitude less than the plot RhWT concentration).

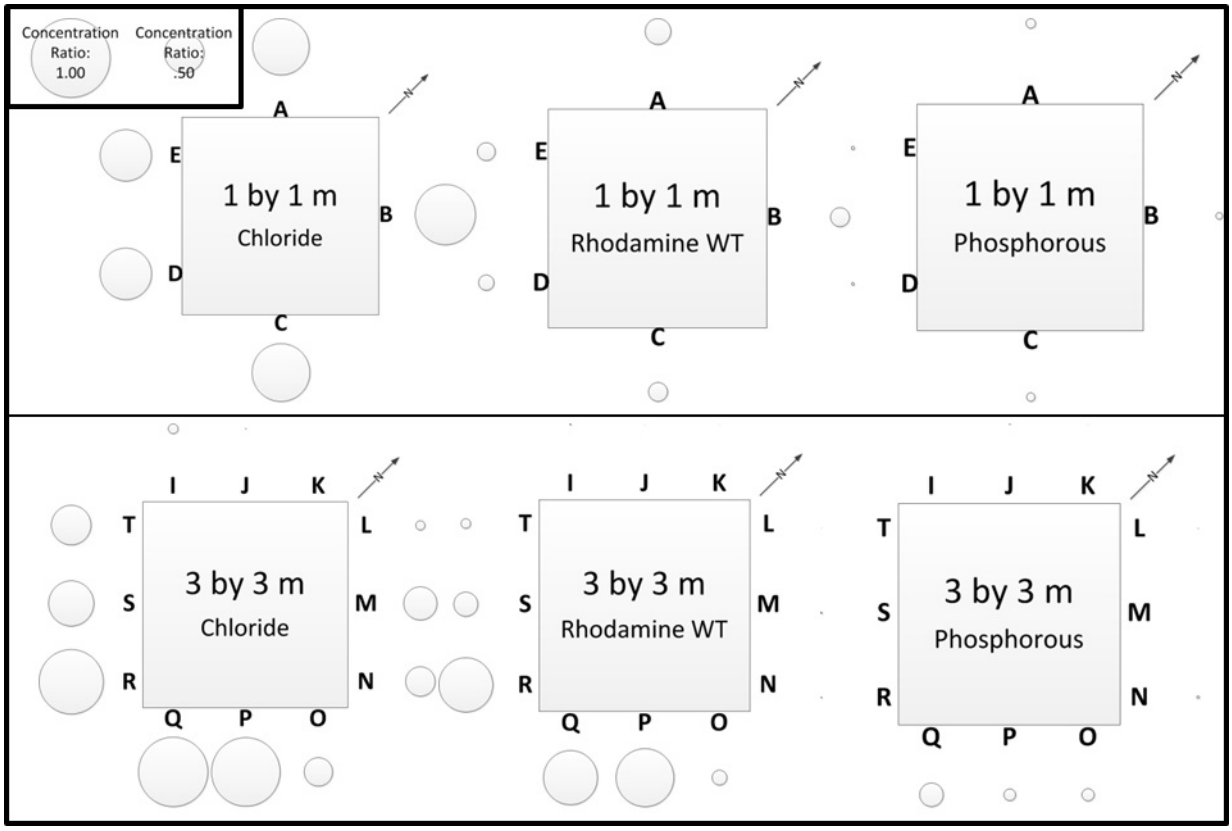


**Figure 39. Maximum concentrations of samples from each well for the Barren Fork Creek shallow gravel plots. Note that the plots are not drawn to scale. Size of the circle around each given well represents the concentration.**

### *Electrical Resistivity Imaging of Infiltration Plume*

Transient electrical resistivity results showed downward (Figure 40) and lateral (Figure 41) migration of the water and $Cl^-$ plume. For the Barren Fork Creek deep gravel plots, $Cl^-$ was detected in the water table (3 m below ground surface) only 7 hr after the initiation of infiltration for both the 1 m by 1 m and 3 m by 3 m plots. Yet the ERI data shows only 1 to 2 m of infiltration after 19 hr. This indicates that rapid flow and transport may be occurring in macropores which only represent a small volume of the soil column, possible escaping detection by the electrical resistivity equipment. It is also possible that the gravel may have remained mostly unsaturated (except for fingering) while transporting all of the water delivered to it by the silt loam (top 1 m of soil profile). The limited downward movement may also indicate some lateral migration, which would be consistent with the plume observed in the lateral line located 1.5 to 2.5 m down gradient from the edge of the plots (Figures 36 and 41).

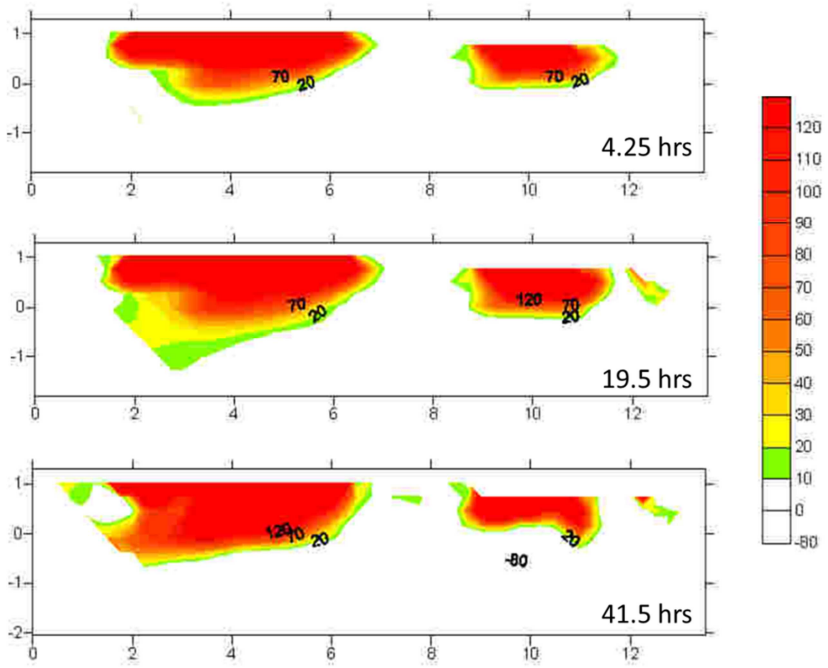


**Figure 40. Vertical profile (y-axis is elevation in m) of percent difference in electrical resistivity of the upgradient lateral line (Figure 36) through the center of the 3 m by 3 m plot (left) and the 1 m by 1 m plot (right) of deep gravel formation at the Barren Fork site, July 13, 2011. Horizontal axis is distance along the electrical resistivity line. Time is the elapsed time from the onset of infiltration.**

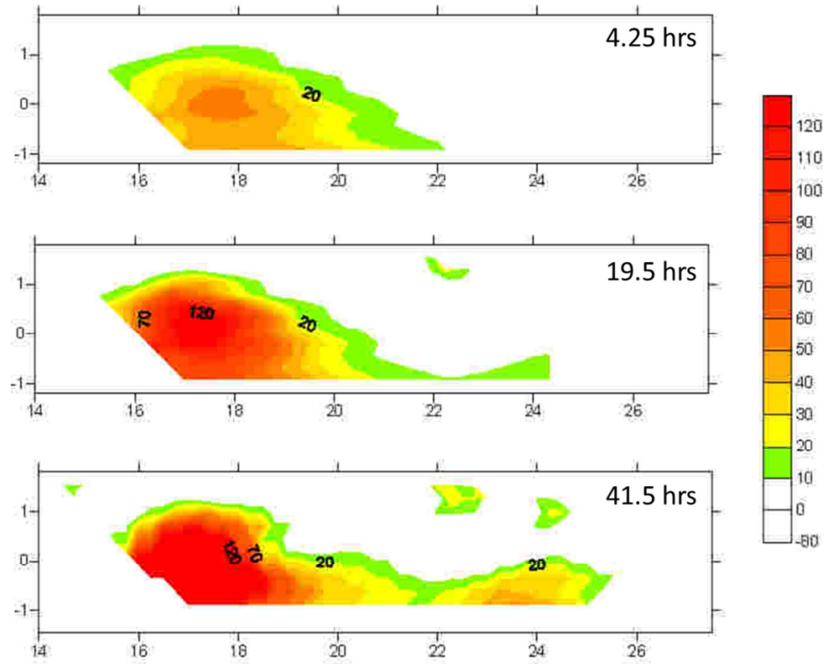


**Figure 41. Vertical profile (y-axis is elevation in m) of percent difference in electrical resistivity of the down gradient lateral line (Figure 36) 3 m down gradient of the center of the 3 m by 3 m plot (left) and the 1 m by 1 m plot (right) of deep gravel formation at the Barren Fork Creek site, July 13, 2011. Horizontal axis is distance along the electrical resistivity line. Time is the elapsed time from the onset of infiltration.**

### Implications

Plot scale experiments simulated field conditions more realistically compared to smaller infiltrometers and laboratory testing. Highly heterogeneous flow and transport indicated that the soils in the floodplains of the Ozark ecoregion are highly complex and not homogeneous. Infiltration rates in gravel outcrops were up to 70 cm/hr. This research highlighted the difference between the conceptual infiltration model of a diffuse wetting front characterized by Richards Equation and actual infiltration in field conditions. Elevated chloride, RhWT, and P concentrations were observed in specific groundwater samples, showing that even a highly sorbing contaminant can be transported through the topsoil and the gravelly subsoils. Since floodplains are hydrologically well-connected to alluvial aquifers and streams in gravelly watersheds, a higher level of agricultural stewardship may be required for floodplains than upland areas. This has implications for the development of best management practices specifically for floodplains in the Ozark ecoregion due to their close proximately and connectedness to streams.

## (G) Plot-Scale Studies - Finite Element Modeling of Phosphorus Leaching (Freiberger, Heeren, and Fox, 2013, Finite element modeling of phosphorus leaching through floodplain soils dominated by preferential flow pathways, ASABE Paper No. 1583250, St. Joseph, Mich.: ASABE.)

Phosphorus is an important nutrient for crop growth and development, but overloading of freshwater systems with phosphorus can induce significant algae growth. Algal blooms and cyanobacteria outbreaks contribute to hypoxic waters and fish kills, as well as reduce the quality of water for consumption and recreational use. Phosphorous (P) transport has been assumed to take place primarily in surface runoff, although a growing collection of research indicates that subsurface P transport can be significant (Osborne and Kovacic, 1993; Cooper et al., 1995; Gburek et al., 2005; Fuchs et al., 2009). Large scale bank storage of P-laden stream water during high flow discharges can result in P-laden groundwater in alluvial aquifers which migrates back to the stream during baseflow conditions (Heeren et al., 2011). These subsurface P transport rates in Ozark floodplains have been shown to be comparable to surface runoff P transport rates (Mittelstet et al., 2011). In many gravelly floodplains, gravel outcrops and macropores are present resulting in high infiltration rates, some of which are reported to be on the order of 70 cm/hr. It has been shown that in porous media with heterogeneous flow properties, the majority of the flow can occur in small preferential flow paths (Gotovac et al., 2009; Najm et al., 2010). Djodjic et al. (2004) performed experiments on P leaching through undisturbed soil columns, and stressed the need to consider larger-scale leaching processes due to soil heterogeneity.

The objective of this research was to evaluate the effectiveness of state of the art variably saturated flow and transport modeling tools to simulate the effects of heterogeneity in porous media on solute leaching. The role of mobile-immobile interactions for solute transport is also demonstrated. Results from this work were used to develop long-term simulations to predict P transport through these soil profiles under different management regimes.

## Methods and Materials

### *Barren Fork Creek Field Site*

The Barren Fork Creek floodplain site was located in the Ozark region of northeastern Oklahoma, which is characterized by karst topography, including caves, springs, sink holes, and losing streams. The erosion of carbonate bedrock (primarily limestone) by slightly acidic water has left a large residuum of chert gravel in Ozark soils, with floodplains generally consisting of coarse chert gravel overlain by a mantle of gravelly loam or silt loam (Figure 42). Topsoil depth in the floodplains ranged from 1 to 300 cm in the Oklahoma Ozarks, and generally increased with increasing stream order. Common soil series include Elsah (frequently flooded, 0-3% slopes) in floodplains; Healing (occasionally flooded, 0-1% slopes) and Razort (occasionally flooded, 0-3% slopes) in floodplains and low stream terraces; Britwater (0-8 % slopes) on high stream terraces; and Clarksville (1-50%) on bluffs.

At the Barren Fork Creek site, located five miles east of Tahlequah, Oklahoma (latitude: 35.90°, longitude: -94.85°) and just downstream of the Eldon U.S. Geological Survey (USGS) gage station (07197000), soils were Razort gravelly loam. The silt loam layer was from 30 to 200 cm thick, and the chert gravel layer, ranging from 3 to 5 m in thickness, extended down to limestone bedrock. The gravel subsoil, classified as coarse gravel based on the Wentworth scale, consists of approximately 80% (by mass) of particle diameters greater than 2.0 mm, with an average particle size ($d_{50}$) of 13 mm (Fuchs et al., 2009). Estimates of hydraulic conductivity for the gravel subsoil range between 140 and 230 m/d based on falling-head trench tests (Fuchs et al., 2009). The gravel layer itself is a complex alluvial deposit (Figure 42) that includes both clean gravel lenses associated with rapid flow and transport (Fox et al., 2011) as well as layers of fine gravel that can cause lateral flow in the silt loam and subsequent seepage erosion (Correll et al., 2013). The anisotropic horizontal layering results in a propensity for lateral flow.

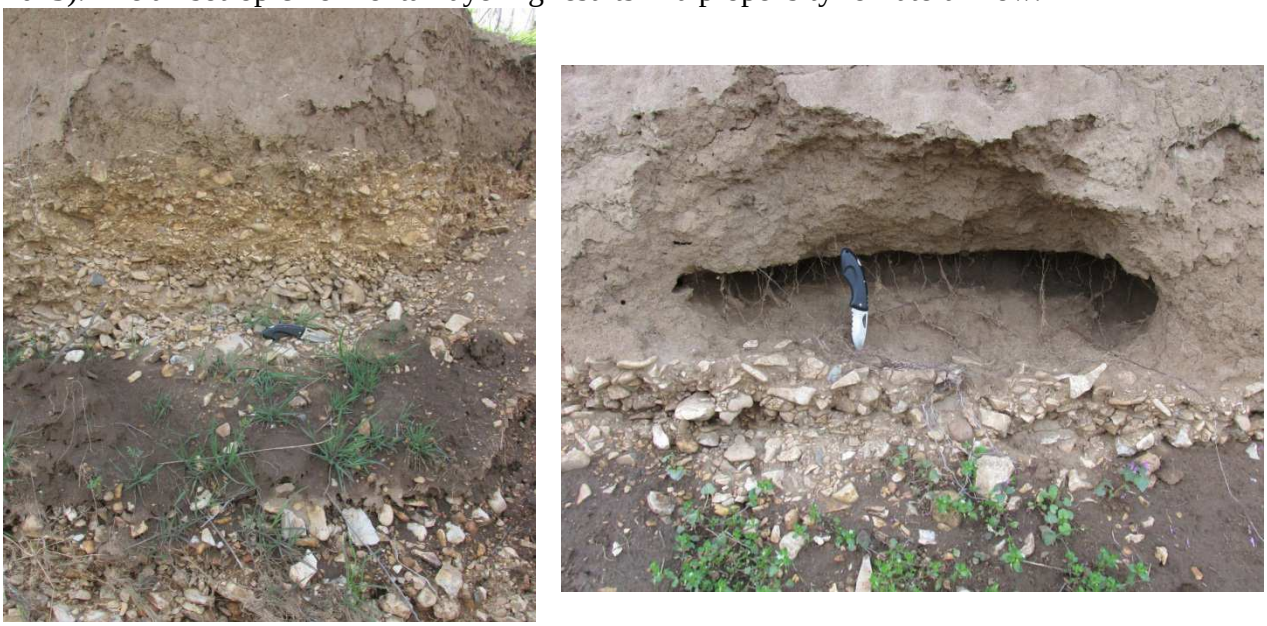

**Figure 42. Streambank at the Barren Fork Creek field site including the bank profile (left) and a seepage undercut (right). Note the sloughed material in the bottom of each picture from recent bank failures. These complex alluvial deposits include both clean gravel lenses associated with rapid flow and transport (left) as well as fine gravel lenses that can cause lateral flow and seepage erosion.**

### *Soil Profile Characterization*

Previous geophysical research was used to characterize the soil profile at the Barren Fork Creek floodplain site (Heeren et al., 2010, 2011; Mittelstet et al. 2011; Miller, 2012). Resistivity mapping involves measuring the electrical properties of near-surface earth materials, which vary with grain size, mineral type, solute content of pore water, and pore-space saturation. Miller (2012) collected electrical resistivity data using a SuperSting R8/IP Earth Resistivity Meter (Advanced GeoSciences Inc., Austin, TX) with a 56-electrode array. Two-dimensional electrical resistivity imaging (ERI) transects were acquired at multiple locations with a 1 m electrode spacing, with an associated depth of investigation of 11 m, and utilized a proprietary routine devised by Halihan et al. (2005) for the resistivity sampling and subsequent inversion. The ERI data from 87 to 94 m along the Barren Fork main roll-along (Figure 43) were used as the ERI base for the modeling. Detailed electrical resistivity data for the Barren Fork Creek site are reported in the appendix of Miller (2012).

Miller (2012) developed a positive linear relationship ($R^2 = 0.57$) to correlate ERI data to hydraulic conductivity using a vadose zone borehole permeameter designed for coarse gravel (Miller et al., 2011). Using the conversion factor of 0.11 m/d per Ω-m, hydraulic conductivity was estimated from resistivity data.

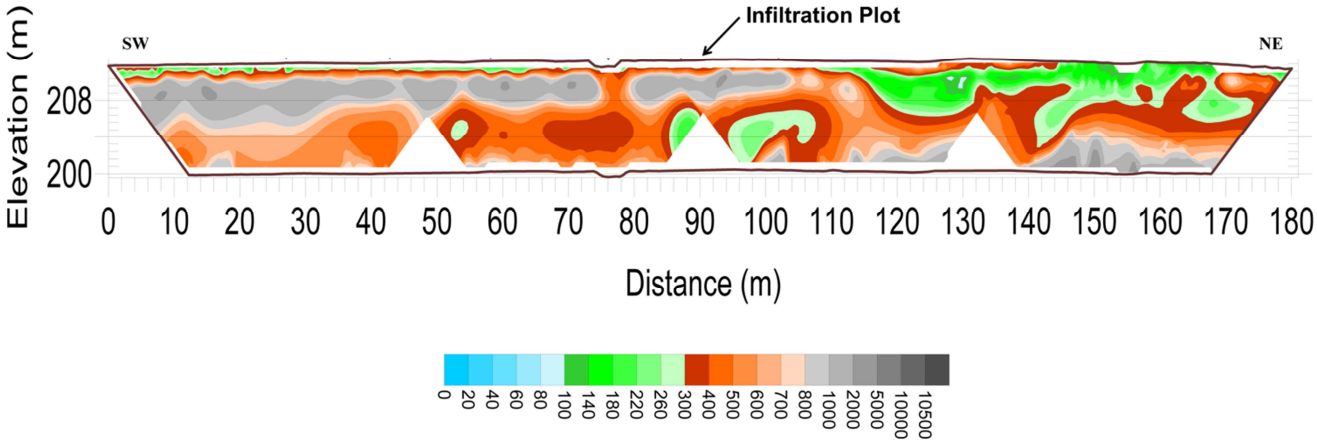


**Figure 43. Electrical resistivity (Ω-m) data from the Barren Fork Creek floodplain site. Gray areas indicate high resistivity course gravels, interpreted to be buried gravel bars. Adapted from Heeren et al. (2010).**

### *Plot Scale Infiltration Experiments*

In this research, a berm method (Heeren et al., 2013a) was used to confine infiltration plots and maintain a constant head of water. An infiltration experiment for a 1 m by 1 m plot at the Barren Fork Creek site was performed for 22 hr. Chloride ($Cl^-$) with a plot concentration of 50.1 mg/L was used as a conservative (nonsorbing) tracer. The RhWT was regarded as a slightly sorbing solute since the soils were expected to have organic matter contents of less than 2%, resulting in a minor amount of Rhodamine WT sorption. Phosphorus (highly sorbing) concentrations of 1.68 mg/L were used to represent poultry litter application rates. Observation wells were installed with a Geoprobe Systems drilling machine (6200 TMP, Kejr, Inc., Salina, KS), and low flow

sampling with a peristaltic pump was used to collect water samples from the top of the water table. Two wells were selected to create a representative sample for the purposes of modeling (Figure 44).

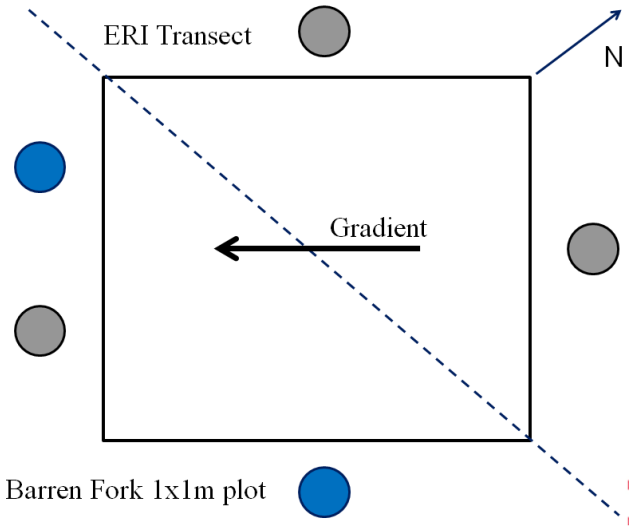


**Figure 44. Overhead view of the shallow gravel 1 m by 1 m test plot. Circles indicate observation wells, with wells in blue indicating those selected for modeling calibration.**

### *Vadose Zone Flow and Transport Modeling*

Solute fate and transport was modeled using the HYDRUS-2D/3D, which utilizes numerical methods to solve the Richards equation for water flow and solute transport equations for movement of heat and contaminants in subsurface systems (Šejna et al., 2011). HYDRUS-2D/3D is capable of solving for water and solute movement in variably saturated media, and is adaptable to varying levels of heterogeneity. HYDRUS-2D/3D can simulate both small- and large-scale water and contaminant transport through unsaturated and saturated soils (Akay and Fox, 2007; Akay et al., 2008).

HYDRUS was set up to model the shallow gravel 1 m by 1 m infiltration plot (June 30, 2011) at the Barren Fork Creek site. A two-dimensional model was developed using the concentration data from the infiltration experiment and hydraulic conductivity data derived from Miller (2012) for the gravelly subsoil. Values for gravel hydraulic conductivity ranged between 130 cm/hr and 580 cm/hr. The effective saturated hydraulic conductivity ($K_{eff}$), calculated to be 9.6 cm/hr based on the plot scale infiltration experiments, was used for the upper silt loam soil layer. A finite element (FE) mesh was developed and was fitted with a media material distribution (Figure 45). The material distribution for each region had an average hydraulic conductivity value that gave a good representation of the region and allowed for the model to operate more smoothly during computations. The FE mesh density was also tailored to allow for optimum computation time and sensitivity of the model. The system was discretized into 450 2 cm by 33.3 cm rectangular units; each unit was composed of two triangular units.

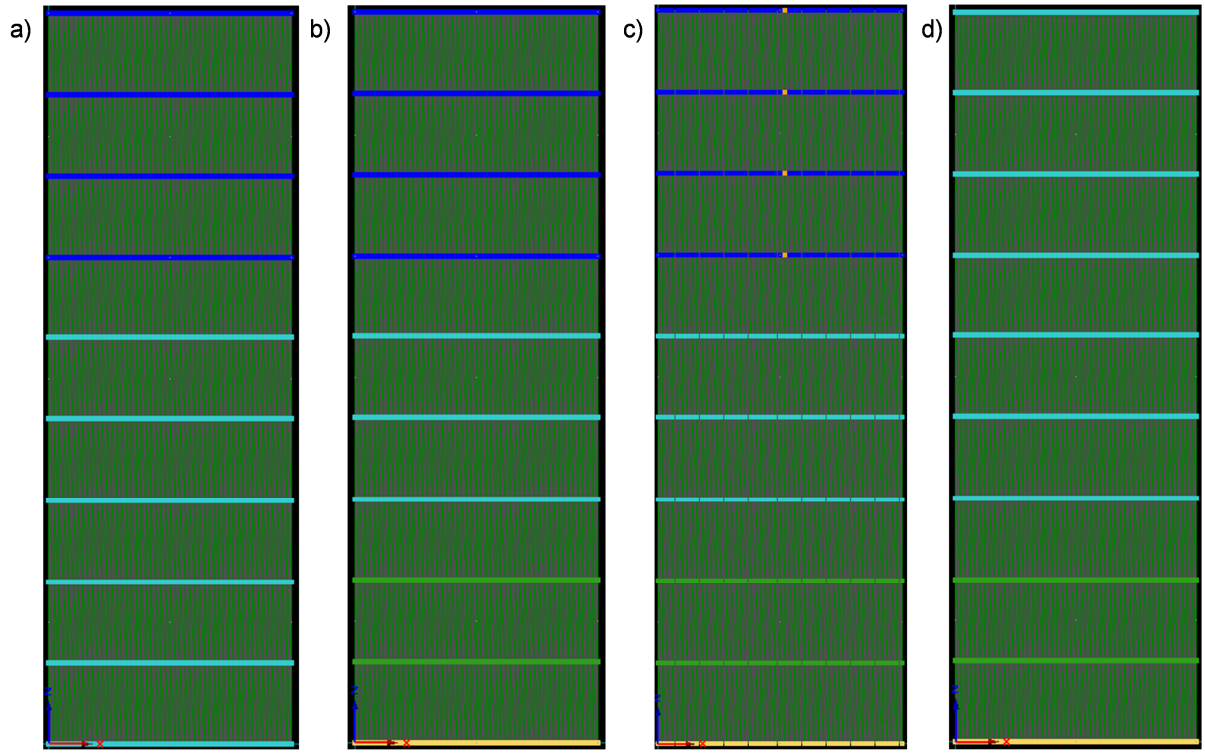


**Figure 45. Vertical FE Mesh overlain with media material distribution. Dark blue indicates a silt loam soil. Other colors indicate gravels of increasing conductivity, with light blue being less conductive and yellow being highly conductive. These profiles show the material distribution for the simple gravel trial (a), multiple gravel trial (b), and physical macropore (c). A fourth profile tested the effect of replacing the topsoil with a gravel outcrop (d). Orientation of the profile is from SW (left) to NE (right). The y-axis extends 3 m, from the water table at the bottom to the soil surface at the top. The infiltration gallery covers the whole 1 m width of the plot.**

Boundary and initial conditions for the trial were established for the model. Rainfall input was set as a variable flux rate. Daily rainfall depths over a 19-year period (Jan. 1994 - Jan. 2013) were taken from Mesonet.org and converted to daily fluxes. Initial pressure head was set to an equilibrium distribution above the water table, and initial concentration was set to match the average background concentration seen in observation wells. Water flow boundary conditions were set to allow for a variable flux across the soil surface boundary and a constant head (atmospheric pressure) boundary at the water table to prevent unnecessary water table mounding. The sides were no-flow boundaries. One solute boundary was set at the soil surface to allow for concentration flux across the boundary. Two observation nodes were placed 1 m apart at the edge of the plot to represent the observation wells selected for calibration trials.

The model also features a mobile-immobile component (Šimůnek and van Genuchten, 2008). Mobile-immobile (MIM) models adapt the porous media to allow for some pores to be closed off to water and/or solute transport (Figure 46). This distinction can yield different results in a system, such as higher pore velocities or reduced solute concentrations in observation wells. For this model, immobile pores were designated as being closed to water flow, but open to solute transport through diffusion.

After initial parameters were input, the model was calibrated with $Cl^-$ data. The $\theta_{im}$ ($cm^3$ mobile pore space per $cm^3$ total soil volume), the immobile porosity, and $\omega$ (1/hr), the solute transport rate between mobile and immobile pores, were optimized by iteratively by changing values and examining the resultant well concentration breakthrough curves. These calibration trials were done using a larger field of view to get a better representation of well capture (Figure 47). The field of view was reduced for the P modeling as flux across the water table boundary, not well capture, was the metric of interest. $Cl^-$ breakthrough curves (BTCs) were also analyzed to determine the effectiveness of different model types on $Cl^-$ transport (Figure 48).

P sorption was simulated using Langmuir isotherm parameters for the gravel subsoil. Values for $K_s$ and $\eta$ for the gravel layers were set at 4.5 L/kg (entered as 4.5 $cm^3$/g in HYDRUS) and 0.048 L/mg (entered as 0.048 $cm^3$/µg in HYDRUS), respectively (Fuchs et. al., 2009). A linear $K_d$ for the silt loam layer was set at 12 L/kg (Khan et. al., 2010) (entered as 12 $cm^3$/g in HYDRUS). Subsequent laboratory analysis on soil samples from this location at the Barren Fork Creek site resulted in Langmuir parameters of 7.28 L/kg for $K_s$ and 0.006 L/mg for $\eta$ for the silt loam layer, and 2.57 L/kg for $K_s$ and 0.002 L/mg for $\eta$ for the gravelly subsoil.

Modeling was done over six trials. Two trials used the default van Genuchten-Maulem model, implemented using a soil regime with a silt loam layer overlaying a homogeneous gravel layer (Trial 1) and a heterogeneous gravel layer based on ERI data (Trial 2). Four trials used the mobile-immobile model in place of the van Genuchten-Maulem model. Soil regimes tested MIM with a heterogeneous gravel layer (Trial 3), incorporating one large physical macropore (Trial 4), and a network of large macropores (Trial 5). One final trial simulated a gravel outcrop in place of the silt loam layer (Trial 6).

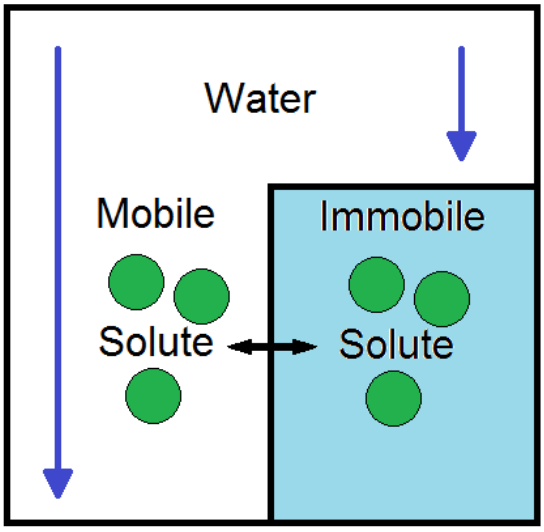


**Figure 46. The mobile-immobile model. This cartoon illustrates a case where water flow is restricted to only a fraction of the pore space, but is open to diffusive solute transfer between the mobile and immobile phases.**

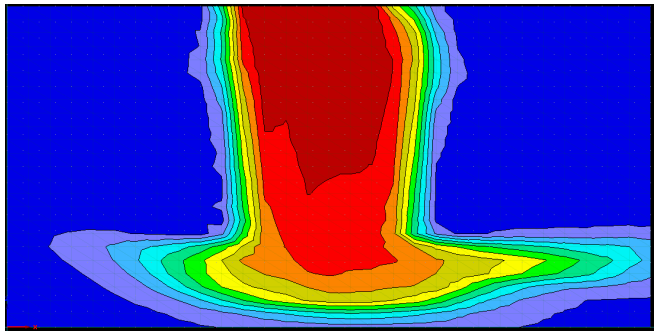

**Figure 47. Cl- transport simulation during the calibration of the mobile-immoble parameters. Plume concentrations ranged from 4.75 mg/L (dark blue) to 50.1 mg/L (dark red).**

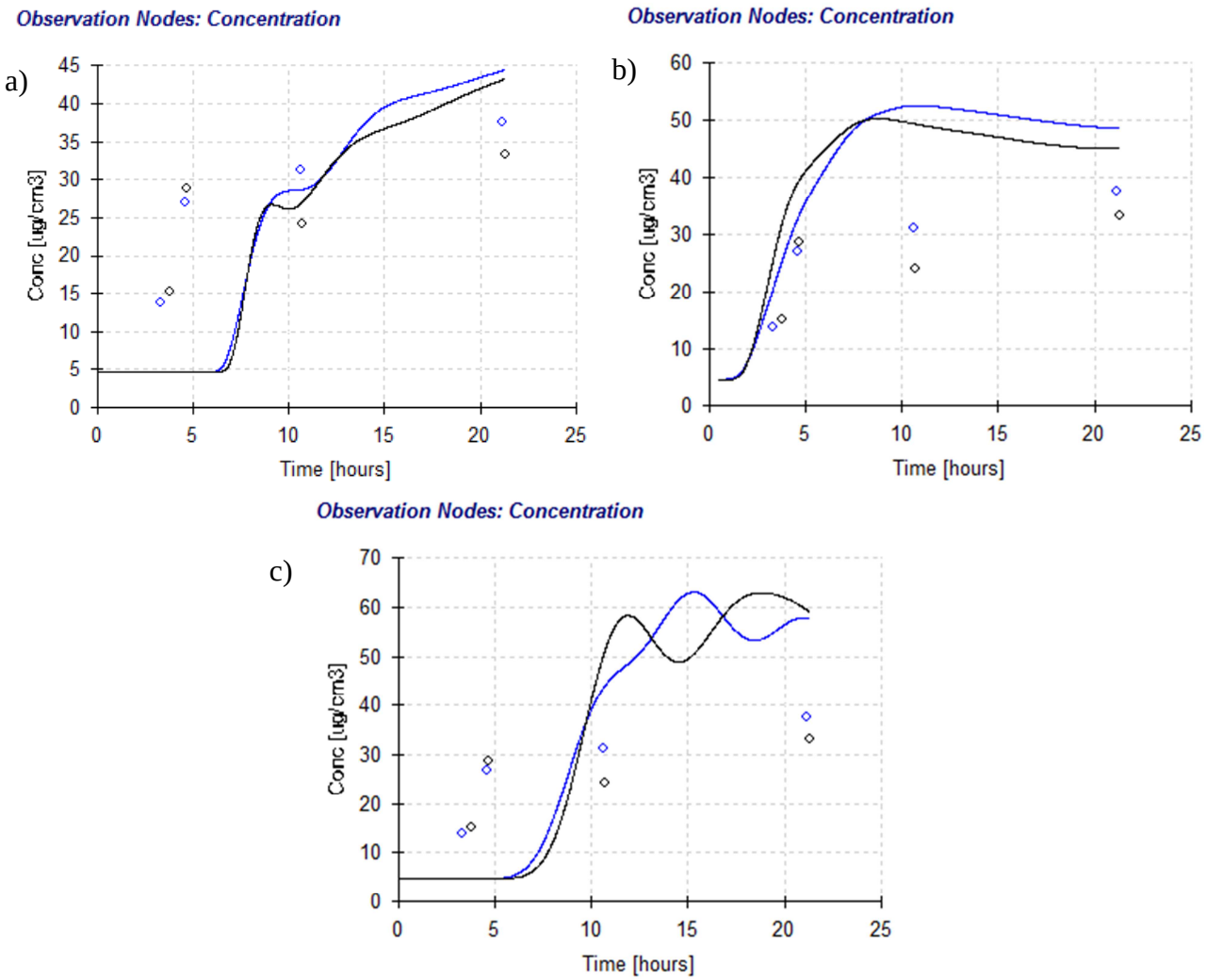


**Figure 48. Cl- BTCs representing water movement through the soil profile with the MIM model (a), with the MIM model and a perched water table (b), and without the MIM model (c). All trials have a heterogeneous gravel layer beneath the silt loam topsoil.**

## Results and Discussion

Trials were analyzed to determine the solute flux across the water table boundary. Trials 1-3 showed clear plume progression throughout the profile. The concentration plume progression for each trial is shown at t = 19 years (Figure 49). It can be seen that the plume approaches the water table, but does not move far enough to cause any major P increase at the water table boundary (Figure 49a). The use of a homogeneous gravel based on a $K_{sat}$ average from all the gravels in the profile does not allow for extensive P movement through the soil profile. The addition of a heterogeneous gravel (Figure 49b) has a significant impact on the plume progression.

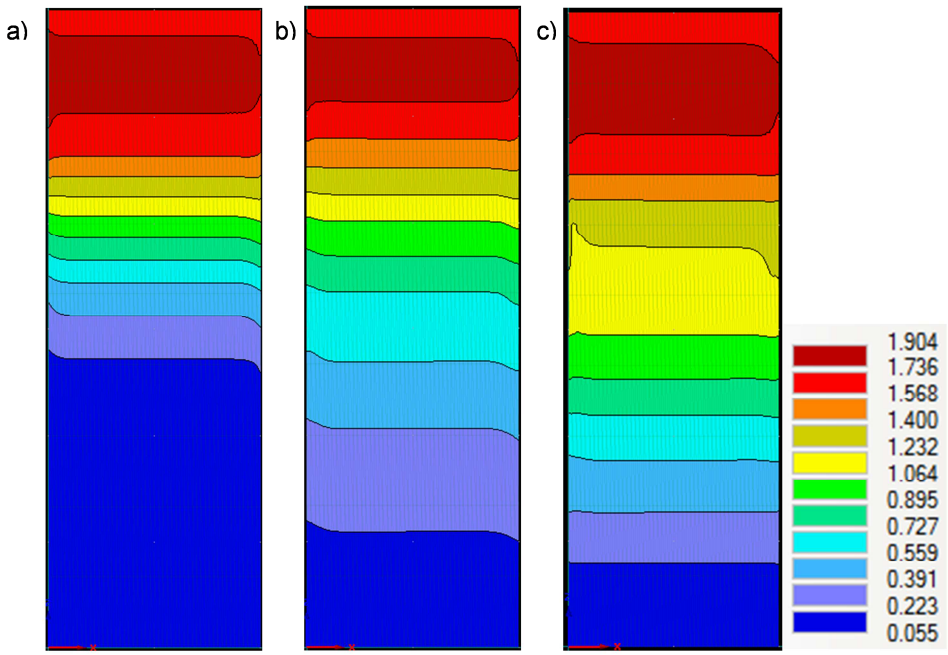


**Figure 49. Vertical downward P front progression at t= 19 years. Slices show the front progression in the homogeneous gravel (a), heterogeneous gravel (b), and heterogeneous gravel incorporating the MIM model (c).**

It can be seen that the plume not only travels deeper into the soil profile, but also has wider bands of solute throughout the plume, indicating more unbounded P is available for continued transport. The use of the mobile-immobile model instead of the standard van Genuchten-Mualem model (Figure 49c) produces more interesting results. Instead of allowing the plume to move through the profile more quickly than with the van Genuchten-Mualem model, the MIM does not seem to progress the plume any deeper into the soil profile than Trial 2. However, it does seem to encourage higher concentrations at all soil depths, and the higher concentrations (indicated by red and yellow) have more representation in the plume than other trials. The P breakthrough curves for Trials 1-3 show the plume progression through the soil profile at t = 19 years (Figure 50). Even though using an MIM and a heterogeneous gravel profile encouraged overall P

transport towards the water table, there was still no significant P flux across this boundary after 19 years. In previous research, significant P increases were seen in observation wells as early as 21 hours after water application began. This suggests that some other process is involved beyond the preferential flow provided by the MIM model alone. The best explanation for the rapid progress of P is the presence of a physical macropore that is significantly larger than existing soil macropores in the model.

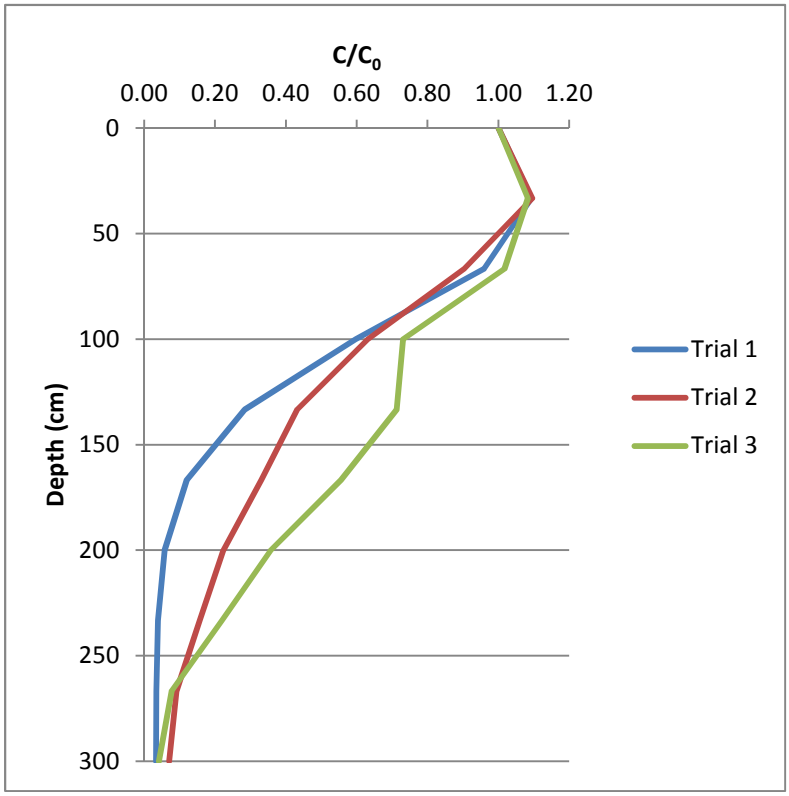


**Figure 50. Breakthrough curves (BTCs) for P for trials 1-3.**

For trial 4, a physical macropore was used in combination with the MIM model and a heterogeneous gravel profile. The physical macropore was simulated as a 2 cm wide, 1.33 m deep gravel pipe with a $K_{sat}$ of 350 cm/hr. This $K_{sat}$ value was found through iteration of the observed data taken from P infiltration plot experiments from previous research (Figure 51). Using these material properties found through this simulation, Trials 4 and 5 looked to simulate this phenomenon using long-term rainfall data. However, the model failed to converge early in these trials, and no usable data was collected.

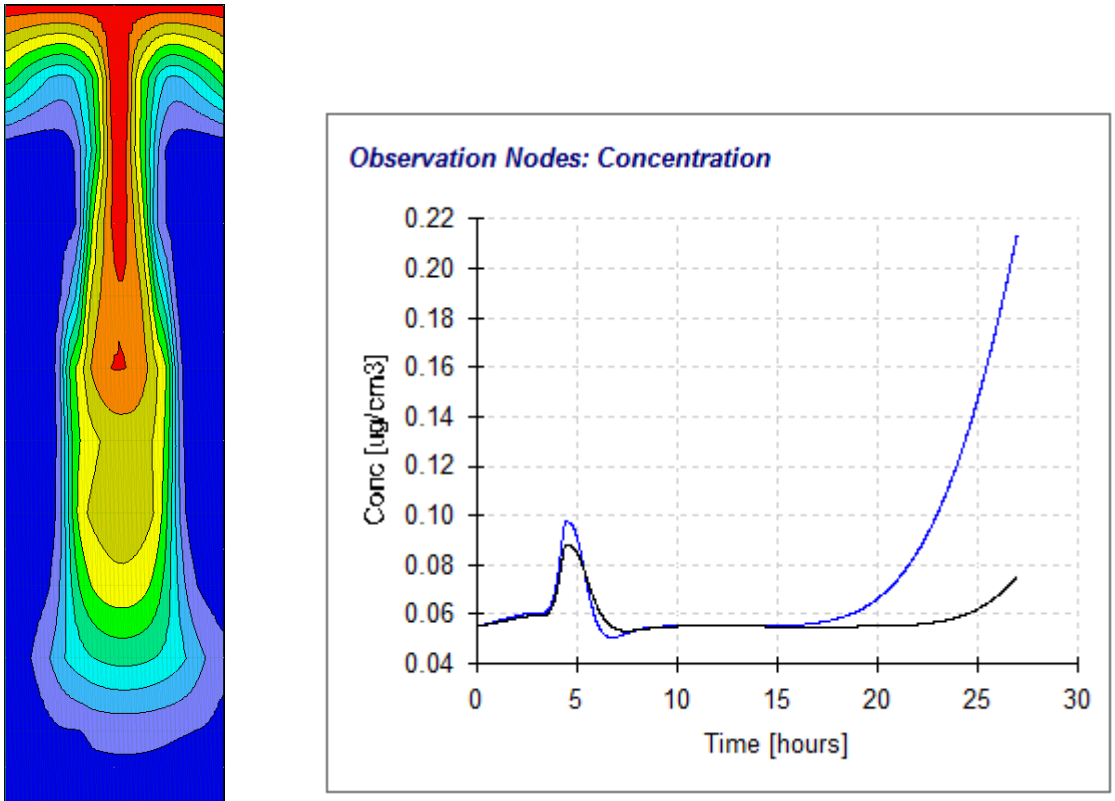


**Figure 51. Calibration results for P infiltration plot leaching. These results tested the effectiveness of a physical macropore in the silt loam layer at P delivery to the observation wells. Results from this testing were used to set material properties for the macropore for future trials.Note the spike in concentration at t= 5 hours caused by numerical dispersion of the model.**

While Barren Fork did not have significant testing with gravel outcrops, other sites in previous research did explore the effects of gravel outcrops on subsurface P transport. Trial 6 created a mock gravel outcrop by replacing the silt loam layer with a layer of gravel with the same properties as the least conductive gravel layer used in the previous simulations (Figure 52). Interpretation of the output data shows that the plume progresses much further than any other successful trial. This trial was also the only trial to show significant P delivery to the water table, and cumulative flux data was analyzed to determine a yearly flux rate across the boundary. A flux curve was developed (Figure 53) and a peak flux rate was calculated to be 876 $g/m^2/yr$. This can be compared to Mittelstet et al. (2011), who reported horizontal transport rates of 30 to 40 g/yr through alluvial aquifers at two small (3 ha) Ozark floodplain sites. In that research the source of P was P-laden stream water infiltrating laterally into the alluvial aquifers, and it was hypothesized that the aquifers were capable of transporting higher rates of P if there was an additional source of P such as leaching from the soil surface.

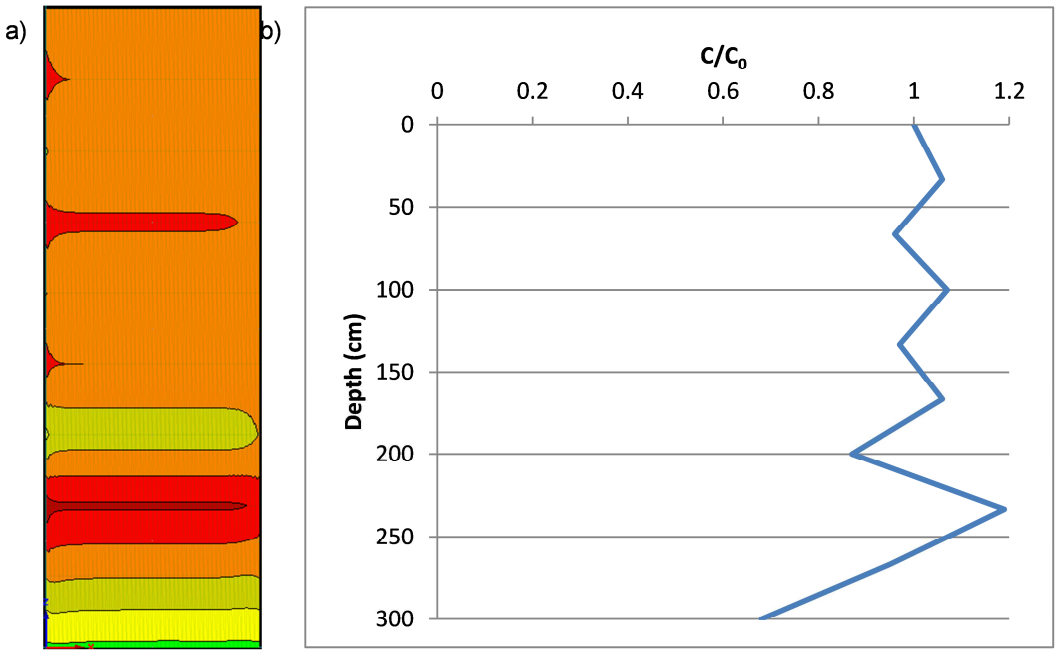


**Figure 52. P front progression (a) and BTC (b) for Trial 6. The P front moved through much farther than any other trial. Note once again the erratic response in the BTC caused by numerical dispersion of the model.**

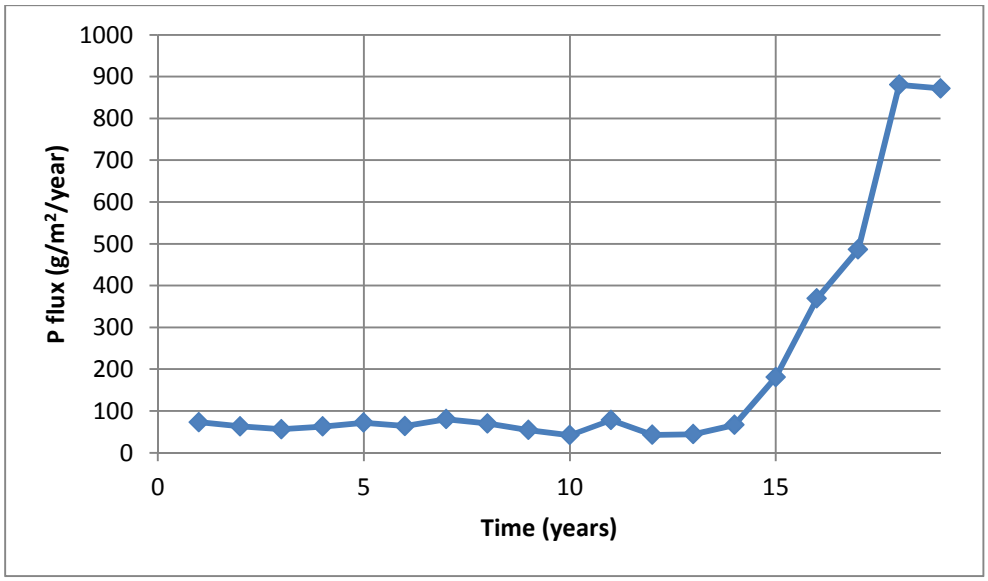


**Figure 53. Yearly P flux for Trial 6. Flux across the boundary is low ( ~70 g/m$^2$/year) until the front reaches the water table boundary around t = 15 years. At this point, the flux rapidly increases. Flux would most likely continue to increase past t = 19 years as water with higher P concentrations move past the water table boundary.**

While some limited success was found in simulating some of these trials, HYDRUS was still overall unsuccessful in simulating the macropore phenomenon to the satisfaction of the researchers. There are several reasons that the researchers feel led to the model's inability to match observed and expected results. Most of the problem with simulation stems from the complexity of the subsurface soil profile. The subsurface is composed of highly variable, highly conductive coarse and fine gravel layers that seem to impair the model's ability to smoothly simulate a water or solute profile over an extended period of time. As a result of this, some of the complexity of the system had to be removed or adjusted to allow for the model to produce results. While some of these results can be useful in determining trends or patterns, they do not accurately represent just how complex the subsurface system is.

Another problem with the model is its inability to simulate gravel pipes and large macropores under non-ponded conditions. Initial simulations with a ponded surface provided some useful results (Figure 49), and helped set the framework for physical macropore trials. However, once the ponded surface was replaced with daily rainfall averages, the macropores were not simulated properly and caused incomplete results for Trials 4 and 5. It is believed that physical macropores must be "activated" by a high intensity rainfall before they will channel significant amounts of water. These high intensity rainfalls may take place over the course of only minutes in a rain event, and are not properly reflected when using historical rainfall amounts on a daily time scale. With the rainfall data available, the researchers were unable to simulate these high intensity flows, and the model was not sophisticated enough to use the input data with these macropores. Finally, numerical dispersion in the model occurred in nearly every trial. This numerical dispersion occurred due to trying to fit numerical models to the complex soil system in these simulations. Numerical dispersion can be most easily seen in the breakthrough curves (BTCs) for each trial. BTCs show plume movement as a fraction of the source concentration ($C/C_0$).

Despite the limitations of the model, however, it is worth mentioning that this process still provides an increased understanding of P leaching through a gravelly soil profile. Other methods currently in practice, such as leaching rates determined only on soil test P data, provide an even more limited understanding of P movement in these systems.

## (3) References


Aharoni, C., and D. L. Sparks. 1991. Kinetics of soil chemical reactions-A theoretical treatment. P. 1-18. In D. Sparks and D.L. Suarez (ed.) Rates of soil chemical processes. SSSA Spec. Publ. 27. SSSA, Madison, WI.

Akay, O., and G. A. Fox. 2007. Experimental investigation of direct connectivity between macropores and subsurface drains during infiltration. *Soil Science Society of America Journal* 71(5): 1600-1606.

Akay, O., G. A. Fox, and J. Simunek. 2008. Numerical simulation of flow dynamics during macropore/subsurface drain interaction using HYDRUS. *Vadose Zone Journal* 7(3): 909-918, DOI: 10.2136/vzj2007.0148.

Allison, J. D., D. S. Brown, and K .J. Novo-Gradac. 1991. MINTEQA2/PRODEFA2, a geochemical assessment model for environmental systems: Version 3.0 users manual. USEPA report number EPA/600/3-91/021. Environmental Research Laboratory, Athens, GA.

Appel, C., D. Rhue, N. Kabengi, and W. Harris. 2013. Calorimetric investigation of the nature of sulfate and phosphate sorption on amorphous aluminum hydroxide. Soil Science, *in print.*

Archie, G. E. 1942. The electrical resistivity log as an aid in determining some reservoir characteristics. *Petroleum Technology* Technical Paper 1422.

Bastian, M. 2011. Water quality credit trading: Does it make sense for the upper Illinois River Watershed? Arkansas Water Resources Center (AWRC) Annual Watershed and Research Conference, Fayetteville, Ark.

Bear, J. 1972. Dynamics of Fluids in Porous Media. Dover Publications: New York, N.Y.

Beauchemin, S., and R. R. Simard. 1999. Soil phosphorus saturation degree: review of some indices and their suitability for P management in Quebec, Canada. *Canadian Journal of Soil Science* 79: 615-625.

Beck, M. A., L. W. Zelazny, W. L. Daniels, and G. L. Mullins. 2004. Using the Mehlich-1 extract to estimate soil phosphorus saturation for environmental risk assessment. *Soil Science Society of America Journal* 68: 1762-1771.

Blackstock, R. B. 2003. Using computer models in court: Challenges for expert witnesses. ASAE Publication Number 701P1503. St. Joseph, Mich.: American Society of Agricultural and Biological Engineers.

Bodhinayake, W., B. C. Si, and K. Noborio. 2004. Determination of hydraulic properties in sloping landscapes from tension and double-ring infiltrometers. *Vadose Zone Journal* 3: 964–970.

Brown, G. O., H. T. Hsieh, and D. A. Lucero. 2000. Evaluation of laboratory dolomite core sample size using representative elementary volume concepts. *Water Resources Research* 36(5): 1199-1207.

Bunte, K., and S. Abt. 2001. Sampling Surface and Subsurface Particle-Size Distributions in Wadable Gravel- and Cobble-Bed Streams for Analyses in Sediment Transport, Hydraulics, and Streambed Monitoring. USFS General Technical Report 74, USDA. Rocky Mtn. Res. Sta. Fort Collins, CO.

Carsel, R. F., and R. S. Parrish. 1988. Developing joint probability distributions of soil water retention characteristics. *Water Resources Research* 24: 755-769.

Chin, D. A., R. M. Price, and V. J. DiFrenna. 2009. Nonlinear flow in karst formations. *Ground Water* 47(5): 669–674, doi: 10.1111/j.1745-6584.2009.00574.x.

Clark, G., D. K. Meuller, and M. A. Mast. 2000. Nutrient concentrations and yields in undeveloped stream basins of the United States. *J. Am. Water Res. Assoc.* 36(4): 849-860.

Cooper, A. B., C. M. Smith, and M. J. Smith. 1995. Effects of riparian set-aside on soil characteristics in an agricultural landscape: Implications for nutrient transport and retention. *Agriculture, Ecosystems, and the Environment* 55(1): 61-67.

Correll, D. A., D. M. Heeren, G. A. Fox, D. E. Storm, C. J. Penn, and T. Halihan. April 4-5, 2013. Transient resistivity imaging of a phosphorous tracer test. Geological Society of America South-Central Regional Meeting, Austin, TX.

Day, P. R. 1965. Particle fractionation and particle size analysis. p. 545-567. In C.A. Black et al. (ed.) Methods of soil analysis. Part 1. Agron. Monogr. 9. ASA, Madison, WI.

DeLaune, P. B., B. E. Haggard, T. C. Daniel, I. Chaubey, and M. J. Cochran. 2006. The Eucha/Spavinaw phosphorus index: A court mandated index for litter management. *J. Soil Water Cons.* 61(2): 96-105.

DeLaune, P. B., P. A. Moore, Jr., D. K. Carman, A. N. Sharpley, B. E. Haggard, and T. C. Daniel. 2004. Development of a phosphorus index for pastures fertilized with poultry litter: Factors affecting phosphorus runoff. *Journal of Environmental Quality* 33(6): 2183-2191.

Djodjic, F., B. Katarina, and L. Bergstrom. 2004. Phosphorus leaching in relation to soil type and soil phosphorus content. *Journal of Environmental Quality* 33: 678–684. DOI: 10.2134/jeq2004.0678.

Easton, Z. M. 2013. Defining spatial heterogeneity of hillslope infiltration characteristics using geostatistics, error modeling, and autocorrelation analysis. *J. Irrig. Drain Eng.* 139(9): 718–727, doi: 10.1061/(ASCE)IR.1943-4774.0000602.

Edwards, D. R., and T. C. Daniel. 1993. Effects of poultry litter application rate and rainfall intensity on quality of runoff from fescuegrass plots. *Journal of Environmental Quality* 22: 361-365.

Engle, B. 2008. Poultry Waste Generation and Land Application in the Illinois River Watershed and Phosphorus Loads to the Illinois River Watershed Streams and Rivers and Lake Tenkiller. Expert Report for *State of Oklahoma v. Tyson Foods, et al.*

Evans, R. G., J. Larue, K. C. Stone, and B. A. King. 2012. Adoption of site-specific variable rate sprinkler irrigation systems. *Irrigation Science* (published online, DOI 10.1007/s00271-012-0365-x).

Fetter, C. W. 1999. Contaminant Hydrogeology. Waveland Press: Long Grove, IL.

Fox, G. A., and C. J. Penn. 2013. Empirical model for quantifying total phosphorus reduction by vegetative filter strips. *Transactions of the ASABE* 56(4): 1461-1469.

Fox, G. A., D. M. Heeren, R. B. Miller, A. R. Mittelstet, and D. E. Storm. 2011. Flow and transport experiments for a streambank seep originating from a preferential flow pathway. *Journal of Hydrology* 403(3-4): 360-366.

Fox, G. A., R. Muñoz-Carpena, and G. J. Sabbagh. 2010. Influence of flow concentration on parameter importance and prediction uncertainty of pesticide trapping by vegetative filter strips. *Journal of Hydrology* 384(1-2): 164-173.

Fox, G. A., R. W. Malone, G. J. Sabbagh, and K. Rojas. 2004. Interrelationship of macropores and subsurface drainage for conservative tracer and pesticide transport. *Journal of Environmental Quality* 33(6): 2281-2289.

Fuchs, J. W., G. A. Fox, D. E. Storm, C. J. Penn, and G. O. Brown. 2009. Subsurface transport of phosphorus in riparian floodplains: Influence of preferential flow paths. *Journal of Environmental Quality* 38: 473-484, DOI: 10.2134/jeq2008.0201.

Gburek, W. J., E. Barberis, P. M. Haygarth, B. Kronvang, and C. Stamm. 2005. Chapter 29: Phosphorus mobility in the landscape. In *Phosphorus: Agriculture and the Environment*, 941-979. Sims, J.T. and A. N. Sharpley, ed. Madison, Wis.: ASA-CSSA-SSSA.

Gotovac, H., V. Cvetkovic, and R. Andricevic. 2009. Flow and travel time statistics in highly heterogeneous porous media. *Water Resources Research* 45, W07402, doi:10.1029/2008WR007168.

Haggard, B. E. 2010. Phosphorus concentrations, loads, and sources within the Illinois River drainage area, Northwest Arkansas, 1997-2008. *J. Environ. Qual.* 39(6): 2113-2120.

Halihan, T., S. Paxton, I. Graham, T. Fenstemaker, and M. Riley. 2005. Post-remediation evaluation of a LNAPL site using electrical resistivity imaging. *Journal of Environmental Monitoring* 7(4): 283-287.

Harvey, O .R., and R. D. Rhue. 2008. Kinetics and energetics of phosphate sorption in a multi-component Al(III)-Fe(III) hydr(oxide) sorbent system. *Journal of Colloid and Interface Science* 322: 84-393.

Heeren, D. M. 2012. Subsurface phosphorus transport and scale dependent phosphorus leaching in alluvial floodplains. PhD diss. Stillwater, Okla.: Oklahoma State University, Department of Biosystems and Agricultural Engineering.

Heeren, D. M., G. A. Fox, and D. E. Storm. 2013a. Berm method for quantification of infiltration and leaching at the plot scale in high conductivity soils. *Journal of Hydrologic Engineering* (in press), doi: 10.1061/(ASCE)HE.1943-5584.0000802.

Heeren, D. M., G. A. Fox, A. K. Fox, D. E. Storm, R. B. Miller, and A. R. Mittelstet. 2013b. Divergence and flow direction as indicators of subsurface heterogeneity and stage-dependent storage in alluvial floodplains. *Hydrological Processes* (in press), doi: 10.1002/hyp.9674.

Heeren, D. M., G. A. Fox, R. B. Miller, D. E. Storm, A. R. Mittelstet, A. K. Fox, C. J. Penn, and T. Halihan. 2011. Stage-dependent transient storage of phosphorus in alluvial floodplains. *Hydrological Processes* 25(20): 3230-3243.

Heeren, D. M., R. B. Miller, G. A. Fox, D. E. Storm, C. J. Penn, and T. Halihan. 2010. Preferential flow path effects on subsurface contaminant transport in alluvial floodplains. *Transactions of the ASABE* 53: 127-136.

Hooda, P. S. 2000. Relating soil phosphorus indices to potential release to water. *Journal of Environmental Quality* 2000. 29: 1166–1171.

Imai, H., K. W. T. Goulding, and O. Talibudeen. 1981. Phosphate adsorption in allophanic soils. *Journal of Soil Science* 32: 555-570.

Jacobson, R. B., and K. B. Gran 1999. Gravel sediment routing from widespread, low-intensity landscape disturbance, Current River Basin, Missouri. *Earth Surface Processes and Landforms* 24: 897-917.

Kabengi, N. ., R. D. Rhue, and S. H. Daroub. 2006a. Using flow calorimetry to determine the molar heats of cation and anion exchange and the point of zero charge on amorphous aluminum hydroxides. *Soil Science* 171: 13-21.

Kabengi, N. J., S. H. Daroub, and R. D. Rhue. 2006b. Energetics of arsenate sorption on amorphous aluminum hydroxides studied using flow adsorption calorimetery. *Journal of Colloid and Interface Science* 297: 86-94.

Khan, Q. U., M. J. Khan, Saif-ur-Rehman, and S. S. Ullah. 2010. Comparison of different models for phosphate adsorption in salt inherent soil series of Dera Ismail Khan. *Soil and Environment* 29(1): 11-14.

Khiari, L., L. E. Parent, A. Pellerin, A. R. A. Alimi, C. Tremblay, R. R. Simard, and J. Fortin. 2000. An agri-environmental phosphorus saturation index for acid coarse-textured soils. *Journal of Environmental Quality* 29: 1561-1567.

Kim, Y., and R. J. Kirkpatrick. 2004. An investigation of phosphate adsorbed on aluminium oxyhydroxide and oxide phases by nuclear magnetic resonance. *European Journal of Soil Science* 55: 243-251.

Kleinman, P. J. A., A. N. Sharpley, A. M. Wolf, D. B. Beegle and P. A. Moore, Jr. 2002. Measuring water-extractable phosphorus in manure as an indicator of phosphorus in runoff. *Soil Science Society of America Journal* 66(6): 1009-2015.

Lai, J., and L. Ren. 2007. Assessing the size dependency of measured hydraulic conductivity using double-ring infiltrometers and numerical simulation. *Soil Science Society of America Journal* 71(6): 1667-1675.

Lee, M., and K. R. Douglas-Mankin. 2011. An environmental trading ratio for water quality trading. *T. ASABE* 54(5): 1599-1614.

Ler, A., and R. Stanforth. 2003. Evidence for surface precipitation of phosphate on goethite. *Environmental Science and Technology* 37: 2694-2700.

Loke, M. H., and T. Dahlin. 2002. A comparison of the Gauss–Newton and quasi-Newton methods in resistivity imaging inversion. *Journal of Applied Geophysics* 49: 149-162.

Machesky, M. L., B. L. Bischoff, and M. A. Anderson. 1989. Calorimetric investigation of anion adsorption onto goethite. *Environmental Science and Technology* 23:580-587.

Maguire, R. O., and J. T. Sims. 2002. Soil testing to predict phosphorus leaching. *Journal of Environmental Quality* 31: 1601-1609.

Massman, J. W. 2003. Implementation of infiltration ponds research. Final Research Report. Olympia, Wash.: Washington State Transportation Commission.

McBride, C. 2011. Oklahoma v. Tyson: Playing chicken with environmental cleanup. *Ecol. Law Quarterly* 38: 603-609.

McDowell, R. W., L. M. Condron, N. Mahieu, P. C. Brookes, P. R. Poulton, and A. N. Sharpley. 2002. Analysis of potential mobile phosphorus in arable soils using solid state nuclear magnetic resonance. *Journal of Environmental Quality* 31: 450-456.

McKeague, J., and J. H. Day. 1966. Dithionite and oxalate-extractable Fe and Al as aids in differentiating various classes of soils. *Canadian Journal of Soil Science* 46: 13-22.

McNeill, J. D. 1980. Electrical conductivity of soils and rocks. Technical Note TN-5. Mississauga, Ontario, Canada: Geonics, Ltd.

Mehlich, A. 1984. Mehlich 3 soil test extractant: A modification of Mehlich 2 extractant. *Communications in Soil Science and Plant Analysis* 15: 1409-1416.

Midgley, T. L., G. A. Fox, and D. M. Heeren. 2012. Evaluation of the Bank Stability and Toe Erosion Model (BSTEM) for predicting lateral streambank retreat on composite streambanks. *Geomorphology* 145-146: 107-114, doi:10.1016/j.geomorph.2011.12.044.

Miller, R. B. 2012. Hydrogeophysics of gravel-dominated alluvial floodplains in eastern Oklahoma. PhD diss. Stillwater, Okla.: Oklahoma State University, Department of Biosystems and Agricultural Engineering.

Miller, R. B., D. M. Heeren, G. A. Fox, D. E. Storm, and T. Halihan. 2011. Design and application of a direct-push vadose zone gravel permeameter. *Ground Water* 49(6): 920-925.

Miller, R. B., D. M. Heeren, G. A. Fox, D. E. Storm, T. Halihan, and A. R. Mittelstet. 2010. Geophysical mapping of preferential flow paths across multiple floodplains. ASABE Paper No. 1008730, ASABE, St. Joseph, MI.

Miller, R. B., D. M. Heeren, G. A. Fox, T. Halihan, D. E. Storm, and A. R. Mittelstet. 2013. The hydraulic conductivity structure of gravel-dominated vadose zones within alluvial floodplains. *Journal of Hydrology* (in review).

Miltenburg, J. C., and H. L. Golterman. 1998. The energy of the adsorption of o-phosphate onto ferric hydroxide. *Hydrobiologia* 364: 93-97.

Mittelstet, A. R., D. M. Heeren, G. A. Fox, D. E. Storm, M. J. White, and R. B. Miller. 2011. Comparison of subsurface and surface runoff phosphorus transport rates in alluvial

floodplains. *Agriculture, Ecosystems, and the Environment* 141: 417-425, DOI: 10.1016/j.agee.2011.04.006.
Mozaffari, M., and J. T. Sims. 1996. Phosphorus transformations in poultry litter-amended soils of the atlantic coastal plain. *Journal of Environmental Quality* 25: 1357-1365.
Muñoz-Carpena, R., G. A. Fox, and G. J. Sabbagh. 2010. Parameter importance and uncertainty in predicting runoff pesticide reduction with filter strips. *Journal of Environmental Quality* 39(2): 630-641.
Murphy, J., and J. P. Riley. 1962. A modified single solution method for the determination of phosphate in natural waters. *Analytica Chimica Acta* 27: 31–36.
Najm, M. R., J. D. Jabro, W. M. Iverson, R. H. Mohtar, and R. G. Evans. 2010. New method for the characterization of three-dimensional preferential flow paths in the field. *Water Resources Research* 46, W02503, DOI: 10.1029/2009WR008594.
Natural Resources Conservation Service (NRCS). 2012. Web Soil Survey (WSS). Washington, D.C.: USDA-NRCS. Available at: http://websoilsurvey.nrcs.usda.gov/. Accessed February, 2012.
Nelson, N. O. and A. L. Shober. 2012. Evaluation of phosphorus indices after twenty years of science and development. *Journal of Environmental Quality* 41:1703-1710.
Nelson, N. O., J. E. Parsons, and R. L. Mikkelson. 2005. Field-scale evaluation of phosphorus leaching in acid sandy soils receiving swine waste. *Journal of Environmental Quality* 34: 2024-2035, DOI: 10.2134/jeq2004.0445.
Niskanen, R. 1990. Sorption capacity of phosphate in mineral soils II: Dependence of sorption capacity on soil properties. *Journal of Agricultural Science in Finland* 62: 9-15.
Oklahoma Water Resources Board (OWRB). 2010. Oklahoma's Water Quality Standards 785:45. Available at: http://www.owrb.ok.gov/util/rules/pdf_rul/RulesCurrent2010/Ch45.pdf. Accessed June, 2013.
Osborne, L. L., and D. A. Kovacic. 2006. Riparian vegetated buffer strips in water-quality restoration and stream management. *Freshwater Biology* 29: 243-258.
Owens, L. B., and M. J.Shipitalo. 2006. Surface and Subsurface Phosphorus Losses from Fertilized Pasture Systems in Ohio. *Journal of Environmental Quality* 35: 1101-1109.
Pautler, M. C., and J. T. Sims. 2000. Relationships between soil test phosphorus, soluble phosphorus and phosphorus saturation in Delaware soils. *Soil Science Society of America Journal* 64: 765–773.
Partyka, S., W. Rudzinski, and B. Brun. 1989. Calorimetric studies of adsorption of anionic surfactants onto alumina. *Langmuir* 5: 297-304.
Penn, C. J., and H. Zhang. 2010. Thermodynamics of phosphorus sorption onto soils: Isothermal titration calorimetry as an indicator of phosphorus sorption behavior. *Soil Science Society of America Journal* 74: 502-511.
Penn, C. J., and J. G. Warren. 2009. Investigating phosphorus sorption onto kaolinite using isothermal titration calorimetry. *Soil Science Society of America Journal* 73: 560-568.
Penn, C. J. and J. M. McGrath. 2011. Predicting phosphorus sorption onto steel slag using a flow-through approach with application to a pilot scale system. *Journal of Water Resources Protection* 3: 235-244.
Penn, C. J., G. L. Mullins, L. W. Zelazny, and A. N. Sharpley. 2006. Estimating dissolved phosphorus concentrations in runoff from three physiographic regions of Virginia. *Soil Science Society of America Journal* 70: 1967-1974.

Penn, C. J., J. G. Warren, and S. Smith. 2010. Maximizing ammonium-nitrogen removal from solution using different zeolites. *Journal of Environmental Quality* 39: 1478-1485.

Penn, C. J., R. B. Bryant, M. A. Callahan, and J. M. McGrath. 2011. Use of industrial byproducts to sorb and retain phosphorus. *Communications in Soil Science and Plant Analysis* 42: 633-644.

Philip, J. R. 1957. The Theory of Infiltration: 1. The Infiltration Equation and Its Solution. *Soil Science* 83(5): 345-358.

Pierzynski, G. M., R. W. McDowell, and J. T. Sims. 2005. Chemistry, cycling, and potential movement of inorganic phosphorus in soils. In Phosphorus: Agriculture and the Environment, Agronomy Monograph No. 46, Sims, J.T., and A.N. Sharpley (eds). American Society of Agronomy: Madison, Wis.

Pittman, H. M. 2011. A legal perspective: Agriculture, water quality, and the Illinois River. In *Proceedings of the Annual Watershed and Research Conference*. Fayetteville, Ark.: Arkansas Water Resources Center (AWRC).

Popov, V. H., P. S. Cornish, and H. Sun. 2005. Vegetated biofilters: the relative importance of infiltration and adsorption in reducing loads of water-soluble herbicides in agricultural runoff. *Agriculture, Ecosystems, and the Environment* 114: 351-359.

Pryor, M., J. Inhofe, T. Coburn, J. Boozman, D. Boren, and S. Womack. 2011. Letter to EPA Administrator Lisa Jackson regarding modeling for TMDL development in the Illinois River Watershed, dated December 9, 2001.

Rao, N. S., Z. M. Easton, E. M. Schneiderman, M. S. Zion, D. R. Lee, and T. S. Steenhuis. 2009. Modeling watershed-scale effectiveness of agricultural best management practices to reduce phosphorus loading. *Journal of Environmental Management* 90: 1385-1395.

Reichenberger, S., M. Bach, A. Skitschak, H.-G. Frede. 2007. Mitigation strategies to reduce pesticide inputs into ground- and surface water and their effectiveness: a review. *Science of the Total Environment* 384: 1-35.

Rhue, R. D., C. Appel, and N. Kabengi. 2002. Measuring surface chemical properties of soil using flow calorimetry. *Soil Science* 167: 782-790.

Ribaudo, M. 2008. Creating markets for environmental stewardship: Potential benefits and problems. *Amber Waves* 6(4): 24-31.

Ryther, J. H., and W. M. Dunstan. 1971. Nitrogen, phosphorus, and eutrophication in the coastal marine environment. *Science* 171: 1008-1013.

Sabbagh, G. J., G. A. Fox, A. Kamanzi, B. Roepke, and J. Z. Tang. 2009. Effectiveness of vegetative filter strips in reducing pesticide loading: Quantifying pesticide trapping efficiency. *Journal of Environmental Quality* 38(2): 762-771.

Sakadevan, K., and H. J. Bavor. 1998. Phosphate adsorption characteristics of soils, slags, and zeolite to be used as substrates in constructed wetland systems. Wat. Res. 32:393-399.

SAS Institute. 2003. SAS user's guide: Statistics. SAS Inst., Cary, NC.

Sauer, T. J., and S. D. Logsdon. 2002. Hydraulic and physical properties of stony soils in a small watershed. *Soil Science Society of America Journal* 66: 1947-1956. DOI: 10.2136/sssaj2002.1947.

Sauer, T. J., S. D. Logsdon, J. Van Brahana, and J. F. Murdoch. 2005. Variation in infiltration with landscape position: Implications for forest productivity and surface water quality. *Forest Ecology and Management* 220: 118-127.

Saunders, W. M. H. 1964. Phosphate retention by New Zealand soils and its relationship to free sesquioxides, organic matter, and other soil properties. *New Zealand Journal of Agricultural Research* 8: 30-57.

Schoumans, O. F. 2000. Determination of the degree of phosphate saturation in non-calcareous soils. p. 31–34. In: Pierzynski, G.M. (Ed.), Methods of Phosphorus Analysis for Soils, Sediments, Residuals, and Waters. Southern Cooperative Series Bulletin No. 396. A publication of SERA-IEG 17. (A USDA-CSREES Regional committee minimizing agricultural phosphorus losses for protection of the water resources.).

Schroeder, P. D., D. E. Radcliffe and M. L. Cabrera. 2004. Rainfall timing and poultry litter application rate effects on phosphorus loss in surface runoff. *Journal of Environmental Quality* 33(6): 2201-2209.

Scott, H. D. 2000. *Soil Physics: Agricultural and Environmental Applications*. Iowa State University Press: Ames, Iowa.

Šejna, M., J. Šimůnek, and M. Th. van Genuchten. 2011. The HYDRUS software package for simulating two- and three-dimensional movement of water, heat, and multiple solutes in variably-saturated media, user manual.

Simard, R. R. 2000. Potential for preferential pathways of phosphorus transport. *Journal of Environmental Quality* 29: 97-105.

Sims, J. T. R. O. Maguire, A. B. Leytem, K. L. Gartley, and M. C. Pautler. 2002. Evaluation of Mehlich 3 as an Agri-environmental soil phosphorus test for the Mid-Atlantic United States of America. *Soil Science Society of America Journal* 66: 2016-2032.

Šimůnek, J., and M. Th. van Genuchten. 2008. Modeling nonequilibrium flow and transport processes using HYDRUS. *Vadose Zone Journal* 7: 782-797, doi: 10.2136/vzj2007.0074.

Šimůnek, J., M. Th. van Genuchten, and M. Šejna. 2006. The HYDRUS software package for simulating two- and three-dimensional movement of water, heat, and multiple solutes in variably-saturated media, Technical Manual, Version 1.0, PC Progress, Prague, Czech Republic, pp. 241.

Sisson, J. B., and P. J. Wierenga. 1981. Spatial variability of steady-state infiltration rates as a stochastic process. *Soil Science Society of America Journal* 45: 699-704.

Soerens, T. S., E. H. Fite, III, and J. Hipp. 2003. Water quality in the Illinois River: Conflict and cooperation between Oklahoma and Arkansas. Diffuse Pollution Conference Paper. Dublin, Ireland: University College Dublin.

Sparks, D. L. 1989. Kinetics of soil chemical processes. San Diego, CA, Academic Press.

Sposito, G. 1994. Chemical equilibria and kinetics in soils. New York, Oxford University Press.

SSSA. 2008. Glossary of soil science terms. SSSA, Madison, WI.

Steel, R. G. D., and J. H. Torrie. 1980. *Principles and procedures of statistics*. New York, N.Y.: McGraw-Hill.

Stoner, D., C. J. Penn, J. M. McGrath, and J. G. Warren. 2012. Phosphorus removal with by-products in a flow-through setting. *Journal of Environmental Quality* 41: 654-663.

Storm, D. E., M. White, M. D. Smolen, and H. Zhang. 2001. Modeling Phosphorus Loading for the Lake Eucha Basin. Final report. Stillwater, Okla.: Oklahoma State University, Department of Biosystems and Agricultural Engineering.

Storm, D. E., P. R. Busteed, A. R. Mittlestet, and M. J. White. 2010. Hydrologic modeling of the Oklahoma/Arkansas Illinois River basin using SWAT 2005. Final report. Stillwater, Okla.: Oklahoma State University, Department of Biosystems and Agricultural Engineering.

Thomas, G. W., and R. E. Phillips. 1979. Consequences of water movement in macropores. *Journal of Environmental Quality* 8(2): 149-152.

Ulen, B. 1999. Leaching balances of phosphorus and other nutrients in lysimeters after application of organic manures or fertilizers. *Soil Use and Management* 15: 56-61.

U.S. EPA (Environmental Protection Agency). 2003. Final Water Quality Trading Policy. Washington, D.C.: U.S. Environmental Protection Agency.

U.S. EPA (Environmental Protection Agency). 2009. Pathogen TMDLs for Clear Creek in Arkansas Planning Segment 3J, U.S. EPA Region 6, Water Quality Protection Division, Dallas, TX.

Vadas, P. A., R. D. Harmel, and P. J. A. Kleinman. 2007. Transformations of soil and manure phosphorus after surface application of manure to field plots. *Nutrient Cycling in Agroecosystems* 77: 83-99.

van Genuchten, M. Th. 1980. A closed-form equation for predicting the hydraulic conductivity of unsaturated soils. *Soil Science Society of America Journal* 44: 892-898.

van Genuchten, M. Th., F. J. Leij, and S. R. Yates. 1991. The RETC Code for Quantifying the Hydraulic Functions of Unsaturated Soils. EPA Rep. No.600/2-91/065, US Salinity Laboratory, USDA, ARS, Riverside, CA.

Violante, A. 2013. Elucidating mechanisms of competitive sorption at the mineral/water interface. P. 111-176. *In* D.L. Sparks (ed.) Advances in Agronomy, Volume 118.

Warren, D. M. 2003. City of Tulsa v. Tyson Foods: CERCLA comes to the Farm—but did arranger liability come with it? *Arkansas Law Review* 59(1): 169-197.

Yandle, B. 2008. Markets for water quality. *Property and Environment Research Center (PERC) Reports* 26(3): 14-17.

Zhang, R. 1997. Determination of soil sorptivity and hydraulic conductivity from the disk infiltrometer. *Soil Science Society of America Journal* 61: 1024-1030.

Zhang, H., J. L. Schroder, J. K. Fuhrman, N. T. Basta, D. E. Storm, and M. E. Payton. 2005. Path and multiple regression analyses of phosphorus sorption capacity. *Soil Science Society of America Journal* 69: 96-106.

## (4) PUBLICATIONS

Heeren, D.M., G.A. Fox, A.K. Fox, D.E. Storm, R.B. Miller, and A.R. Mittelstet. 2014. Divergence and flow direction as indicators of subsurface heterogeneity and stage-dependent storage in alluvial floodplains. *Hydrological Processes* (In Press, Accepted November 28, 2012), DOI: 10.1002/hyp.9674.

Heeren, D.M., G.A. Fox, and D.E. Storm. 2014. Technical Note: A berm infiltration method for conducting leaching tests at various spatial scales. *Journal of Hydrologic Engineering* (In Press, Accepted February 6, 2013).

Penn, C.J., D.M. Heeren, and G.A. Fox. 2014. Application of isothermal calorimetry to the study of phosphorus sorption onto soils in a flow-through system. *Soil Science Society of America Journal* (In Press, Accepted October 4, 2013).

Miller, R.B., D.M. Heeren, G.A. Fox, T. Halihan, D.E. Storm, and A.R. Mittelstet. The hydraulic conductivity structure of gravel-dominated vadose zones within alluvial floodplains. *Journal of Hydrology* (In Review).

## (5) INFORMATION TRANSFER PROGRAM

A project website on subsurface P transport has been created with links to relevant publications and data from the project (http://biosystems.okstate.edu/Home/gareyf/ AlluvialPTransport.htm). A number of publications (shown above), conference proceedings papers, and conference presentations were derived from this research:


Heeren, D. M., R. P. Freiberger, G. A. Fox, D. E. Storm, C. J. Penn, T. Halihan, B. E. Haggard, R. B. Miller, A. R. Mittelstet, and D. A. Correll. 2013. Subsurface phosphorus transport and scale dependent phosphorus leaching in alluvial floodplains. Seminar, U.S. Environmental Protection Agency (EPA) National Center for Environmental Research. Arlington, Va.

Freiberger, R. P., D. M. Heeren, and G. A. Fox. 2013. Finite element modeling of phosphorus leaching through floodplain soils dominated by preferential flow pathways. ASABE Paper No. 1583250. St. Joseph, Mich.: ASABE.

Heeren, D.M., G.A. Fox, D.E. Storm, B.E. Haggard, C.J. Penn, and T. Halihan. 2013. Impact of measurement scale on infiltration and phosphorus leaching in Ozark floodplains. ASABE Paper No. 131621213. St. Joseph, Mich.: ASABE.

Heeren, D.M., C.J. Penn, and G.A. Fox. 2013. Phosphorus sorption and desorption from soils under flow-through conditions: An investigation of the use of thermal heat patterns as indicators or the degree, mechanisms, and kinetics of sorption reactions. ASABE Paper No. 131621201. St. Joseph, Mich.: ASABE.

Correll, D., D.M. Heeren, G.A. Fox, C. Penn, and T. Halihan. 2013. Transient Resistivity Imaging of a Phosphorous Tracer Test. Geological Society of America's South-Central Regional Meeting, April 4, 2013, Austin, TX.

Heeren, D.M., G.A. Fox, and D.E. Storm. 2012. Berm method for quantification of infiltration and leaching at the plot scale in high conductivity soils. ASABE Paper No. 121337098. St. Joseph, Mich.: ASABE.

Heeren, D.M., G.A. Fox, D.E. Storm, P.Q. Storm, B.E. Haggard, T. Halihan, and C.J Penn. 2012. Quantification and heterogeneity of infiltration and transport in alluvial floodplains. ASABE Paper No. 121337097. St. Joseph, Mich.: ASABE.

Heeren, D. M., G. A. Fox, D. A. Correll, R. B. Miller, B. E. Haggard, C. J. Penn, D. E. Storm, T. Halihan, P. D. Hays, and A. N. Sharpley. October 18-19, 2011. Quantification and heterogeneity of phosphorus leaching in Ozark floodplains. Oklahoma Water Resources Research Institute (OWRRI) Oklahoma Water Research Symposium, Norman, Okla.

Heeren, D.M., G.A. Fox, D.E. Storm, B. Haggard. 2011. Influence of Scale on Quantifying Phosphorus Leaching in Ozark Floodplains. Arkansas Water Resources Center, Annual Watershed and Research Conference, July 6-7, 2011, Fayetteville, Arkansas.


## (6) STUDENT SUPPORT

Support has been provided for three graduate students (Ph.D. student in Biosystems and Agricultural Engineering at Oklahoma State, a Master of Science student in Environmental Sciences at Oklahoma State University, and a Master of Science student in Biological and Agricultural Engineering at the University of Nebraska) and six undergraduate students. Also,

the research supported a 2010-2011 Oklahoma State University Wentz Research Scholars project for an additional undergraduate student.

| Student Status | Number | Disciplines |
|---|---|---|
| Undergraduate | 6 | Biosystems Engineering |
| M.S. | 2 | Environmental Sciences (Geology), Biosystems Engineering |
| Ph.D. | 1 | Biosystems Engineering |
| Post Doc | 1 | Biosystems Engineering |
| Total | 9 | |

## (7) STUDENT INTERSHIP PROGRAM

No students completed an internship during the reporting period.

## (8) NOTABLE ACHIEVEMENTS AND AWARDS

U.S. EPA STAR Graduate Fellowship – Derek Heeren (2011-2012)

Outstanding Graduate Student Presentation. 2012. Heeren, D. M., G. A. Fox, D. E. Storm, P. Q. Storm, D. A. Correll, B. E. Haggard, T. Halihan, and C. J. Penn. Quantification and heterogeneity of infiltration and phosphorus leaching in alluvial floodplains. Student Water Research Conference, Stillwater, Okla.

Invited presentations at both Oklahoma and Arkansas Water Resources Research Symposiums